EQUILIBRIUM AND KINETIC STUDIES OF SORPTION OF ACTINIDES AND FISSION PRODUCTS AT SOLID/LIQUID INTERFACE

By

SUMIT KUMAR

CHEM 01200604015

Bhabha Atomic Research Centre, Mumbai

A thesis submitted to the
Board of Studies in Chemical Sciences

In partial fulfillment of requirements
For the Degree of

DOCTOR OF PHILOSOPHY

of

HOMI BHABHA NATIONAL INSTITUTE

October, 2012

Homi Bhabha National Institute

Recommendations of the Viva Voce Board

As members of the Viva Voce Board, we certify that we have read the dissertation prepared by **Shri Sumit Kumar** entitled "**Equilibrium and Kinetic Studies of Sorption of Actinides and Fission Products at Solid/Liquid Interface"** and recommend that it may be accepted as fulfilling the dissertation requirement for the Degree of Doctor of Philosophy.

Date: 28.01.2013

Chairman - **Dr. K. L. Ramakumar**	
Guide / Convener - **Dr. B. S. Tomar**	
Member 1 - **Dr. A. Goswami**	
Member 2 - **Dr. P. K. Mohapatra**	
External Examiner – **Prof. A. K. Singh**	

Final approval and acceptance of this dissertation is contingent upon the candidate's submission of the final copies of the dissertation to HBNI.

I hereby certify that I have read this dissertation prepared under my direction and recommend that it may be accepted as fulfilling the dissertation requirement.

Date: January 28, 2013

Place: Mumbai

STATEMENT BY THE AUTHOR

This dissertation has been submitted in partial fulfillment of requirements for an advanced degree at Homi Bhabha National Institute (HBNI) and is deposited in the Library to be made available to borrowers under rules of the HBNI.

Brief quotations from this dissertation are allowable without special permission, provided that accurate acknowledgement of source is made. Requests for permission for extended quotation from or reproduction of this manuscript in whole or in part may be granted by the Competent Authority of HBNI when in his or her judgment the proposed use of the material is in the interests of scholarship. In all other instances, however, permission must be obtained from the author.

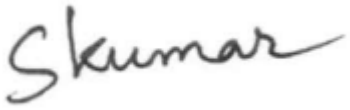

Sumit Kumar

DECLARATION

I, hereby, declare that the investigation presented in the thesis has been carried out by me. The work is original and has not been submitted earlier as a whole or in part for a degree / diploma at this or any other Institution / University.

Sumit Kumar

ACKNOWLEDGMENTS

A cherished wish is hence fulfilled. And I am thankful to a number of people.

Guidance and mentoring of my research guide, Dr. B. S. Tomar, and his encouragement during the thesis work have been torch light in the marching path.

Insightful comments by my doctoral committee members, Dr. K. L. Ramakumar, Dr. V. K. Manchanda, Dr. A. Goswami, and Dr. P. K. Mohapatra, kept me pursuing the goal.

My sincere thanks are due to Dr. Neetika Rawat, Smt. Aishwarya S. Kar, and Ms. Sharayu Kasar for stimulating discussions and cooperation during the thesis work. I express sincere thanks to my colleagues at Radioanalytical Chemistry Division, BARC. Help from Dr. R. M. Sawant, Shri S. Jaykumar, Smt. V. V. Raut, was very timely and constructive.

I am also thankful to my friends and collaborators at Radiochemistry Division (Dr. S. V. Godbole, Dr. M. S. Murali, Dr. P. N. Pathak, Dr. Kathi Sudarshan, Dr. A. Bhattacharyya, Dr. Chhavi Agrawal, Dr. Siraj Ansari, Shri D. R. Prabhu, and Shri Avinash Kanekar), Fuel Chemistry Division (Dr. K. T. Pillai, Shri T. V. Vithal Rao), Material Science Division (Dr. S. Ramanathan), Applied Spectroscopy Division (Dr. D. Bhattacharya, Shri A. Poswal), Technology Development Division (Dr. R. K. Bajpai), and Waste Management Division (Dr. C. Kaushik, Dr. A. S. Pente).

At this time, it gives me immense pleasure to remember a few nice people in my life: my parents, two of my school-time teachers (Mr. Rakesh Sinha and Mr. Madan Singh), my wife, Swagata, and son, Mihir.

Sumit Kumar

CONTENTS

Synopsis

Introduction

The discovery of nuclear fission by Hahn and Strassmann and the realization that "energy released per unit mass from fission is a million times greater than the energy released in the combustion of fossil fuels" prompted the peaceful as well as strategic usage of uranium and plutonium [1]. This generated an inventory of radionuclides having half life ranging from seconds to millions of years, not yet present in the environment. Owing to suitable nuclear properties, many of those radioisotopes were successfully applied in other areas, such as, $^{99}Tc^{m}$ in diagnostic application, ^{241}Am in smoke detector, ^{238}Pu as heat sources, etc. During the wartime development of nuclear weapons, when the impact of environmental radioactivity was neither known nor was of primary concern, relatively large amount of long lived fission products and actinides were released to the environment through soil, rivers, ponds and holding tanks. The scenario changed later when mining, nuclear materials processing and waste management began to be designed to reduce the waste and to isolate the radioactivity from human exposure. Though the environmental footprint of radioactivity produced in front end of the nuclear energy program is now more localized, total clean up of global fallout from earlier above-ground weapons testing and nuclear accidents is far from over [2]. With the construction of newer nuclear power reactors, safe disposal of the spent fuel and the reprocessed nuclear high level waste is an issue. Somewhat counterbalancing this build up is more complex nuclear fuel cycles and transmutation strategy. The fact which, however, underlines the growth of nuclear technology from big experiment of early twentieth century to present day beneficial applications in industry, science, health and national security, is that entry of radionuclides

to the environment is quite probable and a safe nuclear program should rest upon the sound understanding of their geochemical behavior.

Sources of radionuclides in the environment are mainly two folds: natural and anthropogenic. Natural sources, like ^{40}K, ^{232}Th, ^{235}U, ^{238}U and their daughter products are present on the earth from the beginning being formed in the course of nucleosynthesis and are called primordial radionuclides. Anthropogenic sources relate to the radioactivities produced in the nuclear energy and weapons program. These include radioisotopes like fission products $^{134,135,137}Cs$, $^{89,90}Sr$, ^{99}Tc, ^{79}Se, ^{129}I and actinides ^{237}Np, $^{239,240}Pu$, $^{241,243}Am$ and $^{244,245}Cm$. Major fission products ^{137}Cs, ^{90}Sr have significant radioactivity for a period of about 200 years after their production while transuranics having atomic content 1% or less in the spent fuel are prevalent up to a million year and beyond [3]. With respect to concentration and radiotoxities leading to radiation dose and other hazards to the common population, fission products are of concern for the first few hundred years while minor actinides dominate after that up to million years period [4].

Once in the geosphere, radionuclides' chemical behavior is governed by complexation, redox reactions, colloid formation and interactions with mineral surfaces [4, 5]. Water is recognized as the dominant transport medium in the environment [6] and its chemical condition defines the oxidation state, the prevailing species and solubility of the radionuclides. Most natural waters have low salinity (ionic strength below 1 M), near neutral pH (5-9) with a wide range of redox potentials (Eh) (from -300 to +700 mV) [7]. Geochemical interactions of radionuclides primarily stem from their oxidation states. Under a given experimental condition of pH and Eh, redox sensitive radionuclides, viz, Tc, Pu, Np, easily form multiple oxidation states, which complicates the prediction of their behaviour in environment in comparison to single oxidation state radionuclides, such as

Am(III) & Cm(III). Bicarbonate / carbonate and hydroxide are main inorganic complexing ligands present in aquatic system. Many other inorganic ligands such as fluoride, sulfate, silicate or phosphate can play a role by complexing radionuclides, but outcompete hydroxide and carbonate only under exceptional site-specific circumstances, such as chloride because of its high concentration in brines found around geological salt formations. Organic chelating molecules present in the environment range from molecular citrate, oxalate, etc., to macromolecular, polyelectrolytic humic substances.

Radiolysis caused by highly energetic alpha particles in chloride-based brines form highly oxidizing species HClO and ClO^- in neutral pH conditions thereby producing actinides in their higher oxidation states V and VI [8, 9]. The concentration of contaminant radionuclides in environment is decided [1] by the solubility of their solid phase formed under the prevailing condition by the interplay of above mentioned factors (pH, Eh, ligands, etc) [5].

Tetravalent and hexavalent fission products and actinides bind several inner-sphere water molecules and hydroxides to form dimeric, trimeric or polymeric species. These species polymerize further and aggregate to form colloids, relatively low molecular weight species that can remain suspended. This type of colloids is termed real or intrinsic colloids. These colloids are of concern because of their high stability at near-neutral pH, their resistance to disintegration, and their ability to raise the radionuclides level in aqueous phase. At the low concentration of radionuclides expected in surface and groundwater, the sorption of fission products and actinides on mineral surfaces most likely control their fate in the environment. It can be argued that plutonium introduced into subsurface environment should be relatively immobile owing to its low solubility in ground water and strong sorption on mineral surfaces [5]. Following the $^{240}Pu/^{239}Pu$ isotope ratio Kersting et al.

however established that Pu sorbed onto particulate surfaces was responsible for its migration 1.3 kilometer south of the origin site at Nevada test site [10]. These particles are submicrometer sized colloids, consisting of inorganic and/or organic compounds and occur at up to 10^{17} particles per liter in ground water. Aquatic colloids having sorbed radionuclides are termed pseudo-colloids. Nano-secondary ion mass spectrometry elemental maps revealed Pu(IV) sorption on amorphous iron oxide colloids, reinforcing the colloid assisted transport of plutonium in the far-field of the Mayak Production Association, Ural, Russia [11]. The solid geological matrices can immobilize the radionuclides while the high surface area/reactivity of colloidal particles may increase the radionuclides concentration in natural waters by many orders of magnitude over the values expected from solubility calculation. The greater the extent to which a contaminant partitions into the mobile phase, the greater its concentration available for transport in the ground water.

Colloidal particles involved in radionuclides transport process are formed by physical erosion of soils, man-made materials (i.e., cement, glass), surrounding clay and rock formations. They typically comprise of mineral oxides (silica, iron oxides, etc), calcite and clay minerals. Numerous studies devoted to long-lived radionuclides sorption onto these colloids under conditions simulating the near as well as far-field of the deep geological repositories of nuclear high level waste are available in open literature [12]. pH, Eh, complexing ligands, temperature, surface coverage and nature of solid surfaces have been found to significantly influence the sorption behaviour [13]. Owing to their very high complexing ability, presence of humic substances in aquatic environment greatly alters the radionuclide sorption behaviour [14]. The empirical approach of distribution or sorption coefficient, K_d, describe the radionuclide immobilization or migration in site-specific solid-

aqueous medium condition. Transport of radionuclides in geosphere is expected to undergo through variety of hydrogeochemical condition. It is therefore requisite to couple macroscopic and field level radionuclide behaviour with mechanistic understanding of the sorption process.

In the present thesis, sorption of actinides and fission products on mineral oxides and natural smectite rich clay has been investigated using batch sorption, modeling and spectroscopic studies. Effect of pH, ionic strength, surface coverage, presence of inorganic and organic complexants, and nature of solid surface on the sorption process has been delineated through surface complexation modeling of the responsible interfacial sorption reactions. Kinetic and spectroscopic techniques revealed the speciation in aqueous phase and on solid surfaces. Finally a sorption model has been proposed for americium sorption on natural clay to describe the effect of ground water composition, effect of minor phase of the clay and competitive reactions from other cations. Aim of these studies has been to make more robust the mechanistic description of sorption of actinides and fission products on mineral oxides and clay surfaces.

The thesis has been divided into six chapters and a brief description of each chapter is as follows.

Chapter 1: Introduction

In this introductory chapter, an account of the sources of radioactivity present in geosphere has been given. Starting from the historical evidence of radioactivity from Oklo natural reactor, description of radioactively contaminated sites worldwide and future inventories of long-lived actinide and fission products in view of expanding nuclear applications has been discussed. Water has been considered the major transport vector in

radionuclide migration [6]. How its chemistry creates the boundary condition for radionuclide speciation and solubility has been presented in this chapter. Migration of radionuclides to far-field areas may cause exposure of biosphere to these hazardous contaminants. Safety assessment of nuclear operation sites, such as, near surface waste disposal site or deep underground high level waste disposal sites takes recourse of transport modeling based on partition coefficient, K_d, determined in site-specific geochemical condition. As K_d based empirical approach is devoid of taking consideration of the changing chemical conditions in the migration route, thermodynamic description of interfacial sorption of radionuclides proposed in recent modeling exercises has been discussed [6]. This mechanistic approach is based on the geochemical interaction of radionuclides and a short account of those interactions has been discussed. Finally, a review detailing the literature understanding of the sorption of actinides and fission products on mineral oxides and clay and prompting the work carried out in this doctoral dissertation has been presented.

Chapter 2: Experimental details

This chapter discusses the methodology of the experiments and modeling carried out in the present work. To understand the mechanistic aspect of the interfacial sorption process, equilibrium and kinetic data of the sorption systems has been produced in batch sorption experiment while identification and characterization of radionuclides' surface speciation has been done by Fluorescence and X-ray absorption Fine structure spectroscopies. Effect of different chemical conditions, such as pH, surface coverage, presence of humic acid (HA), etc., on the sorption process has been delineated through linear additive modeling and surface complexation modeling. Development of this chapter

is as follows: details of the characterization of different sorbents and HA involved in the experiments, description of the radionuclidic characteristics of various fission products and actinides used along with the production procedure of ^{95m,96}Tc isotopes employed in the Tc experiments, solvent extraction based procedure for plutonium oxidation state determination, procedure of the batch sorption experiment, and theoretical description of linear additive modeling and surface complexation modeling. The chapter ends with the introductory, experimental and analysis details of the spectroscopic techniques used in this thesis work.

Chapter 3: Sorption of fission products on mineral oxides

In this chapter sorption of cesium (Cs(I)) and technetium (Tc(IV), Tc(VII)) on mineral oxides has been described [15-17]. Effect of pH, ionic strength and HA on Cs(I) sorption on silica (amorphous phase) has been studied in batch sorption experiment [15]. Cs sorption on silica starts after pH 7 and reaches ~ 30% by pH 10. There is no effect of the ionic medium (0.05-0.1 M $NaClO_4$) on Cs sorption. Nearly 60% of HA gets sorbed on the silica surface at lower pH values while the sorption percentage decreases by 50 % at pH 10. In the Cs-HA-Silica sorption system, presence of humic acid significantly enhances Cs sorption at lower pH while there is no effect at higher pH values. In the solvent extraction experiment to study Cs-HA interaction, stability constant of Cs-HA species was found to be very small ($\log \beta = -1.86 \pm 0.23$). These observations lead to the conclusions: (1) More than electrostatic factor, it is the complexing ability of metal ions which govern the sorption behaviour, and (2) interaction ability of surface sorbed HA is different from the aqueous phase HA. Linear additive modeling of the Cs-HA-silica system substantiated the second conclusion. ^{99}Tc is a long lived fission product (half-life 2.13×10^5 yrs) with high fission

yield 6.13 % produced in thermal neutrons induced fission of ^{235}U. It exists in pertechnetate form (Tc(VII), TcO_4^-) in oxic condition and is reduced to highly immobile form $TcO_2 \cdot n H_2O$ (Tc(IV)) under reducing environment. Change in speciation could significantly affect Tc migration and to investigate this aspect, Tc(VII, IV) sorption on hematite and alumina was carried out with shorter half life gamma emitting isotope of Tc (^{95m}Tc and ^{96}Tc). These isotopes have been prepared by $^{96}Mo(p,xn)$ reaction using Pelletron accelerator at TIFR, Mumbai. Sorption of TcO_4^- on hematite decreases with pH and conforms to the typical anionic sorption reported in literature. Presence of HA in the sorption system does not change the sorption significantly [16]. Similar observation was found for Tc(VII) on alumina surface though not exactly same. Tc(IV) sorption on alumina was, however, found significantly altered by the presence of HA [17]. Quantitative sorption of Tc(IV) was achieved at lower pH while the presence of HA in the aqueous phase lowered the sorption percentage at higher pH values. Modeling of Tc(IV)-HA-alumina system by linear additive modeling indicates higher complexing ability of surface sorbed HA while surface complexation modeling indicates ligand bridged species of Tc(IV) on alumina surface ($\equiv AlOL_1TcO$) responsible for the enhanced sorption. These studies conclude the role of solid surface in defining sorption profile, changing sorption pattern with changed oxidation state and enhanced complexing ability of HA when sorbed on solid surface.

Chapter 4. Sorption of Actinides on mineral oxides

Sorption of americium (Am(III)) and plutonium (Pu(IV)) has been reported in this chapter [18-20]. Am sorption on alumina in varying pH (3-10), ionic strength (0.005-0.1M), and metal ion concentration (10^{-7}-10^{-4} M) was studied using batch sorption method [18]. There is no effect of ionic strength on Am sorption whereas sorption percentage increases

sharply over pH 3-6. This shows inner sphere complex formation of Am with alumina surface sites. Inactive Eu, an analogue for Am, was used to achieve higher metal ion concentration in the sorption study. Time resolved fluorescence spectroscopic investigation of Eu (10^{-4} M) sorbed on alumina surface over pH 3-7 indicated the presence of two surface species with lifetime values ~110 and 325 μs. There is pH dependent increase in shorter life time value while the other is not much sensitive to pH variation. XAFS study of Am sorbed at alumina surfaces at pH 6.18 (as discussed in the next paragraph) reveals bidentate binding of Am with alumina sites in the second species. Surface complexation modeling of the sorption profile under varying pH and metal ion concentration conditions indicates the predominance of bidentate species at highest metal ion concentration while the other species, monodentate Am species, is the governing surface speciation in lower metal ion concentration condition.

To further investigate the speciation of Am at highest metal ion concentration over pH 6-8, transmission mode X-ray absorption fine structure spectroscopy was carried out for Eu sorbed on alumina [19]. As per the solubility of $Eu(OH)_3$, this pH range stands for undersaturation to oversaturation state of Eu in the sorption system. X-ray absorption near-edge spectroscopy (XANES) revealed the presence of Eu in III oxidation state in all the sorption samples and reference samples (Eu_{aqua}, Eu_2O_3, $Eu(OH)_3$). Extended X-ray absorption fine structure spectrum, however, indicated the absence of $Eu(OH)_3$ as surface speciation and revealed the formation of Eu surface species with dissolved alumina. As silica has higher solubility than alumina, this type of species should form more with silica and similar experiment of Eu sorbed on silica at pH 6-8 revealed the expected conclusion. The difference in basic unit, silicate and aluminate, was however observed to cause difference in the formation pattern of these surface species.

Plutonium exhibits multiple oxidation states in ground water ranging from III to VI [5]. In its IV oxidation state, the solubility product for $Pu(OH)_4$ is very low and it should therefore be immobile. Its high complexing ability in IV oxidation state should also cause strong sorption on geological surfaces to make it immobile. However, the field study at Nevada test site and other places showed plutonium migration away from the place of origin. In the sorption/desorption study of Pu(IV) on silica and alumina surface, the source term of Pu migration from near field nuclear high level waste repositories condition to far-field areas has been investigated. This study aims at exploring the nature of the migrating Pu, apart from the already accepted colloid facilitated migration pathway. Silica was found governing the sorption at pH values < ~5.5 while both the surfaces quantitatively sorb the metal ion at higher pH values. Kinetic data of the sorption indicate faster sorption on alumina compared to silica. On comparing the kinetic data of Pu(IV) with that of Th(IV), Pu sorption can be explained to follow fast sorption characteristic of mononuclear species followed by a slow process. The slow process could be attributed to polymerization of Pu mononuclear species on the sorbent surfaces. Leaching experiment however, negates the formation of PuO_2(am) as surface speciation. Oxidation state determination of surface sorbed Pu by leaching followed by solvent extraction method confirmed IV as the oxidation state of Pu. It can thus be concluded that Pu(IV) sorbs on the surfaces in small polymeric species but not in PuO_2 form. The relative difference in the sorption ability of two substrates, however, causes the difference of oxidation state of Pu in the supernatant; Pu(V) is the dominant species in the supernatant of silica with Pu(VI) being the corresponding species in alumina supernatant.

These studies conclude: (1) Surface speciation changes under different chemical conditions, (2) near the source point where there is higher concentration of metal ions in

comparison to far-field areas, surface speciation may be very different, (3) dissolution of the solid surfaces affects the surface speciation, and (4) apart from the colloid facilitated transport, transport modeling of Pu need to take into consideration desorption and oxidation state transformation for correct modeling.

Chapter 5. Sorption of actinides on natural smectite rich clay

Sorption of Am(III) on smectite rich natural clay under granitic water condition is the subject of this chapter. This clay has been collected from the Barmer region of western India and aim of this wok has been to develop a sorption model for Am on this clay describing the effect of granitic ground water composition, effect of minor phase (Kaolinite) present in clay and competition of other cations, such as, calcium [21]. Batch sorption of Am(III) on washed, Na-homoionic well characterized (for chemical composition, structural phases, surface area, size, etc.) clay has been carried out under the varying condition of pH, ionic strength, and anions. Ion exchange is the sorption mechanism at lower pH values while surface complexation of Am is the mechanism at higher pH values. Presence of anion (chloride, sulphate, and nitrate) has no effect on the sorption experiments carried out in 0.01 M medium while sorption is more than 95 % in the pH range 3-10. In another experiment Am sorption on montmorillonite (main component of the clay) was found independent of Kaolinite fraction (0-20 wt%). These studies confirm montmorillonite as the phase controlling Am sorption on the clay and a sorption model incorporating ion exchange and surface complexation aspects of montmorillonite has been developed using surface complexation modeling of batch sorption data, and Am sorption on calcium - equilibrated-clay.

Chapter 6. Conclusions

In this concluding chapter findings of the thesis work have been summarized. Briefly, sorption characteristics of fission products and actinides on mineral oxides and natural clay under various controlling conditions of pH, ionic strength and the presence of complexing anions have been discussed. Application of inputs from kinetic experiment, spectroscopic studies and surface complexation modeling in delineating the interfacial sorption reaction has been presented. Significant advances towards the understanding of sorption mechanism are as follows:

1. Predictive modeling of ternary systems of radionuclides, humic substances and mineral surfaces,
2. Delineation of surface speciation of americium in conditions of higher surface coverage,
3. Role of solid sorbent dissolution in surface speciation, and
4. Application of understanding gained in the sorption by mineral oxides to complex natural substrates.

References

1. G. Friedlander, J. W. Kennedy, E. S. Macias, J. M. Miller, Nuclear and Radiochemistry, Third edition, 1981, John Wiley & Sons, USA.

2. L. R. Morss, N. M. Edelstein, J. Fuger, The Chemistry of the Actinides and Transactinide Elements, Fourth edition, 2010, Springer, The Netherlands.

3. K. H. Lieser, Radionuclides in the Geosphere: Sources, Mobility, Reactions in Natural waters and Interactions with Solids, Radiochim. Acta 70/71, 355 - 375, 1995.

4. J. I. Kim, Significance of actinide chemistry for the long-term safety of waste disposal, Nucl. Eng. Technol. 38, 459-482, 2006.

5. R. J. Silva and H. Nitsche, Actinide environmental chemistry, Radiochim. Acta 70/71, 377 - 396, 1995.

6. W. Stumm and J. J. Morgan, Aquatic chemistry: Chemical equilibria and rates in natural waters, Third edition, 996, John Wiley & Sons, New York, USA.

7. L. G. M. Baas-Becking, I. R. Kaplan, D. Moore, Limits of the natural environment in terms of pH and oxidation-reduction potentials, J. Geol. 68, 243-284, 1960.

8. K. Büppelmann, J. I. Kim, C. Lierse, The redox-behaviour of plutonium in saline solutions under radiolysis effects, Radiochim. Acta, 44/45, 65-70, 1988.

9. I. Pashalidis, J. I. Kim, C. Lierse, J. C. Sullivan, The Chemistry of Pu in Concentrated Aqueous Sodium Chloride Solution: Effects of Alpha Self-Radiolysis and the Interaction between Hypochlorite and Dioxoplutonium(VI), Radiochim. Acta, 60, 99-101, 1993.

10. A. B. Kersting, D. W. Efurd, D. L. Finnegan, D. J. Rokop, D. K. Smith, J. L. Thompson, Migration of plutonium in ground water at the Nevada Test Site. Nature, 397, 56-59, 1999.

11. A. P. Novikov, S. N. Kalmylov, S. Utsunomiya, R. C. Ewing, F. Horreard, A. Merkulov, S. B. Clark, V. V. Tkachev, B. F. Myasoedov, Colloid transport of plutonium in the far-field of the Mayak production association, Russia, Science 314, 638-641, 2006.

12. M. D. Siegel and C. R. Bryan, Environmental Geochemistry of Radioactive contamination, Handbook of geochemistry, 206-250, 2004.

13. J. Bruno and V. Montoya, From aqueous solution to solid solutions: A process oriented review of the work performed within the FUNMIG project, App. Geochemistry, 27, 444-452, 2012.

14. N. D. Bryan, L. Abrahamsen, N. Evans, P. Warwick, G. Buckau, L. Weng, W. H. Van Riemsdijk, The effects of humic substances on the transport of radionuclides: Recent improvements in the prediction of behaviour and the understanding of mechanisms, Appl. Geochemistry, Doi: 10.1016/j.apgeochem.2011.09.08.

15. S. Kumar, B. S. Tomar, V. K. Manchanda and S. Ramanathan, Effect of humic acid on adsorption behaviour of ^{137}Cs on silica colloids, Radiochim. Acta 94, 369-373, 2006.

16. S. Kumar, N. Rawat, B. S. Tomar, V. K. Manchanda, S. Ramanathan, Effect of humic acid on the sorption of technetium on hematite colloids using ^{95m}Tc and ^{96}Tc as tracers, Journal of Radioanalytical and Nuclear Chemistry, 274 (2), 229-231, 2007.

17. S. Kumar, N. Rawat, A. S. Kar, B. S. Tomar and V. K. Manchanda, Effect of humic acid on sorption of technetium by alumina, Journal of Hazardous materials, 192 (3), 1040-5, 2011.

18. S. Kumar, S. V. Godbole and B. S. Tomar, Speciation of Am(III)/Eu(III) sorbed on γ-Alumina: Effect of metal concentration, Radiochim. Acta (Accepted).

19. S. Kumar, A.S. Kar, B. S. Tomar, D. Bhattacharya, XAFS Spectroscopy study of Eu(III) sorption products on Amorphous Silica and γ-Alumina: Effect of pH and substrate, Polyhedron, 33, 33-40, 2012.

20. S. Kumar, S. U. Kasar, and B. S. Tomar, Interfacial sorption/desorption studies of Pu(IV) on Silica and alumina surfaces, Radiochim. Acta (Communicated).

21. S. Kumar, A. S. Pente, C. P. Kaushik, R. K. Bajpai, B. S. Tomar, Americium sorption on natural Clay in granitic water condition, Appl. Geochemistry (Communicated).

List of Figures

List of Tables

Chapter 1

Introduction

1.1 Environmental relevance

Discovery of artificial radioactivity by Irene Curie and Frederick Joliot in 1934 opened a new chapter in the peaceful uses of radioisotopes in diverse fields, such as, health, agriculture, industry, etc. Major step forward in this direction, however, took place with the discovery of nuclear fission in 1939 by Hahn and Strassmann. It opened up a frontier for utilization of the vast natural resources of uranium for electricity generation as an alternative to fossil fuels.

Associated with its usage, one major concern before environmentalists, policy makers, and common people regarding radioactivity has been its unregulated presence in geosphere. Exploitation of radioactivity during war time and its numerous subsequent applications has introduced large amount of radioactivity into environment. Apart from chemical toxicity, radionuclides cause radiation hazard by emanating ionizing radiations, α, β, γ, and neutrons. Radionuclides' application has, therefore, been put under strict regulations worldwide. With everyday increasing demand on nuclear applications, chances of appearance of radioactivity in the environment cannot be discounted. A safe and scientific approach to deal with this issue lies in developing robust understanding about the environmental geochemistry of radioactive contaminants. This will help not only in assessing the risk posed by future applications but also in remediating the present contaminations.

1.2 Sources of radionuclides in geosphere

Radioisotopes are present in the geosphere both naturally as well as from artificial production routes (Leiser, 1995; Siegel and Bryan, 2009; Runde and Neu, 2010).

1.2.1 Natural radioactivity

Natural radioactivity is present in the form of uranium-thorium decay series wherein ^{238}U (4n+2), ^{235}U (4n+3), and ^{232}Th (4n) decay through intermediate daughter products to ^{206}Pb, ^{207}Pb and ^{208}Pb respectively. On mining and milling, large amount of these activities are brought to the earth surface. Residue (mill tailings) of the milling process are dumped on the low lying areas (mill tailing ponds) which creates a potential source of long lived radioisotopes of Th, U, Ra, and Po in the geosphere. Other naturally occurring radioisotopes such as ^{14}C, and ^{3}H are being continuously formed in environment due to cosmic ray bombardment; their concentration is, however, not a matter of concern owing to the low level of radioactivity.

1.2.2 Nuclear weapon tests

A large number of atmospheric tests were conducted by the US, the USSR, UK, France and China, between 1946 and 1962. After the atmospheric test ban treaty in 1963, underground nuclear tests have been conducted by them along with countries like India, Pakistan, and North Korea. Only France and China continued atmospheric testing till 1974 and 1980, respectively (Runde and Neu, 2010). All these nuclear tests have resulted in the contamination of the geosphere with actinides and long lived fission products.

1.2.3 Accidental releases from nuclear facilities

There have been a few disastrous accidents in the history of nuclear industry. Radioactivity was released from (i) the fire accident at the reactors in Windscale in UK in 1957, (ii) loss of coolant accident at the Three Mile Island nuclear reactors in US in 1979, (iii) explosions at the Chernobyl reactor in USSR in 1986, and recently (iv) release of gaseous fission products from the spent fuel storage bay at Fukusima in 2011 due to the post Tsunamic events. These accidental

releases have resulted in the contamination of the large geographical area and atmosphere with long lived fission products and in some cases actinides as well. In addition there have been releases of actinides and fission products from the spent fuel reprocessing plants, viz., (i) leakage from the Hanford high level radioactive liquid waste storage tanks near the Columbia river, (ii) routine and accidental discharges from the Mayak plutonium production complex in USSR, to list a few.

1.2.4 Nuclear Applications

^{238}Pu has been used as a power source in satellites. Some of the satellites have reentered the earth's atmosphere upon the completion of their life cycle in space or as a result of the incomplete mission. ^{238}Pu thus spread in the upper atmosphere and might have ended up partly in the geosphere (Kim, 1986).

$^{99}Tc^{m}$ is widely used in nuclear medicine for diagnostic applications. The daughter product of this isomer is $^{99}Tc^{g}$ which has a long half life and hence remains in the geosphere for millions of years after the use.

1.2.5 Nuclear waste

The reprocessing of spent nuclear fuel to recover plutonium and uranium results in various waste streams, such as low level waste (LLW) (< 1 mCi/L), intermediate level waste (ILW) (1 mCi/L to 1 Ci/L), and high level waste (HLW) (> 1 Ci/L) depending upon the level of radioactivity. ILW is concentrated in cementous solid matrices and stored in shallow trenches, while the HLW is vitrified in a suitable glass matrix and after an interim storage period, is planned to dispose of in deep underground repositories (Schwyn et al., 2012).

Current and potential future inventories of radioactivity in environment may thus be grouped in three main classes:

- Legacy sources such as contaminated geographical areas, etc.
- Nuclear applications and accidents.
- Nuclear energy: With expanding nuclear energy program in country like India, increasing inventory of nuclear HLW increases the relevance of understanding of geochemical behaviour of long lived radionuclides in environment.

1.3 Actinides and long lived fission products

Actinide isotopes, such as, ^{235}U, ^{239}Pu, ^{233}U, etc. undergo neutron induced fission in nuclear reactors, thermonuclear explosions, etc. A host of fission products spanning the atomic number 35 to 63 with varying yield are produced. Most of the fission products have shorter half-lives and hence do not remain relevant over a longer period of time. Fertile isotopes of actinides can undergo neutron capture reaction to produce a large number of actinide isotopes, most of them having long half lives, viz.,

$$^{232}\text{Th}\,(n,\gamma)\,^{233}\text{Th} \xrightarrow{\beta^-} {}^{233}\text{Pa} \xrightarrow{\beta^-} {}^{233}\text{U}\,(1.593\times10^5\ \text{y})$$

$$^{238}\text{U}\,(n,\gamma)\,^{239}\text{U} \xrightarrow{\beta^-} {}^{239}\text{Np} \xrightarrow{\beta^-} {}^{239}\text{Pu}\,(2.411\times10^4\ \text{y})$$

$$^{239}\text{Pu}\,(n,\gamma)\,^{240}\text{Pu}\,(n,\gamma)\,^{241}\text{Pu}\,(n,\gamma)\,^{242}\text{Pu}\,(n,\gamma)\,^{243}\text{Pu} \xrightarrow{\beta^-} {}^{243}\text{Am}\,(7370\ \text{y})$$

$$^{241}\text{Pu} \xrightarrow{\beta^-} {}^{241}\text{Am}\,(432.2\ \text{y})$$

$$^{241}\text{Am}(n,\gamma)\,^{242}\text{Am} \xrightarrow{\beta^-} {}^{242}\text{Cm}\,(162.94\ \text{d})$$

$$^{243}\text{Am}\,(n,\gamma)\,^{244}\text{Am} \xrightarrow{\beta^-} {}^{244}\text{Cm}\,(18.1\ \text{y})$$

Table 1.1 and 1.2 give the nuclear data of the long lived actinides and fission products typically present in nuclear HLW.

Table 1.1: List of long-lived fission products present in HLW

Radionuclide	Half-life	Yield (%) in $^{235}U(n_{th},f)$ and $^{239}Pu(n_f,f)$*	Radiation type	Energy
^{90}Sr - ^{90}Y	28.5 y	5.772 (2.088)	Pure β	0.5, 2.3 MeV
^{93}Zr	1.5×10^6 y	6.375 (3.734)	Pure β	0.06 MeV
^{99}Tc	2.1×10^5 y	6.074 (5.608)	Pure β	0.3 MeV
^{106}Ru - ^{106}Rh	368 d	0.4019 (4.5219)	γ	512 keV
^{107}Pd	6.5×10^6 y	0.1914 (3.5776)	Pure β	0.03 MeV
^{125}Sb	2.77 y	0.0253 (0.1964)	γ	426, 601 KeV
^{129}I	1.57×10^7 y	0.8533 (0.922)	β, γ	0.2 MeV, 40 KeV
^{134}Cs	2.06 y	4e-06 (1e-03)	β, γ	0.7 MeV, 605 KeV
^{135}Cs	2×10^6 y	6.726 (7.449)	Pure β	0.02 MeV
^{137}Cs	30.17 y	6.2295(6.6255)	β γ	0.5, 1.2 MeV 662 KeV
^{144}Ce - ^{144}Pr	284 d	5.4492 (3.6089)	β γ	0.3, 3.0 MeV 133,697 KeV
^{147}Pm	2.62 y	2.2551 (2.0263)	Pure β	0.2 MeV
^{151}Sm	93 y	0.435 (0.8202)	Pure β	0.1 MeV
^{152}Eu	13.33 y	5.28e-07 (2.05e-05)	γ	121.8 KeV, etc.
^{154}Eu	8.8 y	0.00017 (0.00449)	γ	123 KeV, etc
^{155}Eu	4.96 y	0.03328 (0.2579)	β γ	0.1, 0.2 MeV 87, 105 KeV

*in bracket

Table 1.2 List of transuranium isotopes present in HLW

Radionuclide	Half life (y)	Radiation type	Radiation energy (MeV)
^{237}Np	2.14×10^{6}	α	4.788
^{239}Pu	2.411×10^{4}	α	5.155
^{238}Pu	87.74	α	5.499
^{240}Pu	6550	α	5.168
^{241}Pu	14.4	β	0.02
^{241}Am	432.6	α	5.486
^{243}Am	7370	α	5.275
^{244}Cm	18.11	α	5.805
^{245}Cm	8500	α	5.362

The radioactivity of the radionuclides decays exponentially with time and hence once formed they contribute differently to the total radioactive burden depending upon their half lives. Variation of the radioactivity of different actinides and long-lived fission products present in the HLW produced by an Indian PHWR is plotted as a function of time in figure 1.1. Bulk of radioactivity initially is due to short-lived fission products ^{137}Cs and ^{90}Sr. After 1000 yrs the radioactive hazard is due to transuranics ^{241}Am, ^{243}Am, ^{239,240}Pu, and ^{237}Np and during the longest time periods a mixture of the isotopes ^{99}Tc, ^{237}Np, ^{210}Pb, and ^{226}Ra dominates the small amount of radioactivity that remains (Figure 1.1).

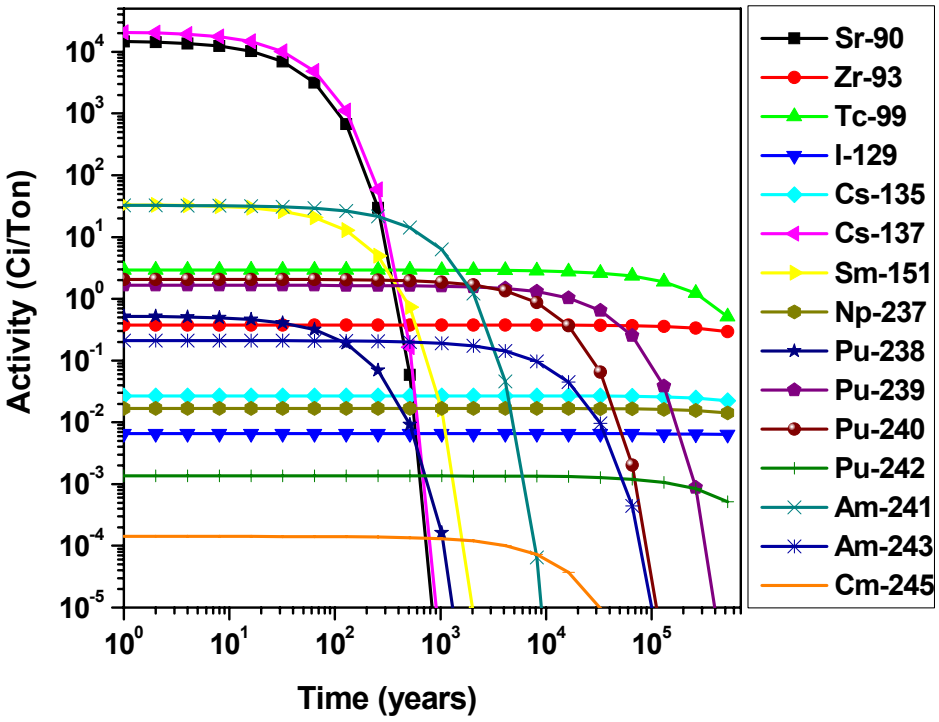

Figure 1.1 Profile of activity of long lived radionuclides present in HLW per ton of spent PHWR fuel (6700 MWD/t). Assuming 99% of Pu is removed.

1.4 Fate of actinides and long lived fission products in geosphere

Once released into the environment, the radionuclides may migrate to the far field areas. Water acts as the dominant transport medium (Stumm and Morgan, 1995; Siegel and Bryan, 2009). Fate of the radionuclides in geosphere is thus decided by the hydro-geochemistry of radionuclides and transport phenomena. Flux of radionuclide available for transport is generally determined in terms of partitioning coefficient (K_d) of a radionuclide between aqueous phase and the radionuclide' sorbing phase and transport is modelled on its basis. As the chemical condition over the flow path cannot be considered same, it is required that all the pertinent chemical

reactions of radionuclides in environmental aquatic medium should be identified and understood in framework of robust thermodynamic model.

1.5 Hydrogeochemistry of actinides and long lived fission products

Geochemistry of fission products in aquatic system is relatively simple compared to actinides. Though the present section details about actinides, chemical reactions applicable to both the class of metal ions are similar.

Solubility and Speciation in groundwater

Solubility of metal ions is primarily decided by their oxidation state. Early actinides (Th - Pu) exhibit multiple oxidation states (+3 to +6 in aquatic medium) owing to the small difference in the energy of 6d and 5f orbitals. +3 becomes the dominant oxidation state of actinides beyond americium (Am) as 5f orbital gets stabilized with increasing atomic number. (Eh, pH) condition of the aquatic body affects the stability of the oxidation state. Complexing ligands present in the aquatic body could also change the oxidative state of redox sensitive elements. Pu exhibits multiple valencies some of which coexist in natural water.

Dominant inorganic complexing ligands of aqueous systems are hydroxide, carbonate, and chloride. Solubility limiting solid phase of actinides are thus oxides, hydroxides or carbonates. The general pattern of solubility of actinides in different oxidation states is: $+4 < +6 < +5 < +3$. In absence of large scale precipitation reaction, higher valent actinides may hydrolyze, form colloidal sized (hydr)oxide polymer and remain suspended in the aqueous medium. Such particulate species are termed “intrinsic colloids” of actinides. Secondary solid phase formation of actinides with silicate ions has also been observed (Wronkiewicz and Buck, 1999).

In dilute natural aqueous system, speciation of metal ions is dominantly decided by the complexation with inorganic and organic ligands. Actinides are hard acids and interact strongly with hard donor ligands. For a given oxidation state, the relative stability of actinide complexes with hard base ligands can be divided into three groups in the order: CO_3^{2-}, OH^- > F^-, HPO_4^{2-}, SO_4^{2-} > Cl^-, NO_3^-. However, speciation gets severely changed in presence of large molecular weight humic substances (HS) and metal ion complexation with HS becomes the speciation governing chemical reaction in the neutral pH range (Choppin, 1988).

Sorption at the solid-liquid interface

Sorption onto geologic materials regulates the mobility of radionuclides in environment. It refers to a host of chemical processes - adsorption, absorption, (co)precipitation, and diffusion into the solid matrix - happening at the solid-water interface, whereby sorbing metal ion gets accumulated at the surface (Bruno and Montoya, 2012). Extensive laboratory scale sorption studies have been carried out to investigate sorption of actinides and fission products on geological materials (Langmuir, 1997, Triay et al., 1997, Jenne, 1998, Sterne et al., 1998, Siegel and Bryan, 2003, Runde and Neu, 2010). The focus of these studies has been on the determination of distribution coefficient in a purely empirical approach, to the use of adsorption isotherms, surface complexation models, and spectroscopic techniques (Geipel, 2006; Denecke, 2006; Edelstein et al. 2006, Zaera, 2012) to delineate the sorption mechanism. To this two compartment (solid-liquid) description of sorption process, observation of colloidal particle assisted migration of radionuclides has added another dimension (Honeyman, 1999; Kersting et al., 1999; Novikov et al., 2006; Utsunomiya et al., 2009). Here, radionuclides ride on the surface of colloidal sized inorganic/organic particles and migrate with the colloidal particles. Inorganic

particles are the weathered products of surrounding solid surfaces while organic particles are mainly HS.

Surface complexation models extend the concept of aquatic complexation to the sorption reaction. It visualizes the solid surface as populated by surface sites formed on the hydration/hydroxylation of dangling terminated bond, such as ≡SiOH on silica surface. Sorption occurs as a result of the interaction of metal ion with the surface sites. Surface interaction includes both electrostatic as well as complexation reaction. Putting sorption process into a complexation description made the model susceptible to chemical conditions and an internally consistent robust sorption model promises to bring the sorption process on predictive level.

1.6 Objective of the thesis

Experimental studies of actinides and fission products have shown their sorption process as dependent on environmental variables such as pH, ionic strength, and temperature, the presence of complexing ligands such as carbonate or organic species, and surface coverage. Attempts of surface complexation models along with spectroscopic and microscopic inputs have been successful to investigate such effects in model systems (Geckeis and Rabung, 2008), but complexities of natural sorption systems are yet to be fully understood (Lützenkirchen, 2012).

Natural sorbents are generally heterogeneous with regard to mineral composition and with the presence of natural organic matter. Changing chemical condition of the aquatic medium can turn sorption mechanism from surface complexation to surface precipitation. Presence of small inorganic as well organic complexants adds complexity by introducing competition between sorbent surface and complexants for metal ions. Understanding of the complexities of the natural

systems in framework of surface complexation models is thus required for more accurate prediction of transport process. The present thesis aims to identify some of the complexities of the natural sorption systems and delineate the sorption mechanism of radionuclides under such complexities.

Complexities investigated in the present thesis

Interactions of Radionuclides with mineral surfaces in presence of HS can be depicted schematically as in figure 1.2. HS are polydisperse, polyelectrolyte and undergo fractionation

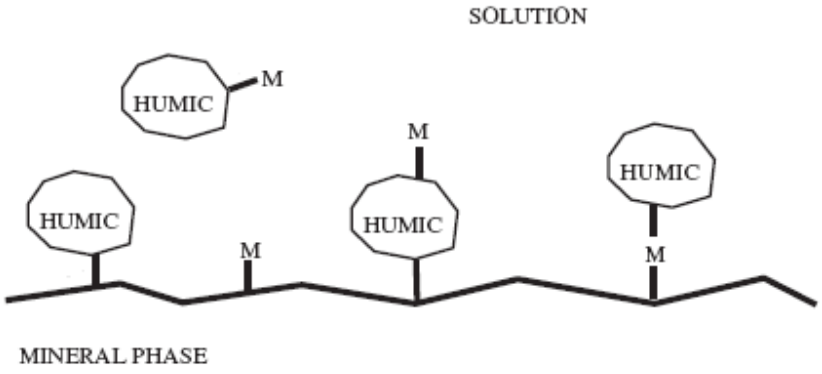

Figure 1.2 Interactions in ternary sorption system of radionuclides - humic acid - mineral (Bryan et al. 2012).

during sorption on mineral surfaces (Davis and Gloor, 1981; Zhou et al., 2001; Hur and Schlautman, 2003). Being polyelectrolyte, humic acid complexation with metal ions increases with pH (Choppin, 1988; Tipping, 1998, Kinniburgh et al., 1999). In view of an array of simultaneously operating interactions in the ternary systems, predictions of radionuclides sorption behaviour in such systems are hard (Fairhurst et al., 1995). Complexity to such systems is further added by the fact that interaction mechanisms between humic substances and minerals

are uncertain, and the mechanism of sorption of humic substance-metal ion complexes is not fully understood (Bryan et al. 2012).

Solid sorbents participate in the sorption reactions differently (Banwart, 1997; Piasecki and Sverjensky, 2008). This is attributed to the difference in their surface characteristics (Tournassat et al., 2004). Depending upon the electro-negativity of the structural atom, solid surface may behave as acidic or basic in the pH range. Dissolution of the solid sorbents also changes with the change of surface central atom. Structural arrangement of the surface atoms has been found guiding the formation of surface species (Cheah et al., 1998). Transition of surface complexation to surface precipitation involves continuum of chemical process where mononuclear surface complex leads to multinuclear complex, to precipitation of metal ions in pure homogenous phase or coprecipitation with dissolved species of solid surface, and finally to formation of a new phase on the surface (figure 1.3) (Banwart, 1997). How the structural characteristics relates with the

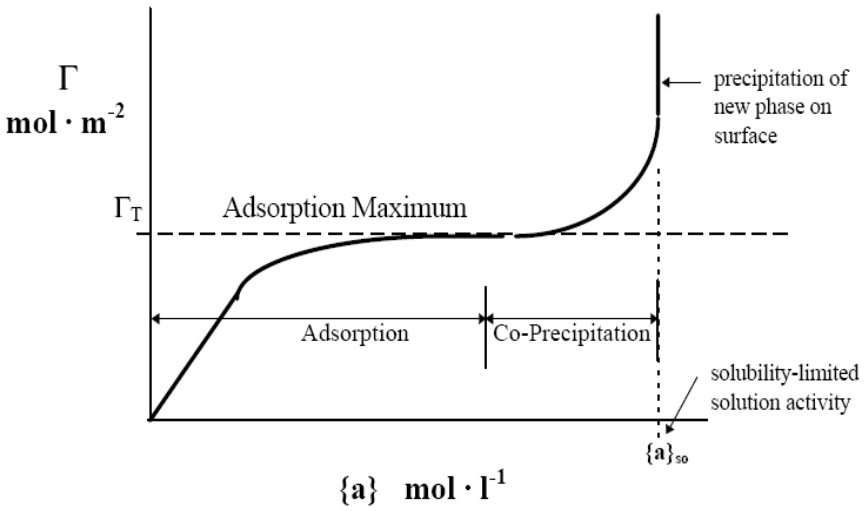

Figure 1.3 Typical adsorption isotherm obtained in metal ion sorption on solid surfaces (Banwart, 1997).

sorption behaviour needs to be investigated for accurate description of sorption process.

Sorption of actinides and fission products on clay minerals has been studied and modelled using ion exchange and surface complex reactions. These processes get significantly affected by the presence of various cations and anions (Bradbury and Baeyens, 2005; Bachmaf et al., 2008). Sorption process may change by the overlapping sorption characteristics of different mineral phases present in the natural sorbents (Missana et al., 2009; Bradbury and Baeyens, 2011). Different "top-down" and "bottom-up" approaches have been tried in the literature for modelling sorption of radionuclides on natural sediments (Altmann, 2001). In top-down strategy, the natural system is modeled on the basis of bulk system parameters while in the alternate "bottom-up" approach one identifies all the significant components of the system and attempts to systematically understand and model the interactions of each component with the contaminant of interest. The latter approach involves detailed study of both the mineralogy of the solid phase and the chemistry of the aqueous phase and works in agreement with molecular level informations. Such studies in site specific conditions may serve as link between laboratory scale experiment and field level observations and may help in calibrating the sorption models to predict real system transport behaviour.

Focus of the studies in this thesis

- Understanding the sorption mechanism of Cs(I) and Tc(IV) on mineral oxides in presence of humic acid (HA) with an aim to explore the role of humic acid in determining the sorption behaviour of the ternary system of metal ion – HA – oxide surfaces.

- Investigation of Am(III) speciation on alumina-water interface under varying surface coverage. Emphasis is on spectroscopic identification of speciation at higher surface coverage and study the evolution of surface speciation under varying surface coverage.
- Role of oxides surface characteristics in governing Pu speciation on surface as well as solution, and
- Development of surface complexation model for Am sorption on smectite rich natural clay from granitic ground water.

1.7 Outline of the thesis

The thesis is composed of six chapters. This (chapter 1 Introduction) is the first chapter. Chapter 2 describes the experimental methods and techniques employed in the thesis work. The next three chapters details the studies carried out for the thesis work and the last chapter (chapter 6 Summary and Conclusions) summarizes the findings.

In chapter 3, the sorption mechanism of Cs(I) and Tc(VII, IV) on mineral oxides – silica, alumina, hematite – in presence of humic acid have been investigated using batch sorption experiment and surface complexation modelling. The study revealed the non additivity of the ternary system and emphasized the requirement of understanding humic acid sorption on mineral surfaces for modelling such systems. Interaction of metal ion with humic acid governs the sorption of Tc(IV) while presence of humic acid affects the sorptivity of Cs(I) even though Cs(I) interacts weakly with humic acid.

In chapter 4, role of surface reactivity in guiding sorption process was studied by Am(III) and Pu(IV) sorption on silica and alumina surfaces. The objective was to study surface reactivity due to surface charge, dissolution of solid sorbents, and structural difference. Batch sorption,

kinetics experiments and molecule level spectroscopic techniques – Time Resolved Fluorescence Spectroscopy and Extended X – ray Absorption Fine Structure Spectroscopy – were employed to reveal the change in surface speciation with the change of surface reactivity.

In chapter 5, Am(III) sorption on smectite rich natural clay from granitic ground water was studied and modelled using a surface complexation model. Study on model clay mixtures – montmorillonite and Kaolinite - helped in identifying the mineral surface governing sorption in the complex natural sorbent. Role of cations and anions present in groundwater was studied by investigating effect of their presence in individual experiments. Based on the informations obtained from these experiments, a ion exchange and surface complexation based sorption model was developed for Am(IIII) sorption on natural clay from simple electrolyte medium with varying pH and ionic strength. Finally, the model prediction was checked for Am(III) sorption on natural clay from granitic ground water.

Chapter 2

Experimental Methods and Techniques

2.1 Introduction

Mechanistic description of sorption process requires delineation of the chemical reactions occurring at the solid liquid interface. Various approaches to investigate the sorption mechanism span from determination of metal ion partitioning in different chemical conditions such as, varying ionic strength of the sorption medium, through semi-empirical (Langmuir and Freundlich isotherms) approaches, to modelling of sorption processes assuming probable surface chemical reactions, to application of molecular level spectroscopic techniques. While the partition coefficient infers some important information such as formation of outer/inner sphere complex formation (Hayes and Leckie, 1987), fitting of sorption data into isotherm equations cannot by itself provide information about the reaction involved (Sposito, 1984; Scheidegger and Sparks, 1996). Surface complexation model (SCM) has been most successful in revealing the sorption mechanism; though various variants of the SCMs have been found to fit the sorption data equally well (Westall and Hohl, 1980) making prediction of surface speciation model dependent. Molecular level spectroscopic techniques help in identifying the surface speciation and thus in fixing the exact mechanism operating at the interface. McBride pioneered the application of spectroscopic techniques in studying surface speciation of Cu(II) on iron oxide surface by electron paramagnetic resonance spectroscopy. These spectroscopic techniques are however fraught with the lower sensitivity in view of dilute samples of environmental origin. Solubility of actinides and fission products in natural ground water systems is very low (trace to ultra-trace level). Complete understanding of the sorption reactions thus invariably requires synergism of all the methods and the same methodology has been followed in the thesis. The present chapter gives a brief account of the methods and techniques used. Further details can be

found elsewhere (Dzombak and Morel, 1990; Stumm, 1996; Bunker, 2010) and are available in several reviews (Denecke, 2006; Edelstein, et al., 2006; Geipel, 2006; Simoni, 2007).

2.2 Batch Sorption Method

Batch sorption method is used to study the equilibrium distribution of radionuclides between the mineral surface and the aqueous phase under well defined experimental conditions of temperature, pH, ionic strength and solid/liquid ratio. Partitioning is expressed by the distribution coefficient, K_d, defined as:

$$K_d\ (ml/g) = \frac{C_S}{C_L} \qquad (2.1)$$

Where, C_s is the concentration of the metal ion per g of the solid and C_L is the concentration of the metal ion present per ml of the aqueous phase. As the radionuclides may have multiple speciation in the same pH condition, K_d basically represents the combined distribution of the all the species.

Considerable sorption data, especially for single mineral sorbents such as oxides, have been collected describing pH influence on sorption process. The pH sorption edge thus obtained represents percentage sorption of radionuclide on solid surface against pH. Percentage sorption is calculated by the formula given below.

$$\%\ \text{sorption} = \left(\frac{C_i - C_f}{C_i}\right) \times 100 \qquad (2.2)$$

Where, C_i is the concentration of the metal ion added to the sorption system and C_f is the concentration left over in the aqueous phase after the attainment of equilibrium.

2.2.1 Experimental details

Distribution experiments were carried out in 50 ml polypropylene tubes (Oak ridge Centrifuge tubes). The design of the experiments was as follows: Nanometer sized powder samples of mineral solids (oxides and clays) previously characterized for surface characteristics (surface area, mineral phase, surface charge, etc.) were suspended in aqueous phase containing simple electrolyte (NaCl, $NaClO_4$) in fixed solid to liquid ratio for 24 to 48 hours equilibration before metal ion addition. After the addition of the acidic solution of metal ion, pH of the suspension was adjusted over 2-10 by dropwise addition of dilute mineral acid ($HClO_4$) or base (NaOH) under constant stirring of the suspensions. The suspensions were left, in a shaker, for attainment of sorption equilibrium over a time period which was fixed based on the kinetic experiments. After the equilibration period, pH of the equilibrium was checked and suspensions were centrifuged at 16 000 rpm for 45 minutes to separate the two phases present in the suspension. 1 ml of the supernatant was aliquotted and assayed for the determination of metal ion concentration left in the supernatant after equilibration. In sorption systems, where the effect of humic acid presence was investigated, suspensions were first equilibrated with humic acid before metal ion addition. Both the humic acid and metal ion equilibration were carried out at the same pH.

2.2.2 Methods of assaying

As the fission products and actinides used are radioactive, radiometric methods (γ-Counting in NaI(Tl) detector and Liquid Scintillation Counting (LSE) for α-decaying isotope) (Friedlander et al., 1990) were used for assaying the metal ion left in the supernatant while UV-Visible

spectrophotometry (λ=254 nm) was used for assaying humic acid concentration (Stevenson, 1994). ^{137}Cs, $^{95,96}Tc$, ^{241}Am have suitable γ- energies 661, 204, 582, 778, 850, and 59.9 keV, respectively for assay by gamma counting, while ^{238}Pu was assayed by alpha counting in liquid scintillation counter.

2.2.3 Preparation of radiotracer at environmental concentration level

Early actinides and some of the fission products, such as, technetium exhibit multiple valencies and strong hydrolyzing tendency in their higher oxidation states. Solubility of radionuclides in neutral pH conditions is thus very low. To study the sorption of actinides and fission products at environmental concentration level, radioisotopes of lower half life/higher specific activity can be used. In the present thesis to study technetium speciation at picomolar

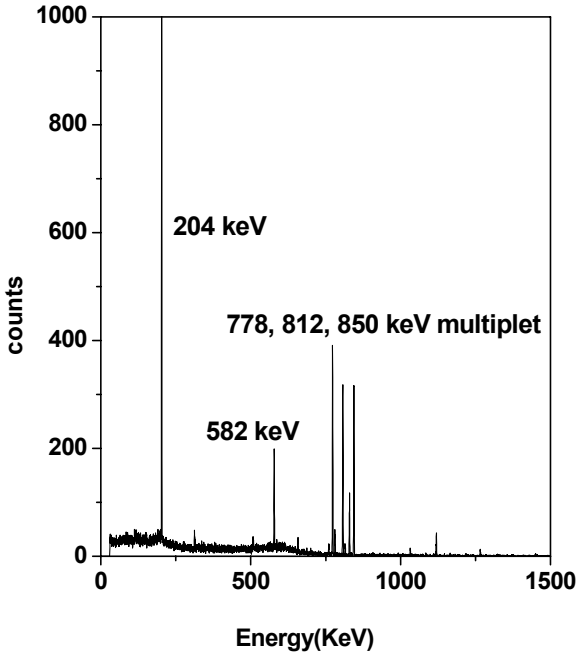

Figure 2.1 Gamma spectrum of $^{96, 95}Tc$ tracers

concentration, $^{95}Tc^{m}$ ($t_{1/2}$ = 60 days) was produced by nuclear reaction $^{96}Mo(p, 2n)^{95}Tc^{m}$. $^{95}Tc^{m}$ is

a γ (204, 582 keV) emitting isotope and does not require much of sample preparation as in liquid scintillation counting. Figure 2.1 shows the gamma spectrum of the ^{95,96}Tc tracer produced by proton induced reaction on natural molybdenum target and followed by radiochemical separation. Schematic of Tc separation from bulk Mo is given in figure 2.2.

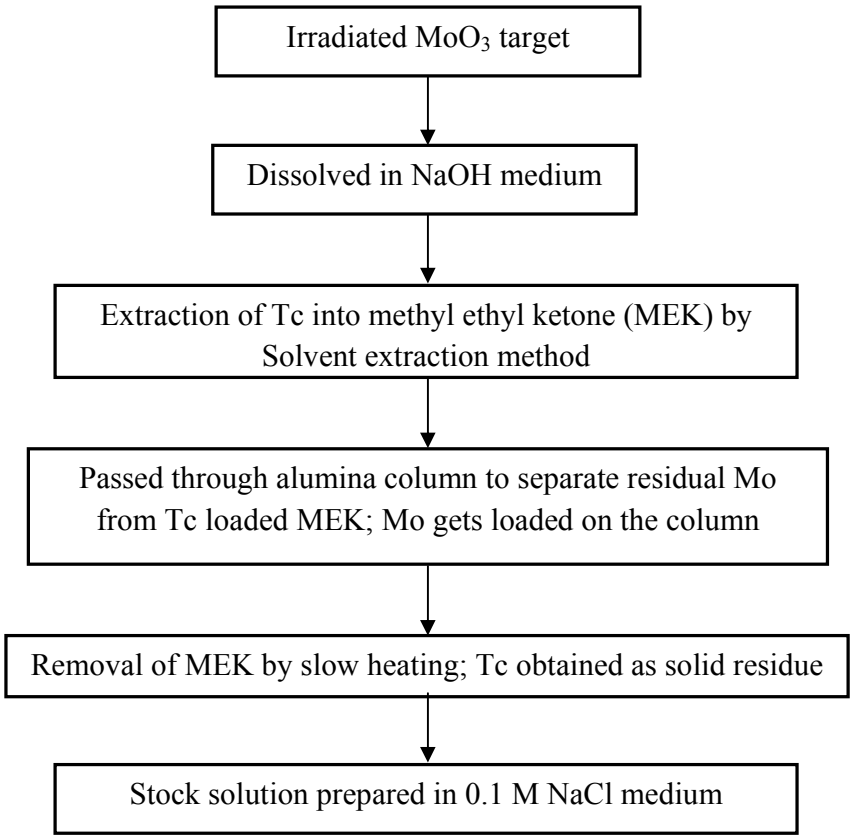

Figure 2.2 Separation scheme of Tc from irradiated Mo target

2.2.4 Error analysis of the sorption data

Owing to higher hydrolyzing tendency of actinides, during sorption they can sorb on the inner wall of the polypropylene container. Neglecting wall sorption in the estimation of the sorption data may result in large errors, especially if the wall sorption is significant. With the

container (polypropylene tubes) used in the present study, sorption on wall was very small (< 5%). Wall sorption was, nevertheless, quantified by leaching the sorbed metal ions with 1.0 M HNO_3. For this purpose, after the equilibrium sorption, the suspensions were removed from the tubes. The tubes were given gentle wash with distilled water, and then the leaching was carried out (overnight) with the same volume of the 1.0 M HNO_3 acid solution as that used in the sorption experiments. The activity leached into the solution was assayed for the radioactivity in a manner similar to the sorption experiment. The wall sorption was calculated as the ratio of activity per ml leached into the leachate to the initial activity per ml before sorption equilibrium.

Experimental uncertainties on the sorption data were determined by calculating the standard deviation of the sorption data obtained with duplicate sorption samples. When this method was not followed, error on the radioactive counting was propagated to calculate the error on sorption data. Program used to calculate the error on sorption data is listed in appendix 1.

2.3 Modelling approaches

Modelling approaches adopted to delineate the sorption mechanisms in the present thesis involve (1) Linear additive modelling (LAM), and (2) Surface complexation modelling (SCM). Linear additive models simulate the ternary system of radionuclides-humic substances (HS)-mineral surfaces in terms of binary interactions, radionuclides-HS, radionuclides-mineral surfaces, and HS-mineral surfaces assuming independence of one binary interaction of the other. On the other hand, SCM considers all possible chemical interactions of the sorption system in thermodynamic terms. Though LAM considers the gross behaviour of the systems and in this way neglects the true intricacies of the ternary system, comparison of the sorption behaviour

with that produced by LAM helps in characterizing the interactions in the ternary system due to the interactions among binary systems. These informations once incorporated into the SCM promise to make the prediction of sorption behaviour more robust.

2.3.1 Formulation for sorption behaviour in ternary system by LAM

Following Davies-Colley et al. (1984), distribution coefficient for a multiple sorbent mixture ($K_{d\text{-}tot}$) is assumed to equal the sorptive contributions of the individual phases:

$$K_{d\text{-}tot} = \sum K_{d,n} \chi_n \qquad (2.3)$$

where, $K_{d,n}$ is the distribution coefficient for the nth phase and χ_n is its mass or surface area fraction. Implicit in equation (2.3) are the following assumptions: (1) the sorbing phases exhibit linear isotherms over the concentration range of interest, and (2) the sorptive contributions of different phases are additive.

Zachara et al. (1994) modified equation (2.3) by incorporating the effect of desorption of HS and aqueous complexation using the following relationship:

$$K_{d\text{-}tot} = \sum K_{d,n} \chi_n \big/ [1+C_{HS} K_{d\text{-}HS}] \qquad (2.4)$$

where, C_{HS} is the aqueous concentration of HS (*g/l*) and $K_{d\text{-}HS}$ is the sorption coefficient of metal ions for dissolved HS.

In the ternary sorption system, mineral surface and the HS compete for the metal ion and therefore eq. (2.4) can be simplified to:

$$K_d = \frac{K_d^0 + K_{d\text{-}HS}\chi_{HS}}{1+C_{HS}K_{d\text{-}HS}} \quad (2.5)$$

where, $K_{d\text{-}HS}$ is the sorption coefficient of metal ions onto dissolved HS, and K_d and K_d^0 are the sorption coefficients of metal ions onto mineral surface in the presence and absence of HS, respectively. While formulating eq. (2.5) following assumptions were made: (1) the affinity of metal ions toward HS molecules is identical for both the mineral-bound and dissolved HS, and (2) the mass of mineral-bound HS is much smaller than the mass of solid sorbent, $\chi_{HS}/\chi_{SS} << 1$; χ_{HS} and χ_{SS} are the mass fractions of HS and solid sorbent in the HS coated sorbent.

The strength of the metal binding with HS can be expressed by an apparent stability constant, β, defined as,

$$M^{n+} + HS \rightarrow M\text{-}HS$$

$$\beta = \frac{[M\text{-}HS]}{[M^{n+}][HS]} \quad (2.6)$$

where, [HS] is the concentration of free HS ligands capable of binding with metal ions, and is almost constant and equal to the total concentration of HS ligands in view of the very low concentration of metal ions generally used in the experiment. The molar concentration of HS is operationally defined as the concentration of carboxylic groups of HS (equivalent per liter). $K_{d\text{-}HS}$ is related to β by the equation,

$$K_{d\text{-}HS} = \beta \times [HA] \times \frac{V}{W_{HS}} \quad (2.7)$$

In eq. (2.7) [HA] is the total (mineral-bound + dissolved) concentration of HS in suspension, and W_{HS} is the total (mineral-bound + dissolved) mass of HS in the suspension of volume, V. χ_{HS} and C_{HS} can be represented by,

$$\chi_{HS} = f_{HS} \times \frac{W_{HS}}{W} \tag{2.8}$$

and $$C_{HS} = (1-f_{HS}) \times \frac{W_{HS}}{V} \tag{2.9}$$

where W represents the mass of solid sorbent in the suspension. f_{HS} is the fraction of HS sorbed on the solid sorbent. Substituting eqs. (2.7-2.9) in eq. (2.5) yields

$$K_d = \frac{K_d^0 + (V/W) f_{HS} \beta [HS]}{1+(1-f_{HS}) \beta [HS]} \tag{2.10}$$

which should represent the sorption behaviour in the ternary system.

2.3.2 Surface complexation model

Surface complexation model (SCM) follows a thermodynamic approach (Schindler, 1981; Sposito, 1984; Schindler and Stumm, 1987) to model the sorption reaction. It extends the ion-association concept of aquatic complexation to the sorption process. Dzombak and Morel (1990) describe the basic postulates of SCM developed for oxides as:

- Sorption on oxide surfaces takes place at specific coordination sites. Such sites are produced by the dissociative chemisorption of water molecules on dangling oxygen atoms present on the surface, such as ≡SiOH on silica surface. These sites are amphoteric in nature and undergo protonation /deprotonation depending on the pH of the suspension, viz.,

$$\equiv SiOH_2^+ \underset{-H^+}{\overset{K_1}{\rightleftharpoons}} SiOH \underset{-H^+}{\overset{K_2}{\rightleftharpoons}} SiO^- \qquad (2.11)$$

- Sorption reactions on oxide surfaces can be described quantitatively via mass law equations. A typical sorption reaction on an oxide surface can be expressed as:

$$\equiv SiOH + M^{n+} \overset{K}{\rightleftharpoons} SiOM^{(n-1)+} + H^+ \qquad (2.12)$$

$$\text{where, } K = \frac{[\equiv SiOM^{(n-1)+}][H^+]}{[\equiv SiOH][M^{n+}]}$$

The activity coefficients of the surface species have been taken as unity.

- Surface charge results from the sorption reactions themselves. Protonation/deprotonation and metal ion binding on the surface sites creates the charge on the surface.
- The effect of surface charge on sorption can be taken into account by applying a correction factor derived from the electrical double layer (EDL) theory to mass law constants for surface reactions. Depending upon the description of the charge distribution in the EDL, different variants of SCM have been proposed (Hayes et al. 1991). A typical expression for surface complexation constant containing the correction factor (exponential term) is given as:

$$K = \frac{[\equiv SiOM^{(n-1)+}][H^+]}{[\equiv SiOH][M^{n+}]} \exp(-\Delta zF\Psi/RT) \qquad (2.13)$$

where, ΔZ is the difference of surface charge produced on surface complexation. F and Ψ are the Faraday constant and surface potential respectively. R and T represent the gas

constant and temperature respectively. Expression of surface potential varies as per the EDL model employed.

Apart from these pH dependent sites, there is another type of surface site on clay surfaces. Clay minerals contain, structurally, silicon and aluminium oxides layers packed together by weak van der Walls interactions. Isomorphous substitution in these oxide layers produces residual charge on the clay surface. These charged sites participate in ion exchange reactions with the sorbing metal ions. SCM developed for clay surfaces should include therefore ion exchange and surface complexation reactions in modelling sorption reactions.

2.3.3 Simulation of sorption behaviour using SCM

FITEQL Software ver. 4.0 (Herbelin and Westall) was used to obtain the formation constant (logK) of the surface species. Formation constant was subsequently used to simulate the sorption behavior. FITEQL considers sorption by a multi-component chemical equilibrium model and operates by formulating the sorption model in a matrix or tableau format (Morel and Morgan, 1971; Morel, 1983; Dozambak and Morel, 1990, appendix B). In this format, every chemical entity is considered as a species in the sorption system, which can be written as the product of a reaction involving only the components. Components are entities which cannot be expressed as the product of an algebric reaction involving only the other components. The components can, thus, be described as a linearly independent basis set spanning species space. Mass action equations are applied for each species while mass balance is taken into consideration for each component. Surface charge is accounted for by the Coulombic exponential term and is factored as a component in the tableau. Finally all the information is expressed in the form of a set of simultaneous equations. Next the equilibrium model is solved at each of the experimental data to

minimize the difference between values calculated from the model and values observed experimentally. This gives the optimized logK values. Details of running the optimization procedure and the best fit values can be found in the manual of FITEQL and chapter 3 of Dzombak and Morel (1990). Appendix 2 gives the FITEQL table produced while simulating Tc(IV) sorption on alumina in presence of humic acid.

2.4 Fluorescence Spectroscopy

Following excitation, the excited electronic state of a metal ion may come to the ground state by radiative decay process. Fluorescence spectroscopy uses this decay mode to determine metal ions speciation in its characteristic coordination environment. Three advantages associated with this spectroscopy make it important in this regard. These are characteristic excitation wavelength, characteristic emission wavelength (figure 2.3), and characteristic fluorescence

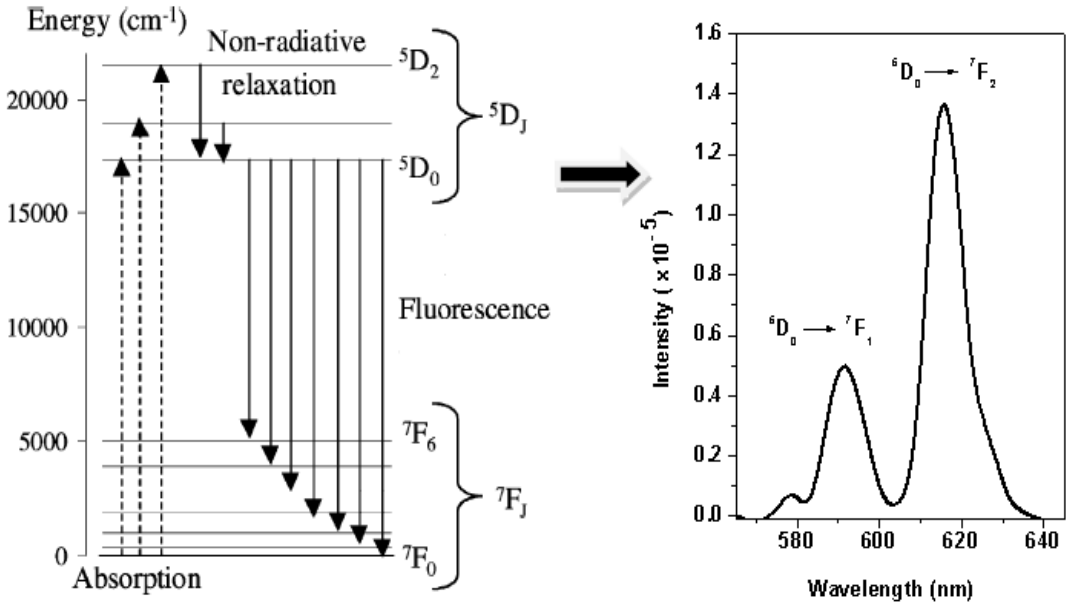

Figure 2.3 Energy- level diagram and characteristic fluorescence spectrum of Eu^{3+}

decay lifetime. The first two characterize the fluorescent probe by representing the energy levels and crystal field splitting of the species while the change in fluorescence lifetime reflects the effect of chemical reactions (such as hydrolysis, complexation, etc.) involving the probe atom. These advantages have been successfully employed to infer about the sorption mechanism.

2.4.1 Fluorescence measurement using chemical analogues

All the metal ions do not fluoresce significantly; actinides are generally less fluorescing than their lanthanide counterparts. Larger spatial expansion of 5*f* orbital and larger spin-orbital coupling in actinides causes smaller crystal field splitting leading to stronger non-radiative decay mode. In the fluorescence spectroscopic measurements reported in the present thesis, Eu(III) has been used to simulate the behaviour of Am(III). Choice of europium depends on its being the good fluorescent probe and chemical analogue of americium.

2.4.2 Instrumentation

Time resolved fluorescence spectroscopy (TRFS) measurements were carried out using Edinburgh F-900 time resolved fluorescence spectrometer consisting of CD-920 controller unit, a micro-second Xe flash lamp as excitation source and an optical multichannel analyzer coupled with M-300 excitation and emission monochromators. The data analysis was carried out using GEM-3 software supplied by M/s Edinburgh Instruments, UK.

2.4.3 Sample preparation and Data analysis

For fluorescence measurements, concentration of Eu(III) in alumina suspension (3 g/l) was fixed at 5.0×10^{-5} M. Sample preparation method was similar to batch sorption experiment. After equilibration, the solid phase was mounted onto quartz plate for spectroscopic measurement.

Excitation wavelength was fixed at 230 nm and fluorescence emission was collected over 550 - 650 nm wavelength range. For recording the lifetime data, the emission wavelength was fixed at 620 nm. The temporal decay data were accumulated up to 4 milliseconds. Fluorescence intensity *I(λ, t)* at wavelength λ and time t can be described as,

$$I(\lambda,t) = \sum_{j=1}^{n} I_j(\lambda,0) \times \exp(-t/\tau_j) \qquad (2.14)$$

where, $I_j(\lambda, 0)$ is the fluorescence intensity of the fluorescing species *j* at time = 0 and τ_j is its lifetime. The factor $I_j(\lambda, 0)$ is a function of experimental set-up (optical path length *l*, excitation source intensity I_0, etc.), molar absorption coefficient and the fluorescence quantum yield of the species *j,* and its concentration in sample. The life time of the surface complexes was obtained by fitting the temporal data into the above equation.

2.5 X-ray Absorption Fine Structure Spectroscopy

This spectroscopy covers both Extended X-ray Absorption Fine Structure Spectroscopy (EXAFS) and X-ray Absorption Near Edge Spectroscopy (XANES), which have their origin in quantum interference effects. When X-ray of suitable energy impinges on a probe atom, electrons are produced in photoelectric absorption process. The outgoing electrons collide with the surrounding atoms and get scattered. Interference between the outgoing and scattered electron waves modulates the absorption coefficient, resulting in an oscillatory pattern above the absorption edge. The spectral region upto ~30 eV above absorption edge is defined for XANES while that beyond this limit is used for EXAFS data. Figure 2.4 depicts a typical spectrum obtained in the XAFS experiment. XANES can be used to determine the valence state and

coordination geometry, while EXAFS is used to determine the local molecular structure of a particular element within a sample. Details on XAFS can be found in standard texts, viz., Koningsberger and Prins (1988) and Bunker (2010). Sample preparation, data collection and analysis suitable for environmental samples have been discussed in details in monographs such as Kelly et al. (2008). A brief description of these aspects as applied in the present thesis work is given below.

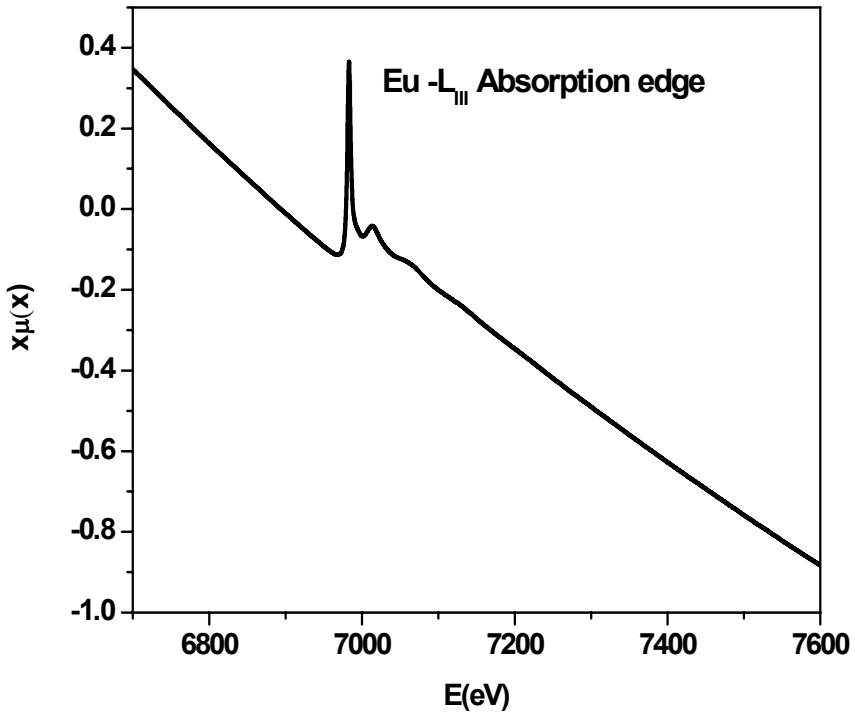

Figure 2.4 A typical XAFS spectrum

2.5.2 Sample preparation and Data acquisition

The initial part of the XAFS sample preparation was similar to the sorption experiment, with the only exception of a larger (250 ml) suspension volume for the XAFS samples. After filtering the suspensions, the solid phase was vacuum dried in an oven at temperature below 40 ^{0}C. A

calculated amount (to get edge step ~ 1 in the Eu–L_{III} X-ray absorption spectrum) of the dried powder was mixed with polyvinyl pyrolidone and pelletized. Homogeneous mixing of binder and the solid powder in the pellet was ensured by thorough mixing and optical examination.

XAFS data were collected using the XAFS beamline at Elettra synchrotron facility. Storage ring was operating at electron energy equal to 2.0 GeV and beam current about 300 mA which decreased with a half life of 35 hours. XAFS spectra were recorded in transmission mode by placing the pellet in the path of the X-ray beam from the Synchrotron. Measurements were carried out with three ionization chambers, one each for initial X-ray intensity (I_0), intensity (I) after transmission through the sample and intensity (I_m) after the monitor foil (Fe) placed downstream of the second ionization chamber for simultaneous energy calibration. Harmonics of the beam were rejected by detuning the second monochromator crystal by 45%. Following Eu–L_{III} edge energy (6977 eV), the spectra were collected over energy range 6700– 7600 eV, with a pre-edge energy step of 5 eV, 0.20 eV in the edge region and thereafter a constant 'k' step of 0.03 $Å^{-1}$ in the extended XAFS region. Data acquisition was limited to 7600 eV as the Eu–L_{II} edge lies just above this energy.

2.5.3 Data analysis

The Eu (L_{III}) edge X-ray absorption spectra of the reference compounds and the samples were analyzed by the software package IFEFFIT. Philosophy of the analysis has been as follows: Determination of structural parameters (co-ordination numbers and distance of surrounding atoms around the probe atom) of a species by EXAFS basically involves the modelling of experimental data. A hypothetical model most suitable for the species to be characterized is proposed and a convergence between experimental data and the data generated for the hypothetical model is searched out. Data analysis is started with the data reduction step in

ATHENA software, where the plot of μx vs. E is corrected for background absorption and normalized for single absorption event. Next the modified plot is brought to momentum (k) space and subsequently Fourier transformed to radial (R) space. For the hypothetical structure, phase-shift and amplitude functions are generated by the theoretical multiple scattering calculations in FEFF program. These calculated functions with associated informations for the model in EXAFS equation (eq. 15) create k and R space data, viz.,

$$\chi(k) = S_0^2 \sum_{i=1}^{n} \frac{N_i}{R_i^2} \frac{F_i(k,R)}{k} e^{-2R_i/\lambda} e^{-2\sigma_i^2 k^2} \sin(2kR_i + \psi) \qquad (2.15)$$

where, χ(k) is the measured EXAFS spectrum, and k is the electron momentum. N_i is the number of surrounding atoms in the i^{th} coordination sphere, R_i is the average radial distance to the i^{th} coordination sphere, and σ^2 is the Debye Waller factor. $F_i(k,R)$, S_0^2, λ, and ψ stand for backscattering amplitude, amplitude reduction factor, mean free path, and phase shift. Optimization of the calculated k or R space data to match the experimental data using non-linear least square fitting program is carried out in Artemis software. Hypothetical structures for the analysis of sorption samples have been based on the structure of oxide, hydroxide and silicate compound of Eu(III).

Chapter 3

Sorption of fission products on mineral oxides: Effect of humic acid

3.1 Introduction

Humic substances (HS) are important reactive fraction of natural organic matter present in soil, sediment, surface water and groundwater. They are polydisperse and heterogeneous mixture of organic molecules, and are formed as a result of the degradation of remains of the dead plants and animals (Stevenson, 1982). Presence of HS in the geosphere is dependent on many factors such as climate, pH, substrate material, topography and time (Stevenson, 1994). In soil, the humic content varies from 0 to 10% with still higher proportion in peat soil, while in water the dissolved organic carbon (DOC), may be as large as 50 ppm in dark water swamps. Samples from surface waters generally have DOC values from 0.1 to 8 ppm. In ocean waters, the DOC ranges from 0.5 to 1.2 ppm. In addition, organic matter is present in suspended sediments in lakes, rivers, estuaries and coastal seawaters. Majority of the DOC as well as the particulate and sorbed organic matter falls within the classification of HS (Choppin, 1988).

HS are divided into three groups based on their solubility in acid-base solutions; (i) fraction insoluble in aqueous medium is called Humin, (ii) the fraction soluble at all pH in water is known as the fulvic acid (FA) and (iii) the fraction soluble only above pH 3.5 in water is called humic acid (HA). A typical separation scheme is shown in figure 3.1. Specific details of HS separation from soil and water can be found in Tipping (2002). To a large extent, the procedures depend upon controlling the electrical charge of the humic matter. Higher the charge of the molecules, (e.g., at high pH), higher the solubility. Lower charge e.g., at low pH, promotes precipitation and adsorption to hydrophobic surfaces.

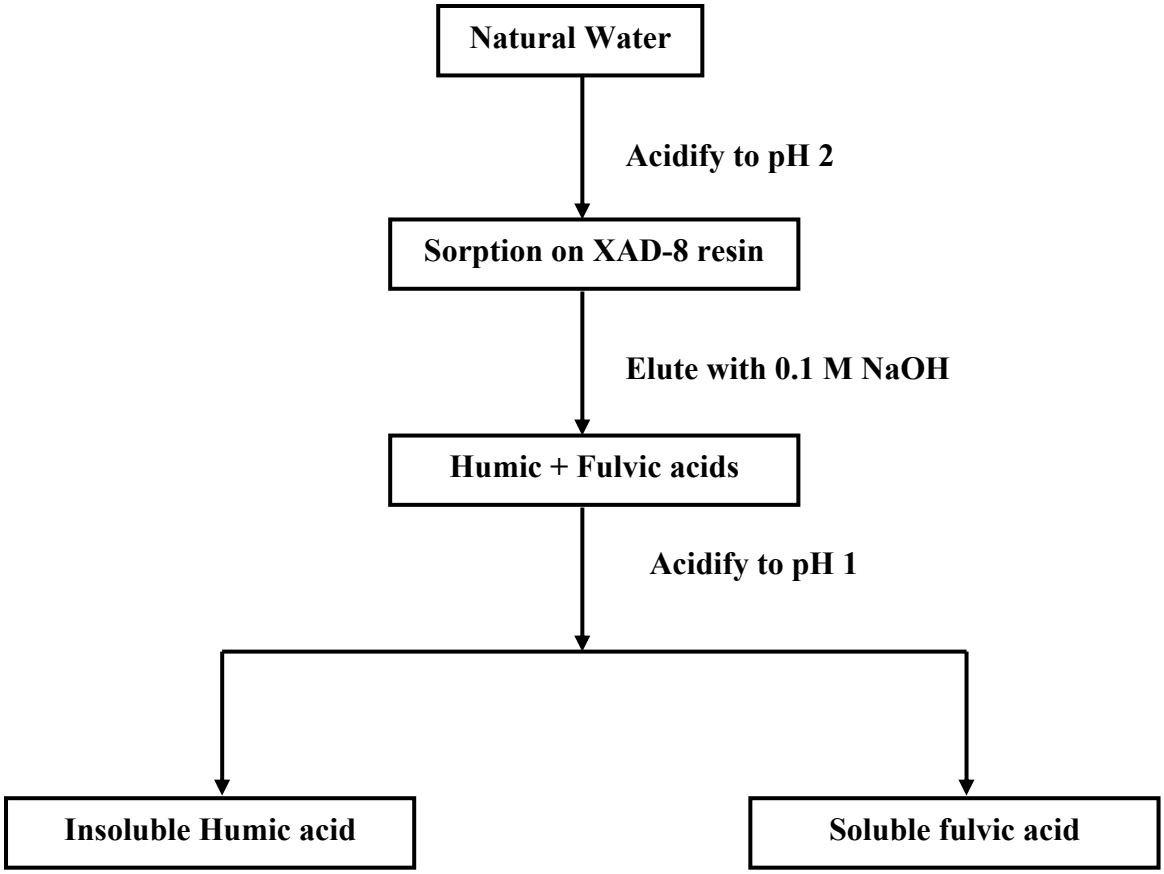

Figure 3.1 Separation scheme for humin, humic and fulvic acids

Unlike the simple organic complexants, the physicochemical properties of HA and FA are hard to define as the true nature of HS structures is still ill-defined despite many decades of research (Hayes et al., 1989). Origin, climatic conditions, pH, mineral surfaces and time cause variable degree of degradation of HS leading to the variable structure. Early concept (polymer model) envisaged humic substances as randomly extended macromolecules that had elongated shapes in basic or low ionic strength solutions, and coiled in acidic or high ionic strength media (Swift, 1999). Later informations gathered using spectroscopic, microscopic, pyrolysis, and soft ionization techniques gave a toss to the "polymer model" and a new concept of humic substances emerged, that of the supramolecular association, in which many relatively small and chemically diverse organic molecules form clusters linked by hydrogen bonds and hydrophobic interactions (Piccolo, 1999). Emphasizing molecular interactions

over molecular components has been the essence of the newer understanding of humic substance structure (Sutton et al. 2005). Amidst these structural ambiguities, distinguishing characteristics of humic and fulvic acids have been delineated. Fulvic acids are more aliphatic and less aromatic than humic acid and have lower molecular weight, 300 – 2000 amu, compared to 1000 to 5000 amu typical for aquatic humic acid. Main functional groups of humic and fulvic structures are carboxylic and phenolic groups along with minor presence of nitrogen based functional groups like amine, amide, etc. A hypothetical structure proposed for humic acid is shown in figure 3.2 (Stevenson, 1982).

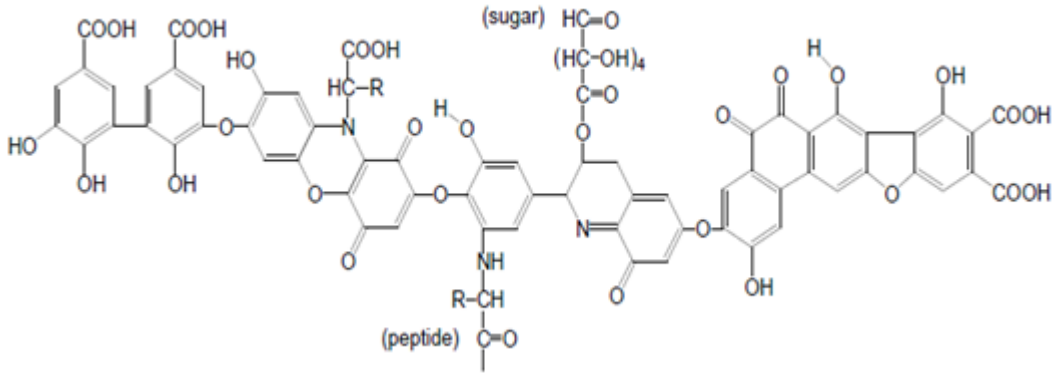

Figure 3.2 A hypothetical structure of humic acid

Humic substances exhibit strong complexing affinity towards metal ions and significantly alter the metal ion speciation with their presence (Tipping and Hurley, 1992). They may also interact with mineral surfaces and thereby affect the sorption and migration of radionuclides in environment (Ticknor et al., 1996; Choppin, G., 1992; Maes, et al., 2006; Reiller, 2002). In an extensive evaluation of sorption of trace metals on natural sediments, Wang et al. (1997) concluded a correlation between sorption and hydrolysis of metal ions (termed as Linear Free Energy Relation) dependent on the proportion of total organic carbon and the mineral oxide component in the sorbent. Distribution coefficient (K_d) of Am(III) and Pu(IV) on Zeolitized tuff samples collected from the Rainier Mesa tunnel system, Nevada Test Site, were upto two

orders of magnitude lower in water with high DOM (15-19 mg C/L) compared to the same water with DOM removed (< 0.4 mg C/L) or in naturally low DOM (0.2 mg C/L) groundwater (Zhao et al. 2011). It is, therefore, pertinent that speciation and sorption of metal ion in presence of mineral surfaces and HS should be understood mechanistically and parameterized for predictive modelling.

Interactions in ternary systems of metal ions - mineral surfaces - HS, are governed by metal ion interactions with mineral surfaces and humic substances, both dissolved and sorbed on mineral surface (figure 1.2). Formation of "ternary complexes" may result from interaction between any two binary systems namely, metal ions-HS, metal ion-mineral surface, and HS-mineral surface. There are generally two types of ternary complexes. In type 1, the humic molecule acts as the bridge between metal ion and mineral surface, whilst in type 2, the metal ion acts as the bridge. Interplay of these interactions results in variable sorption characteristics (Fairhurst et al., 1995). Dominance of different interaction modes has further been seen by changing the addition order of components in the ternary systems (Kar et al. 2011; Reiller, 2005). Existence of different ternary complexes has also been shown in spectroscopic results (Alacacio et al., 2001, Siato et al., 2005). Description of ternary systems in terms of these interactions is, however, simplistic as intrinsic characteristics of humic substances – polyelectrolyte material, heterogeneous mixture of organic molecules which undergo fractionation on sorption (Meier et al. 1999), electrostatic aspects – need to be considered in the framework of these interactions. In spite of functional groups similarity, differences observed in the effect of humic and fulvic acids on meal ion sorption have been attributed to their intrinsic characteristics. Fulvic acid having smaller molar mass behaves like simple inorganic ligand and is present near the surface layer during sorption on mineral surface whereas humic acid with higher molar mass/size extends away from the sorbent surface into diffuse layer around the mineral surface.

Metal ions interaction with humic substances

Metal ion interaction with humic and fulvic acid needs to deal with three aspects: site-specific binding, electrostatics and heterogeneity of the HS. Different predictive models have been developed ranging from conceptually simpler models (e.g., Mixture model, Triprotic acid model, Tipping, 2002), to operationally simpler models (e.g., Charge Neutralisation model, Kim and Czerwinski, 1996)), to computationally involved models where all the three aspects have been included to reproduce the interaction behaviour (Model VI and NICA models, Tipping, 1998; Milne et al. 2003). The Model VI simulates the chemical heterogeneity with a finite number of discrete binding sites and the NICA model uses a continuous distribution approach. These two models have been successful specially in predicting metal ion binding to humic and fulvic acid largely independent of source and improved the understanding of mechanisms, such as denticity or coordination number in metal ion-humic acid complex.

Sorption of Humic substances onto mineral surfaces

Sorption of HS on surfaces such as Mn, Fe, Al oxides and clays has been studied using batch experiments. A number of mechanisms have been suggested for the binding of HS to inorganic surfaces (Lenhart and Honeyman, 1999): ligand exchange; cation/anion exchange; cation bridging; entropy driven physical sorption; hydrogen bonding and van der Waals / hydrophobic interactions. Chemical fractionation of HS has also been reported by several authors. Wang and Xing (2005) observed that the aliphatic fractions were preferentially adsorbed onto a kaolinite surface, while Feng et al. (2006) found that the aromatic components of a terrestrial humic acid are preferentially adsorbed onto montmorillonite. Varying fluorescence spectra of Eu(III) complexes in sorption of HS onto α-Al_2O_3 has been attributed to fractionation (Claret et al. 2005, 2008).

Metal ion interaction with mineral surfaces in presence of HS

Metal ion sorption on mineral surfaces in presence of humic substances is more than that expected based on the binary interactions (Bryan et al., 2012). This is so because binary interactions modify the response of the minerals surface and the humic acid towards metal ion.

Linear additive modelling (LAM) has been used to reveal interactions in ternary sorption systems. Here, the behaviour of the ternary systems is simulated just with the separate binary models. This has not been always successful. Bruggeman et al. (2010) found that sorption of Eu(III) in an illite/humic acid ternary system could be modelled by an additive approach using Tipping Model VI to simulate Eu(III)-humic acid interaction and a non electrostatic surface complexation model for the metal ion-mineral surface interaction. Interestingly in this study the humic substance was not interacting with the mineral surface. In sorption systems where the HS sorbs on mineral surface, there is also contrasting behaviour. Cd(II) sorption to humic acid-hematite systems was found to be more than the sum of the Cd(II) adsorptivites to individual component (Vermeer et al., 1999) with the difference increasing with the pH. Interaction of Ca(II) and fulvic acid at the goethite-water interface resulted in reduced sorption at lower pH values and enhanced adsorption pH at high pH (Weng et al. 2005). Warwick et al. (2006) studied the ternary systems of Cs(I), Cd(II), Ni(II) and Eu(III) with goethite, montmorillonite and kaolinite in presence of HS and successfully explained the data with the LAM approach. For modelling humic substances and metal ion speciation in ternary systems at equilibrium, the Ligand charge distribution (LCD) has been developed by van Riemsdijk et al (2006). It has also been used to simulate the ternary sorption systems. For example, in the case of Ca/goethtite/fulvic acid ternary system, where the LAM does not work, the LCD was able to simulate the behaviour taking into account ternary complexes

(Weng et al. 2005). Interestingly, the model predicted that the main interaction between Ca(II) and sorbed fulvic acid is electrostatic, and virtually all the sorbed Ca(II) is bound directly to the surface.

Literature Studies on fission products sorption in presence of HS

Though extensive studies have been performed for the effect of HA on the sorption of actinides and europium on oxides surface, there are very few studies devoted to investigate such effect in the sorption of fission products. This could be due to the relatively short life of fission products and /or their chemistry. For example, the mono and divalent metal ions are weakly interacting with HS while a longer half life fission product such as technetium is anionic. A few studies have been carried out on sorption of ^{137}Cs on clays, such as montmorillonite (Dumat et al., 2000) where HA was found to decrease the sorption of Cs on the clay at pH 7. In another work on sorption of ^{137}Cs by silica gel, no effect of HA was observed (Hakem, et al., 2004). In oxic conditions and under neutral pH conditions, Tc exists as TcO_4^- and interacts very weakly with mineral surfaces and HS (figure 3.3) (Kumar et al. 2007, 2011). Tc(VII) may, however, be reduced to Tc(IV) under reducing condition and by

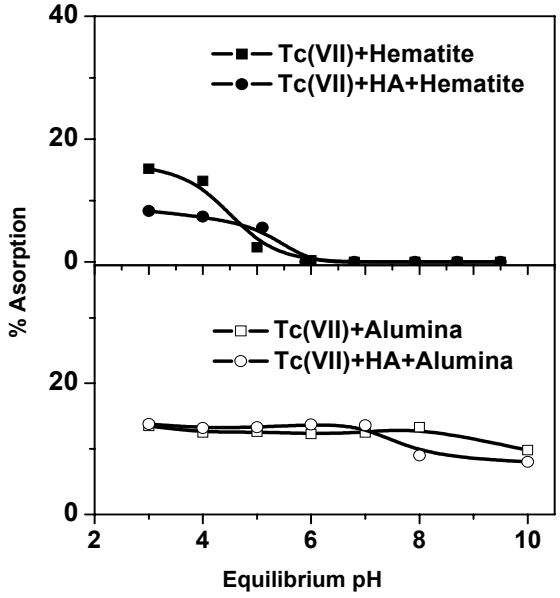

Figure 3.3 Effect of humic acid on Tc(VII) sorption on hematite and alumina

reductants like Fe(II) and Mn(II) present on various solid sorbent, thereby enhancing its interaction with HS. Maes et. al (2003) observed Tc(IV) associated with HS enhancing solubility up to the order of 2×10^{-6} M. Evidence for the aggregation of Tc(IV) colloids with humic substances has been obtained in EXAFS and XANES studies (Maes et al., 2004; Geraedts et al. 2002). Artinger et al. (2003) carried out extensive studies on humic colloid mediated transport of Tc(IV) in Gorleben ground water and found the presence of humic substances enhancing the transport rate of Tc(IV). Tc(IV)-humic complexes have been suggested to be the dominant chemical species in deep groundwater containing humic substances, and the complexation reaction may control the mobility and fate of Tc under reducing environments (Sekine et al. 1997). While Cs(I) interacts with mineral surface and HS weakly, Tc(IV) interacts with both of them strongly. It is therefore important to study the effect of HS in their sorption on mineral surface.

Present Study

In the present work, the role of humic acid on the sorption of Cs(I) and Tc(IV) on mineral oxides has been investigated. Mineral oxides chosen for the study are silica and alumina. Silica is an important naturally occurring mineral oxide, originating basically from various weathering actions on rock, clays and sediments. Though alumina does not exist in nature in its pure phase; it has been of research interest due to following reasons: (1) alumina is structurally similar to iron oxides, such as hematite, magnetite. Iron oxides are produced in aquatic system by the corrosion of iron/steel containers and have been found interacting significantly with environmental radioactivity; (2) Unlike iron oxides, they are amenable to spectroscopic techniques such as TRLFS.

Among the binary interactions, there exists stronger interaction between Cs and mineral surfaces while Tc(IV) interacts strongly with humic acid. Studies of the present chapter aim

to investigate the sorption of Cs(I) and Tc(IV) on oxide surfaces in presence of humic acid and thereby understand the role played by HA in deciding the sorption behaviour of ternary systems.

3.2 Experimental details

3.2.1 Characterization of mineral oxides

Nanometre sized silica and alumina powders were purchased from AEROSIL and Degussa India Ltd respectively, and were used without purification. X-ray diffraction based characterization showed that silica was amorphous in nature while alumina was present in its γ-phase. Both the sorbents were found free from any other structural phase impurities. Specific surface area and porosity of these solid particles were determined using N_2 gas based BET analysis. The surface area was found to be 180 and 203 m^2/g, for silica and alumina respectively. Pore volumes obtained in BET analysis are 0.269 and 0.067 cc/g for silica and alumina, respectively, indicating insignificant porosity. Zeta potential of the silica and alumina suspensions prepared by suspending particles in 0.01 M $NaClO_4$, was measured at varying pH values using a Malvern zetasizer (4.0 mw He-Ne laser at 633 nm). The instrument measures electrophoretic mobility of the particles using dynamic light scattering data and obtains the zeta potential by putting velocity data into Henry's equation (eq. 3.1).

$$U_E = \frac{2\ \varepsilon\ z\ f(K_a)}{3\ \eta} \tag{3.1}$$

where, U_E, ε, z, η stand for electrophoretic mobility, dielectric constant, zeta potential, viscosity and $f(K_a)$ is Henry's function. Its value is 1.5 under Smoluchowski approximation. The iso-electric points, that is, pH corresponding to zero potential, were found to be 2.4 and

8.9, for silica and alumina respectively, which are in agreement with the PZC (point of zero charge) values available in literature (Silva and Nitsche, 1995).

Site density (≡AlOH) and hydrolysis constants of sites present on alumina surface were determined by titrating alumina suspension (strength 7.5 g/l in 0.1 M $NaClO_4$) in N_2 environment with 0.1 M HCl and NaOH solutions and modeling the titration data using FITEQL V. 4.0 software. A constant time interval (2 min.) was provided between the consecutive titrant additions.

3.2.2 Humic acid characterization

Humic acid (HA) in the sodium form was procured from ACROS, Belgium, and was purified by repeatedly dissolving in alkali followed by precipitation in perchloric acid medium. Purified HA was characterized for elemental composition using CHNS-O (EA-1110) elemental Analyser, Radiochemistry Division, BARC and the values compare well with the literature reported values (Table 3.1) (Kim et al., 1990).

Table 3.1 Elemental composition of the purified humic acid

Element	% Obtained	Literature value (%)
C	48.82	50-60
H	4.415	4-6
N	0.82	2-6

The UV-Visible spectrum of humic acid (100 mg/l solution of humic acid in 0.05 N $NaClO_4$) was recorded using the JASCO V-530 UV/VIS spectrophotometer. The spectrum showed a featureless continuum without recognizable peaks. A slight hump at ~ 250 nm was, however, observed in the UV region. The ratio of absorbance at 465 and 665 nm (E4/E6), which is an indication of the humification or the condensation of aromatic humic constituents

(Kim et al., 1990), was found to be 5 and was comparable to that for Gorleben HA (Kim et al. 1990). The IR spectrum of humic acid in Nujol medium was obtained with Philips PU-9500 IR spectrophotometer. Prominent peaks in the 1600-1650 cm^{-1} wave number region characterize carboxylate group present in HA (figure 3.4). Fulvic acid shows a reduced absorption compared to humic acid in this region.

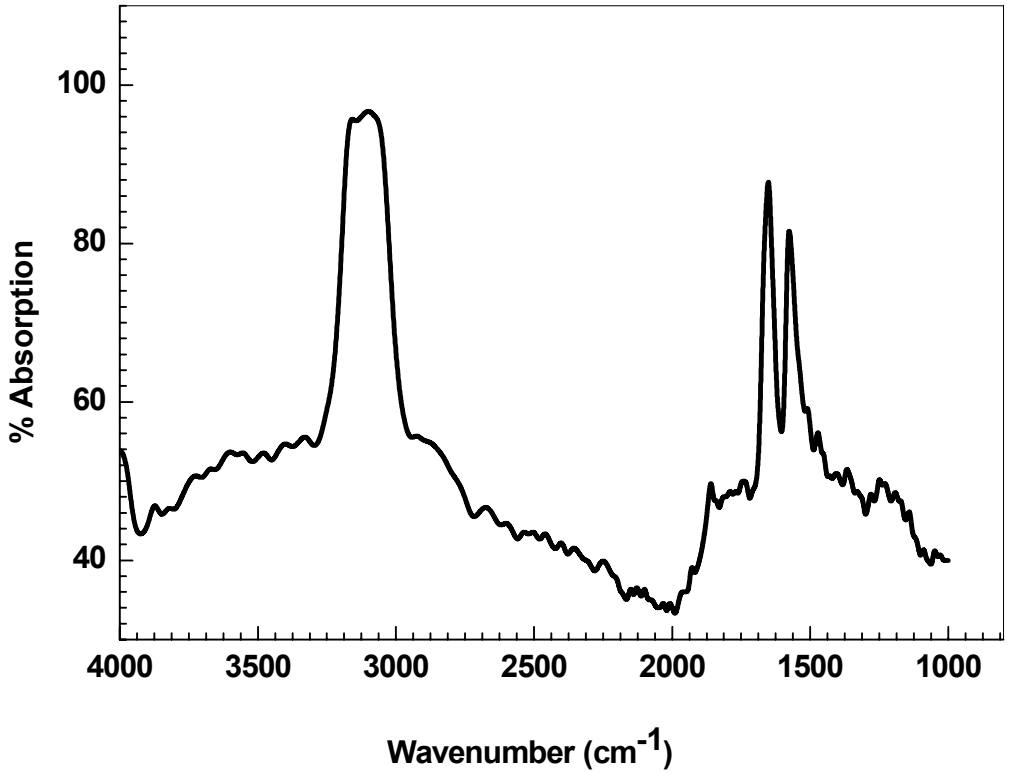

Figure 3.4 IR spectrum of humic acid

The proton exchange capacity (PEC) for HA was determined by potentiometric titration (4.6 ± 0.1 meq/g) and by the Baryta method (4.8 ± 0.1 meq/g) (Stevenson, 1994). Baryta method is based on the complete neutralization of HA with excess $Ba(OH)_2$, followed by titration of the unused base with a standard acid. pK_a values for HA functional groups were obtained in the framework of triprotic acid model (discrete 3-sites (HL_i; i=1-3) for proton affinity (Tipping, 2002) using potentiometric titration and modelling of the titration data in FITEQL. During this titration, pH of the HA solution (0.04 g HA in 0.1 M NaCl) was first

brought to 2.97 by adding 0.1 M HCl dropwise and then the titration was continued with the successive addition of 0.2 ml of the base (0.02 N NaOH + 0.08 M NaCl) up to nearly 10 ml.

3.2.3 Determination of stability constant of Cs(I)-HA

The average stability constant for Cs-HA system in 0.05 M $NaClO_4$ medium was determined using Schubert's ion exchange method (Lenhart et al. 2000). Schubert's method is based on measuring the distribution of metal ion between the solution phase and a cation exchange resin, in the presence and absence of a metal complexing ligand. If λ_0 and λ stand for the distribution ratio in absence and presence of humic acid, respectively, relationship between distribution ratios and ligand concentration as per the Schubert's method can be expressed by eq. 3.2.

$$\left(\frac{\lambda_0}{\lambda}-1\right)=\frac{\beta_{1,n}\left[L\right]^n}{\Pi} \qquad (3.2)$$

Where, $\beta_{1,n}$ stands for stability constant of mononuclear metal ion complex with *n* number of ligands. The term Π accounts for metal ion reactions with ligands present in the system other than HA, e.g., OH^-. Log $\beta_{1,n}$ can be determined from a plot of $\log\{(\lambda_0/\lambda)-1\}$ versus log [L]. The conditions necessary for the application of Schubert's method include, excess concentration of ligand over the metal ion concentration, so that that the Ligand concentration can be treated as constant even after some of it is complexed with the metal ion. Dowex-50W×8, a strong cation-exchange resin, was converted into the sodium form and used in the metal ion distribution experiment. HA concentration was varied in the range of 0-100 mg/l. pH of the experiments (4.0 and 6.5) was adjusted using sodium acetate-acetic acid buffer and dilute $HClO_4$/NaOH solutions. The ion exchange capacity (2.7 $\pm$ 0.1 meq/g) of the resin employed in the study was measured titrimetrically. The mass of the resin in each sample was fixed at 0.03 g. The equilibration time of 48 hr for the ion-exchange experiment was based on

the preliminary kinetic experiment. Control experiments were also conducted to determine the sorption of HA onto the resin.

3.2.4 Sorption experiments and Modelling exercises

Details of sorption experiments and the modelling protocol followed in the present work have been discussed in chapter 2. Specific details pertaining to this chapter are as follows. Both silica and alumina suspensions used in the experiment have solid to liquid ratio 5 g/l. During sorption 24 hrs was given for metal ion equilibration with mineral surfaces while 48 hrs equilibration was employed when HA was present in the sorption system. In ternary sorption system, HA was equilibrated with mineral surface before metal ion addition. To reduce Tc(VII) to Tc(IV), Sn(II) (10^{-6} M $SnCl_2$ in suspensions) was used in acidic condition and reduction was ensured by Tetraphenyl arsonium chloride (in chloroform) based solvent extraction procedure, wherein TcO_4^- gets extracted to organic phase while Tc(IV) species remain in aqueous phase.

Humic acid sorption on silica and alumina was separately studied over pH 3-10 in $NaClO_4$ medium (0.05 and 0.1 M, respectively). 2 mg/l HA was contacted with the suspensions at different pH for 48 hours. On equilibration, the suspensions were centrifuged and assayed using UV visible spectroscopy to measure HA sorption.

In surface complexation modelling, constant capacitance model (C = 1.2 F/m^2) was used for surface electrostatics. In order to determine the protonation / deprotonation constants and concentration of alumina surface sites (≡Al-OH), potentiometric titration of the alumina suspension (7.5 g/l) in 0.1 M $NaClO_4$ was carried out with the continuous addition of either 0.1 M HNO_3 or 0.1 M NaOH under N_2 gas environment. A constant time interval (2 min.) was provided between the consecutive titrant additions. Potentiometric data was modelled

using FITEQL and optimized protonation/deprotonation constants were kept constant during the modelling of the Tc(IV) sorption data.

3.3 Results and discussion

3.3.1 Acidity of silica and alumina surface sites

Figure 3.5 shows the zeta potential of silica and alumina suspensions in 0.01 M $NaClO_4$ medium. Silica becomes negatively charged above pH 2.3 while alumina is positively

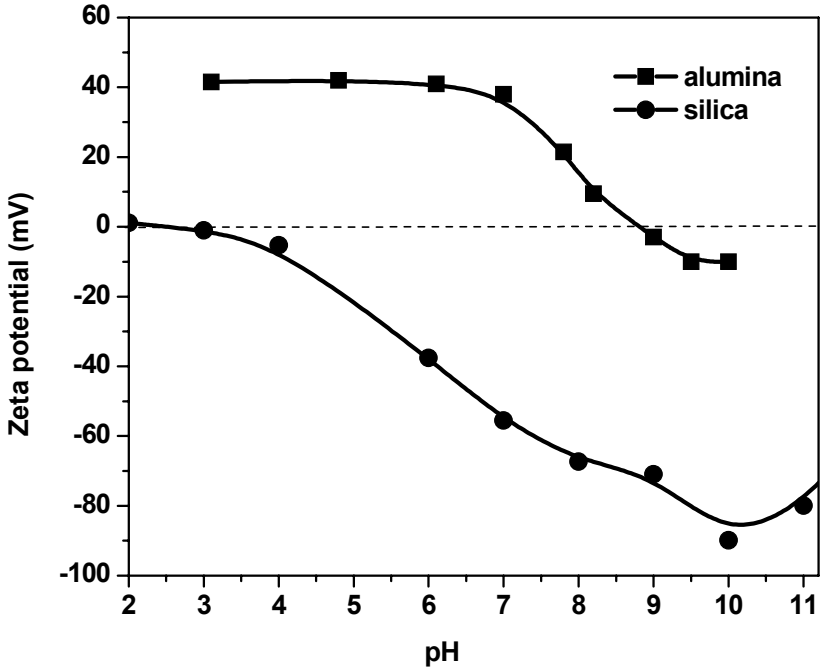

Figure 3.5 Zeta potential of silica and alumina suspensions over pH 3-10 in 0.01 M $NaClO_4$.

charged upto pH ~ 8.9. In absence of any specifically sorbing cation, SCM postulates the formation of surface charge as due to protonation/deprotonation reactions of the surface sites. Negatively charged silica surface thus can be attributed to the deprotonation reaction which in turn is promoted by the higher eletronegativity of Si atoms in comparison to Al atoms. Figure 3.6 shows the potentiometric titration data of γ- alumina with 0.1 M HCl and NaOH

along with its surface complexation modelling under 2-pK formalism for surface complexation and constant capacitance model for electrostatics. Modelling results of potentiometric data is shown in table 3.2. Comparing deprotonation constant of alumina with that of silica (log K = -7.60 ± 0.05; Marmier et al., 1999) higher isoelectric point for alumina (pH = 8.9) is obvious.

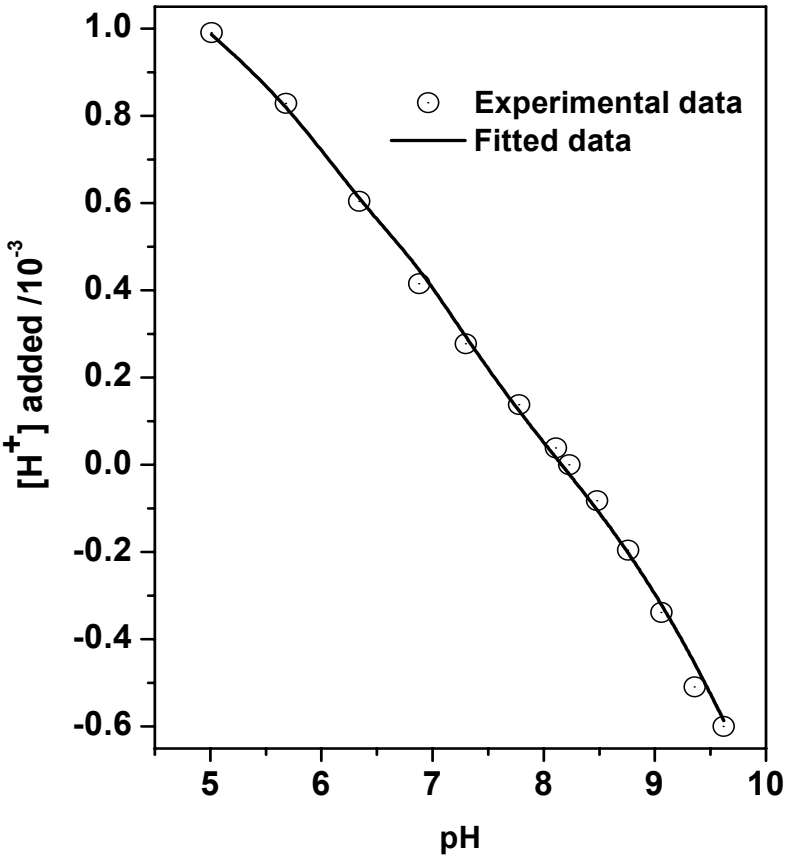

Figure 3.6 Potentiometric titration of alumina suspension. Solid line refers to surface complexation modelling of the titration data.

Table 3.2. Details of potentiometric titration of alumina suspension and SCM fitting

Log K ($\equiv AlOH + H^+ \leftrightarrow \equiv AlOH_2^+$)	7.2 $\pm$ 0.2
Log K ($\equiv AlOH - H^+ \leftrightarrow \equiv AlO^-$)	-9.1 $\pm$ 0.1
Alumina concentration	7.5 g/l
Ionic strength	0.1 M $NaClO_4$
Specific surface area	203 $\pm$ 5 m^2/g
Specific capacitance	1.2 F/m^2
Surface sites ($\equiv SOH$)	1.022×10^{-3} mol/l
WSOS/DF(weighted sum of squares per degree of freedom)	29.5

3.3.2 Proton affinity of HA functional groups

Potentiometric titration data of HA is shown in figure 3.7 (a). The curve exhibits characteristics typical of a polyelectrolyte where the continuous ionization of the functional

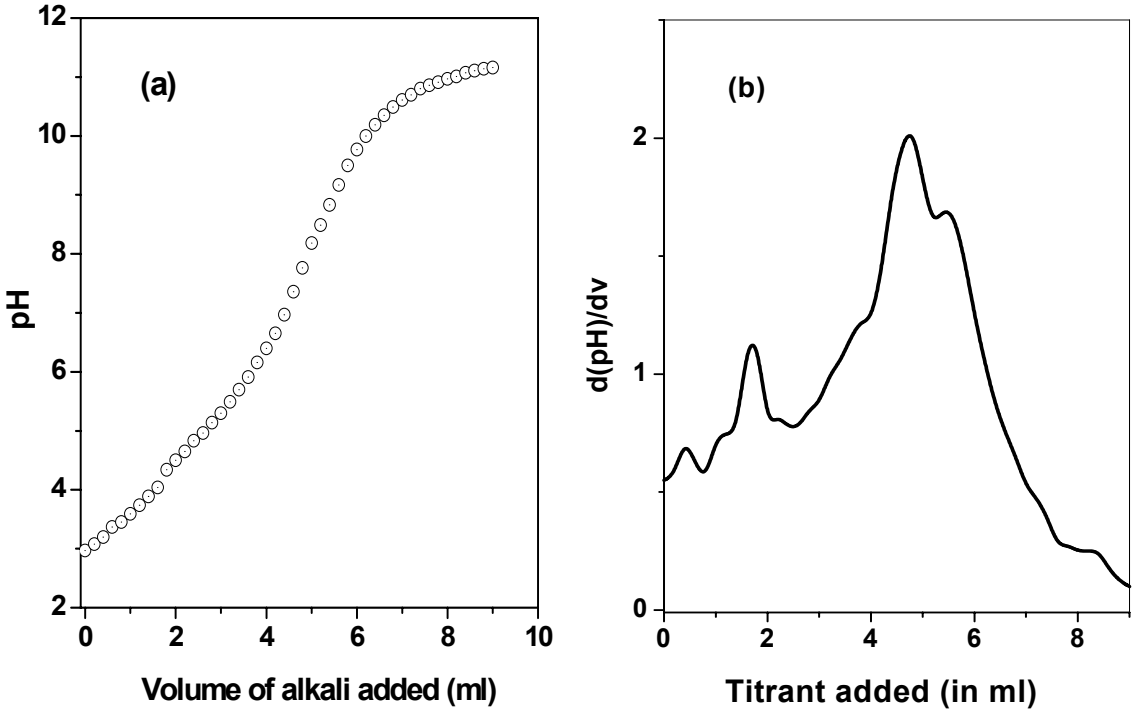

Figure 3.7 Potentiometric titration data of HA

groups creates the pattern devoid of any sharp transition. Derivative of this plot (figure 3.7 (b)) indicates two maxima attributed to the ionization of two broad groups of functional groups with nearly 2 and 5 ml of titrant (NaOH) addition. These peaks have been considered to be represented by carboxylic and phenolic groups, respectively.

Modelling of HA potentiometric titration data was, however, carried out using three discrete sites model (Triprotic model), corresponding to carboxylic, amine and phenolic groups. As the concentration of metal ion (Tc) involved in the study was very small compared to that of HA, only the higher affinity (carboxylic) sites are expected to participate in metal binding. Hence determination of the concentration and affinity constant of this type of site with greater precision was considered necessary and three sites model was adopted for the modelling of potentiometric data. Results of this exercise are listed in table 3.3.

Table 3.3 Modelling result of the humic acid titration data assuming discrete 3-sites model

Site	Concentration (M)	Log K	WSOS/DF
HL_1	5.107×10^{-4}	-3.602	
HL_2	3.715×10^{-4}	-5.885	7.39
HL_3	2.108×10^{-4}	-8.118	

3.3.3 Humic acid sorption on oxide surfaces

Sorption of humic acid on silica and alumina surfaces is shown is figure 3.8. The plot shows the typical behaviour of an anion sorbing on oxide surface; higher sorption percentage at lower pH values and decreasing sorption at increasing pH. However, there is difference in the absolute sorption percentage at these two surfaces; percentage sorption is higher for alumina than that for silica at lower pH values. This observation indicates the involvement of ligand exchange as the predominant reaction mechanism, as silica being negatively charged

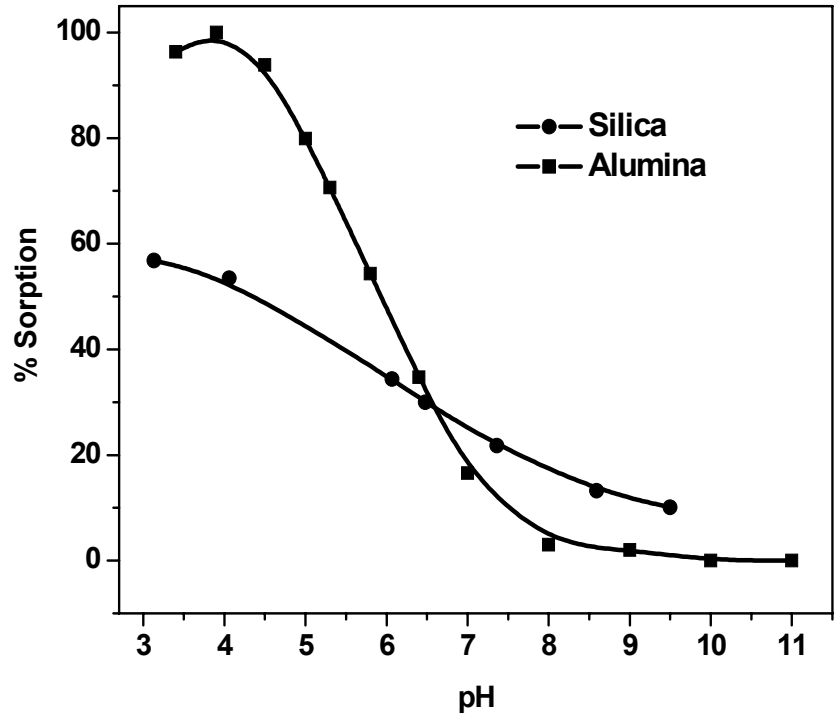

Figure 3.8 Humic acid sorption in silica and alumina

over the studied pH range should have shown negligible sorption of HA. This is further substantiated with the fact that humic acid sorption on silica surface does not change with increased ionic strength (i.e., 0.1 M) (figure 3.14). However, electrostatic factor can not be ruled out entirely as alumina with its positively charged surface sorbs higher proportion of humic acid compared to silica. Participation of other mechanisms such as hydrophobic binding, van der Waals interactions, etc., however, cannot be ruled out in defining the sorption behaviour.

Surface complexation modelling (figure 3.9) of humic acid sorption on alumina using 3-sites model for HA and 2-pK approach for surface complexation on alumina surface, could quantitatively explain the sorption profile reasonably. The optimized surface species (table 3.4) is an outer sphere complex of HA on alumina surface sites ($\equiv AlOH.HL_1$).

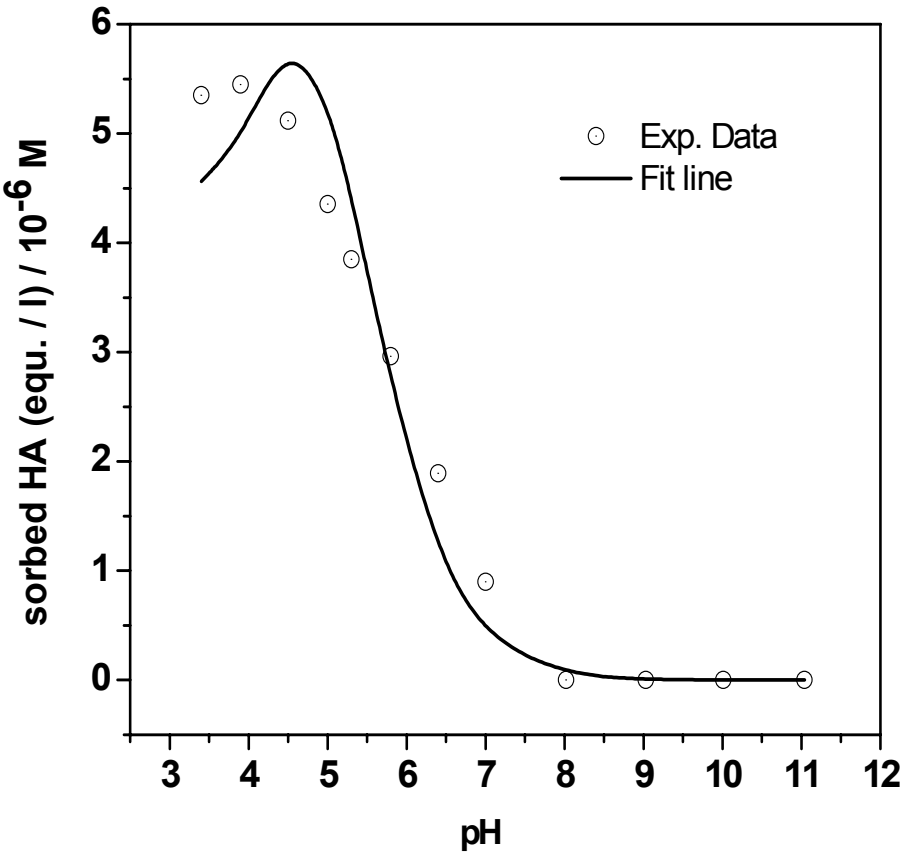

Figure 3.9 Surface complexation modelling of humic acid sorption on alumina.

3.3.4 Cs(I) and Tc(IV) complexation with HA

^{137}Cs activity left in the supernatant after equilibration with the fixed amount of cation-exchange resin was found to be constant, irrespective of varying pH, ionic strength, and HA concentration. A typical plot of $\log(\lambda_0/\lambda-1)$ vs. log[HA] at pH 6.5 and 0.05 M ionic strength is shown in figure 3.10. Concentration of HA has been converted into eq/l using carboxylic acid content in HA and the amount of HA used in the experiment. The results indicate weak interaction of cesium ($\log \beta = -1.86 \pm 0.23$) with humic acid.

Tc(IV) shows strong interaction with humic acid and a conditional constant ($\log \beta$) value of 5 obtained by Maes et al. (1999) has been used in the present work for modelling exercise.

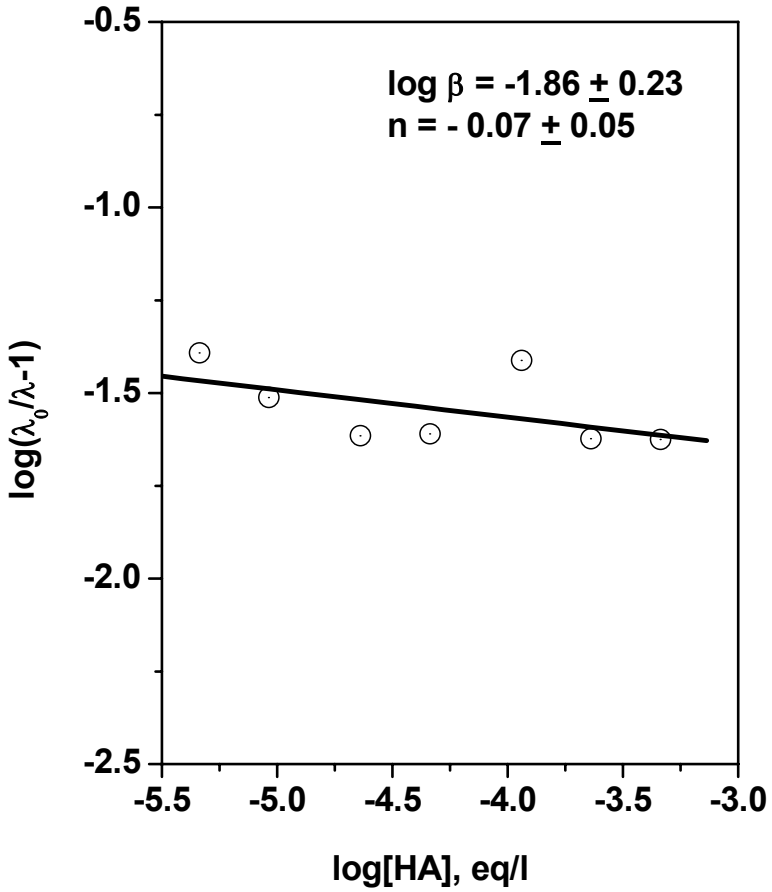

Figure 3.10 Distribution data for the determination of Cs(I)-humic acid stability constant at pH 6.5 in 0.05 M $NaClO_4$ medium

3.3.5 Cs(I) sorption on silica in presence of humic acid

Cs(I) sorption on silica in absence and presence of HA is shown in figure 3.11. In absence of HA, sorption percentage is insignificant till pH 7, above which it increases and attains ~30% value by pH 10. With HA, the sorption percentage at lower pH values shows enhanced profile while there is no difference at higher pH values. Increase at lower pH values has a convex shape with maximum sorption in the pH range of 4 to 6.

Cs(I) sorption on silica has strong competition from Na(I) of the background electrolyte. Further, with lesser ionic potential, it behaves like a weak Lewis acid and therefore, as per the

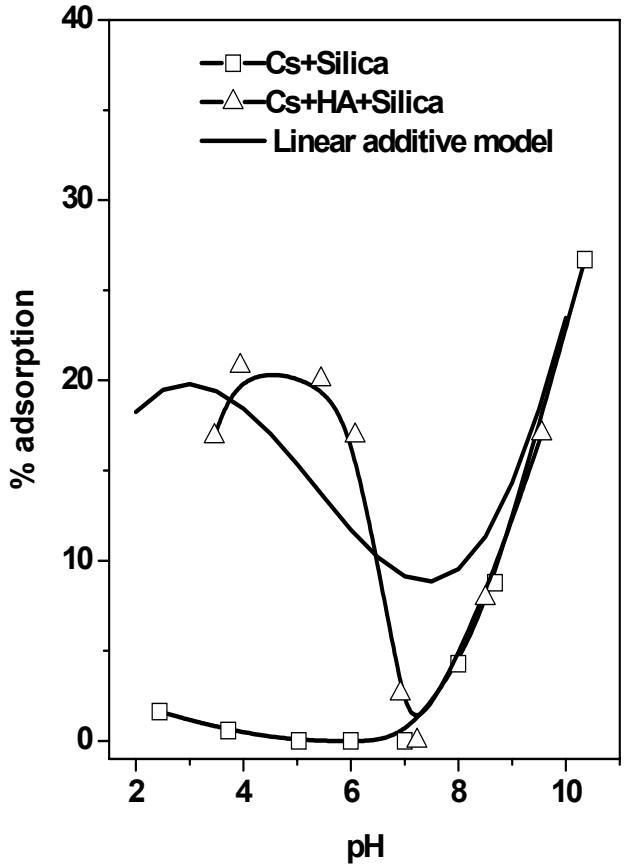

Figure 3.11. Sorption of Cs(I) on silica in presence and absence of humic acid. The solid line represents the linear additive modelling of the ternary system

hard acid-hard base concept, shows weak interaction with strong Lewis base like oxygen of silica surface. Metal ion sorption on oxide surface starts with the formation of outer sphere complex with surface sites and subsequently converts into inner sphere when complexing behaviour of metal ions has increased, such as at higher pH. Cs(I) sorption profile at lower pH can thus be attributed to suppression of outer sphere complexation while the increasing sorption with pH above 7 is due to increasing ionic interaction with $\equiv SiO^-$ group like with hydroxyl ion in Cs(OH) ionic compound.

Increased sorption percentage of Cs(I) at lower pH values in presence of HA indicates stronger binding of Cs(I) with HA sorbed silica surface. As per the formulation of linear

additive model (eq. 2.10), there should be no such enhancement (i.e., $K_d = K_d^0$). To reproduce the sorption percentage, LAM was modified to include the different binding ability of surface bound HA and dissolved HA. Eq. 2.10 gets modified to eq. 3.3 where β_1 and β_2 stand for the Cs(I) stability constant for surface sorbed and dissolved HA.

$$K_d = \frac{K_d^0 + (V/W) f_{HS} \beta_2 [HS]}{1+(1-f_{HS}) \beta_1 [HS]} \quad (3.3)$$

In an iterative fitting of the sorption data of the ternary system in eq. 3.3, β_2 value was varied in step of 0.1 unit from β_1 value. Log β_2 value of 4.6 was found to reproduce the ternary sorption profile. This value is significantly different from stability constant of dissolved HA and substantiate the stronger binding behaviour in the ternary system.

SCM defines sorption as the result of surface complexation and the electrostatic factors. Though interaction ability of HA and surface oxygen atoms with Cs(I) should not change due to sorption, presence of HA on surface could present a cloud of negative charge causing enhanced electrostatic attraction for Cs(I). This is evidenced by the fact that zeta potential of HA-sorbed-silica changes significantly from that of bare silica and comes closer to that of HA (figure 3.12).

Cs(I) is thus present on HA-sorbed-silica surface as counter ion condensate around the polyelectrolyte (HA), wherein Cs(I) can be considered as forming outer sphere complex with HA. This conclusion is substantiated by the facts that Cs(I) sorption on HA-sorbed-silica decreases significantly with increased ionic strength (0.1 M from 0.05 M $NaClO_4$) whereas the same for binary sorption systems do not change with ionic strength (figure 3.14). Similar conclusion was derived in an LCD model application to Ca(II) sorption by goethite surface in presence of FA where, with the enhance capability of the model, the authors could delineate

the interaction between Ca and FA at the surface of goethite as mainly due to the electrostatic effects (Weng et al. 2005).

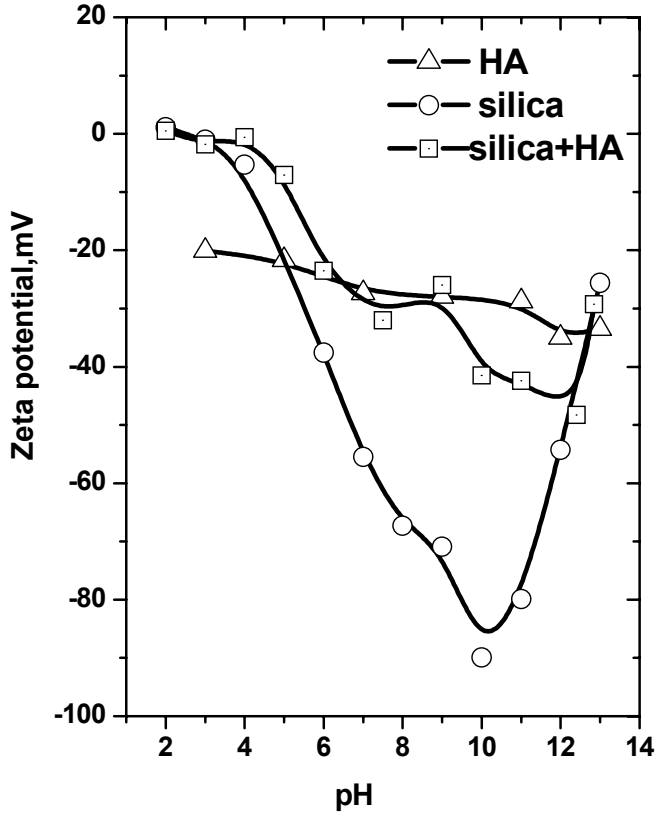

Figure 3.12 Zeta potential measurements of humic acid, silica and humic acid equilibrated silica

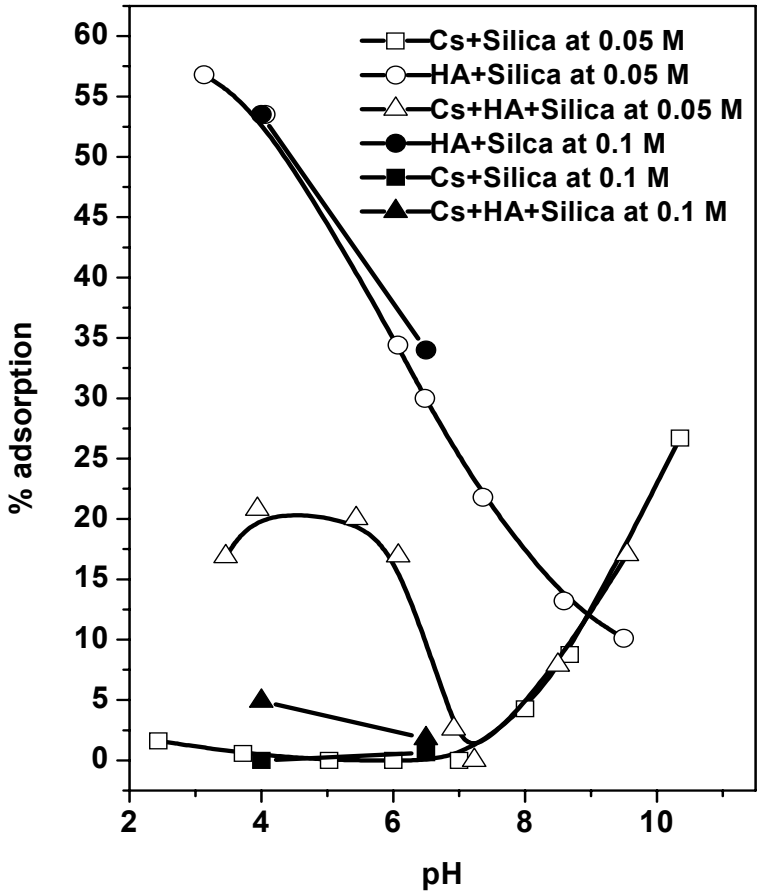

Figure 3.13 Effect of ionic strength in Cs(I) and humic acid sorption systems.

3.3.6 Tc(IV) sorption on alumina in presence of humic acid

Tc(IV) sorption on alumina both in absence and presence of HA is shown in figure 3.14. Sorption in absence of HA remains low (~10-20 %) over the pH range 4 – 11 which is distinctly different from the high sorption percentage expected for tetravalent metal ions (Reiller et al. 2005). Tc in its IV oxidation state exists as TcO^{2+} at lower pH values and hydrolyses to $TcO(OH)^{+}$ and $TcO(OH)_2$ with increasing pH (figure 3.15). Hydrolysed Tc species thus carry lesser effective ionic charge and this decreases the interaction affinity leading to reduced sorption percentage.

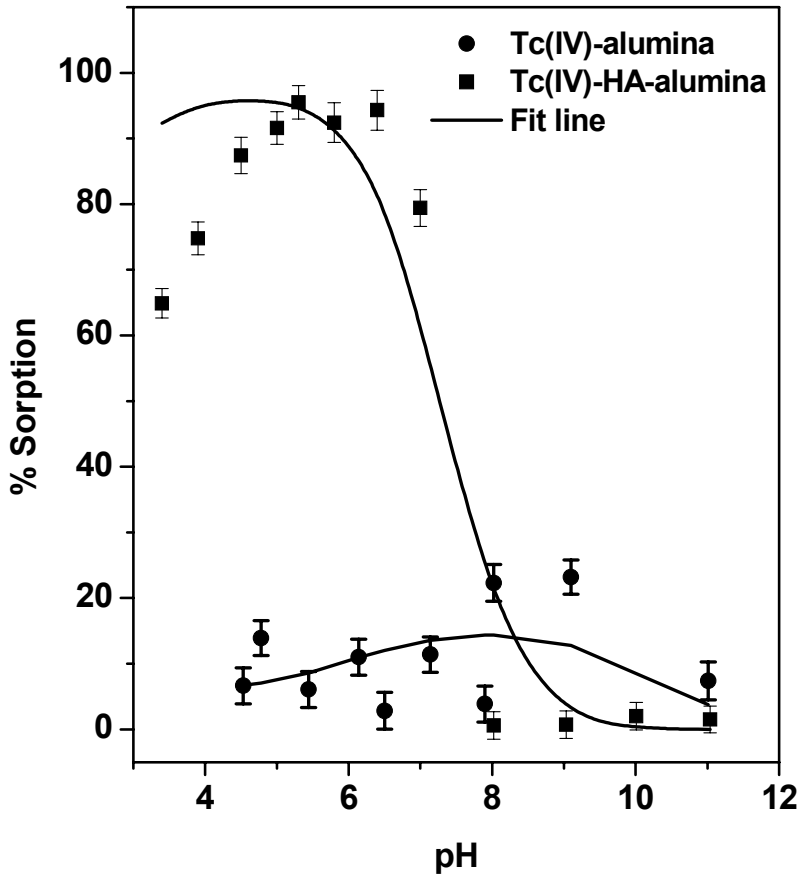

Figure 3.14 Effect of humic acid on Tc(IV) sorption on alumina. Solid lines stand for surface complexation modelling of sorption systems

Sorption of Tc(IV) in presence of HA greatly increases at lower pH values compared to that in absence of HA, reaches quantitative value in the pH range 5-6 (figure 3.14) and decreases at higher pH values. Sorption profile in the ternary system follows the trend of HA sorption on alumina (figure 3.9) indicating that HA sorption by alumina governs Tc(IV) sorption characteristics. LAM of the ternary systems (figure 3.16) considering different metal binding characteristic of dissolved and surface sorbed HA (eq. 3.3) reproduces the sorption profile. The inset in figure 3.17 shows the variation of log β_2 (5.3-6.9) with pH. Considering the effective charge of TcO^{2+} and trivalent actinides/lanthanides, log β_2 value stands in conformity for the value (~ 4.7 - 7) reported in Am(III)/Cm(III) sorption on

hematite in presence of humic acid (Samadafam et al. 2000). The variation does suggest the role of HA in governing the sorption. However, the participation of interactions other than those present in binary systems, governing sorption is also clear as Tc(IV) interaction constants with dissolved and surface sorbed HA are different.

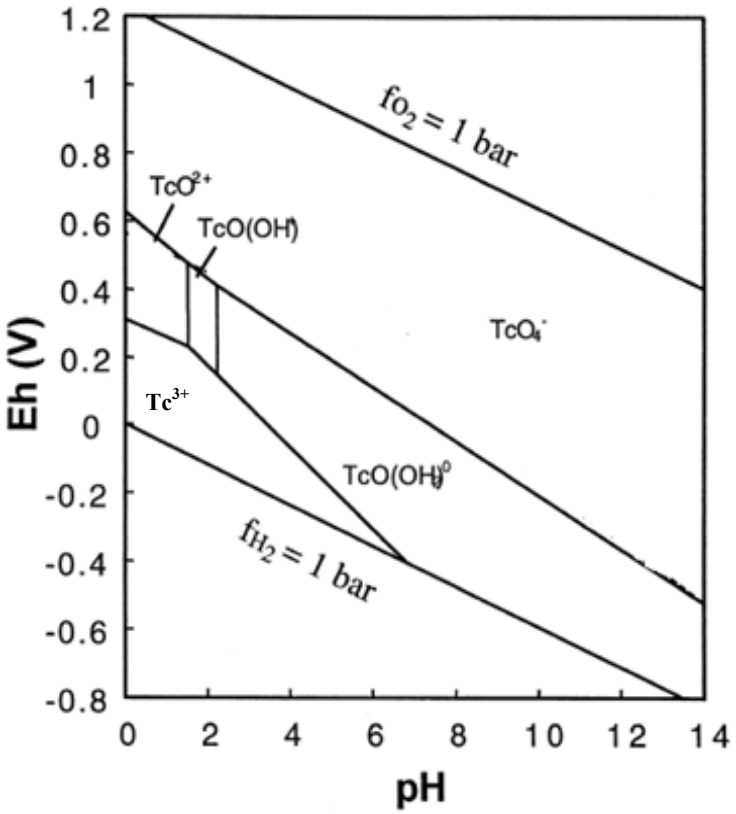

Figure 3.15 Eh-pH predominance diagram of technetium aqueous speciation

SCM of the Tc(IV) sorption on alumina in absence and presence of HA is shown in figure 3.14 and the modelling result is listed in table 3.4. Modelling of Tc(IV) sorption on alumina indicates the formation of two Tc(IV) surface species while ligand bridged Tc(IV) surfaces species forms on alumina sites in ternary system. The log K value obtained for ternary system matches closely with maximum value of log β_2 observed in LAM. Predominance of ligand bridged ternary complex (type 1) in characterising the ternary sorption system seems justified

in view of weak Tc(IV) interaction with mineral surface and stronger interaction of Tc(IV) with HA.

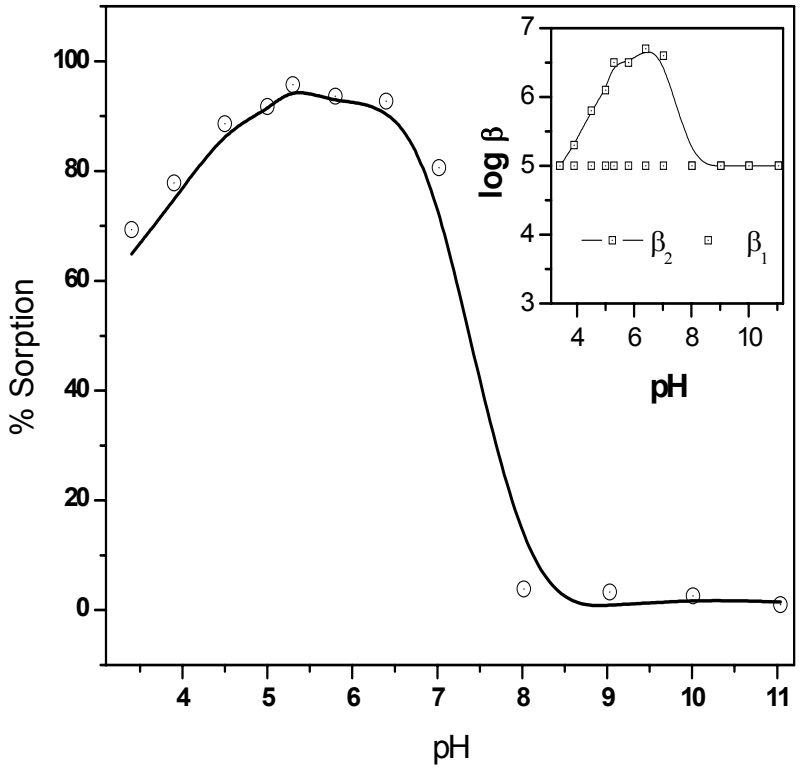

Figure 3.16 Linear additive modelling of Tc(IV) sorption on alumina in presence of humic acid. Inset shows the variation of log β_2 over the pH range of sorption

Table 3.4 Surface Complexation modeling of Tc(IV) binary and ternary sorption systems

Equilibrium reactions	Species optimized	Log K
Tc(IV)-Alumina		
$\equiv AlOH + TcO^{2+} \rightarrow \equiv AlOTcO^{+}$	$\equiv AlOTcO^{+}$	5.80
$\equiv AlOH + TcO^{2+} + H_2O \rightarrow \equiv AlOTcO(OH)$	$\equiv AlOTcO(OH)$	-1.01
HA-Alumina		
$\equiv AlOH + HL_1 \rightarrow \equiv AlOHHL_1$	$\equiv AlOHHL_1$	4.44
Tc(IV)-HA-Alumina		
$\equiv AlOH + TcO^{2+} + HL_1 \rightarrow \equiv AlOL_1TcO$	$\equiv AlOL_1TcO$	6.79

3.4 Conclusion

Presence of humic acid was found to strongly modify the sorption of Cs(I) and Tc(IV) on mineral oxide surfaces. Though the general pattern of HA effect - enhanced metal ion sorption at lower pH values and suppressed sorption at higher pH compared to that in absence of HA – is same , the role played by humic acid varies. In case of Cs(I), it alters the electrostatics at the oxide-water interface while strong Tc(IV) interaction with HA causes the formation of ternary complex in Tc(IV)-HA-alumina system. Complexing behaviour of humic acid governs the sorption in ternary sorption system of Tc(IV)-HA-alumina.

Chapter 4

Sorption of actinides on mineral oxides: Role of surface reactivity

4.1 Introduction

Sorption of metal ions at the solid-water interface involves accumulation of metal ions in the interfacial region. Chemical reactions involved in the accumulation process can be broadly classified as:

- Coordinative bonding of metal ion on the solid surface through outer and inner sphere complex formation.
- Precipitation of metal ions at the surface. This can start from heterogeneous nucleation at the surface in surface complexation step, and proceeds through precipitation / coprecipitation to newer solid phase formation.
- Oxidation state change of metal ions while approaching the surface. This transformation may take place in the aqueous phase as well as in adsorbed phase at solid surface.

Apart from metal ions themselves, the characteristics of the interfacial region also govern chemical reactions involved in the accumulation process (Bargar et al., 1997; Cheah et al., 1998).

A solid surface, such as that of an oxide can be considered as the two dimensional distribution of central atom, forming on the cleavage of bulk three dimensional network (≡S–O–S≡), where S represents the metal ion, viz., Si, Al, Fe, Mn, Ti, etc. Dissociative chemisorption of water molecules on the oxygen atom of the ≡S–O moiety also creates surface sites (≡SOH). These surface hydroxyl groups are structurally and chemically not equivalent, though under mean field statistics the surface can be considered populated by a single type of surface sites (Sposito, 1994), represented simply by ≡SOH. These sites act as surface functional groups in interactions with sorbing metal ions. Depending upon the electronegativity of the central atom, ≡SOH sites can undergo protonation/deprotonation

reactions to produce surface bound charged layer (Stumm, 1992). Counter ions present in the surrounding aqueous phase flock near the surface to form an electric double layer (EDL) structure.

The reactivity of the interfacial region, however, gets primarily defined by the particular details of the solid surface. For example, silica has negative zeta potential over the pH range 3-10 while alumina exhibits positive surface charge over the same pH range (Stumm, 1992). Alumina starts sorbing metal ions well below its pzc while silica resists sorption till higher pH values (Brown, Jr., et al., 1999; figure 29b). High dielectric constant solids have been found forming a different proportion of surface species compared to those with lower dielectric constant (Sverjensky, 2006; Fukushi and Sverjensky, 2007). Piasecki and Sverjensky (2008) concluded a weaker monodentate complex (relative to the tetra-complex) on high dielectric constant solid such as rutile compared to hematite or silica. Geometric constraint of the surfaces as well modifies the pattern of surface speciation. O'Day et al. (1996) suggested the difference in Co(II) sorption on quartz and rutile attributable to the availability of reactive sites on these surfaces, which are structurally favourable for the sorption of octahedrally-coordinated Co(II). XAFS studies of Cu(II) on silica and alumina surfaces at low surface coverage indicate predominately dimeric Cu(II)-surface complex on silica surface along with a minority monomeric species while only a monomeric species forms on alumina surface (Cheah et al., 1998). Role of structural features in dissolution of solid substrates has been emphasized in the coordinative description of the dissolution reaction (Hiemstra and van Riemsdijk, 1990; Berger et al. 1994; Stumm, 1992, chapter 5). Also, change in the oxidation state of surface central atom has been found to affect the dissolution rate significantly (Stumm, 1992, chapter 9). Formation of metal ion outer and inner sphere complexes at the solid-liquid interface influences the dissolution rate differently.

As a result, the importance of precipitation/co-precipitation reaction in the sorption mechanism varies with solid surfaces. Oxidation state variability of surface atom has been found mediating redox reactions of sorbing metal ions. Mixed valence (II/III) iron and manganese oxide surfaces have been found reducing Pu(V/VI) to Pu(IV) with direct correlation to the content of divalent species (Fe(II), Mn(II) (Powell et al., 2004; Shaughnessy et al., 2003; Hixon et al., 2010).

In the present chapter, the sorption of two strongly mineral-interacting actinides, namely, Am and Pu, on the oxide surfaces, has been investigated. Metal ion concentration has been varied in the sorption of Am(III) on alumina surface to understand the evolution of surface species formed below pH 7 (Kumar et al., in press). Precipitation of $Am(OH)_3$ could take place above pH 7 and to delineate the surface speciation of Am(III) in precipitating condition, X-ray absorption fine structure spectroscopy study of Eu(III), an analogue of Am(III), sorbed on alumina was carried out over pH 6-8 and the result was compared with that obtained on silica surface (Kumar et al., 2011). Sorption of Pu, a redox sensitive radionuclide, on silica and alumina surfaces was investigated using sorption, desorption and kinetic studies to understand the role of mineral surface in defining the speciation of Pu in aqueous phase and on the oxide surface (Kumar et al., 2012). The chapter aims to gain insight of the role of surface-reactivity in governing speciation at oxide-water interface.

4.2 Am(III) Sorption on mineral oxides

Sorption of metal ions under the condition of increasing surface coverage can be characterized by the following observations:

- Higher surface coverage studies in literature have been achieved by either increasing metal ion concentration in the sorption system or decreasing the solid amount in the suspension (Marmier et al., 1999; Rabung et al., 2000). While both the conditions cause higher surface coverage, the former can produce homogenous precipitation in the aqueous phase. Metal ions thereby may form "intrinsic colloids" (cf. Chapter 1) and remain suspended in the aqueous phase or the colloidal species may sorb on the surface. In the second case, due to unsaturated condition, homogenous precipitation is not possible. Metal ion may, however, coprecipitate with dissolved species of the solid on the surface and this heterogeneous nucleation on further progress may result in a new solid phase formation (figure 1.3) (Charlet and Manceau, 1992).
- Affinity of surfaces for sorbing metal ions, geometrical distribution of sites on solids surfaces, dissolution of solid surfaces and chemistry of the metal ions have been observed influencing the speciation of metal ions under increasing surface coverage condition (O'Day et al., 1996; Cheah et al., 1998; Powell et al., 2005).

Literature update on sorption of trivalent actinides/lanthanides on mineral oxides under different surface coverage

pH edge for sorption of trivalent actinides/lanthanides on oxide surfaces has been found to shift to higher pH values with increasing surface coverage. Though the sorption profile remained same; sorption percentage increased to quantitative value over small pH difference (2) (Rabung et al., 1998; Rabung et al., 2000; Piasecki and Sverjensky, 2008). Sorption percentage as function of pH has been modelled assuming inner sphere complex formation of

metal ion with surface sites in framework of surface complexation modelling. Metal ion binding (denticity) with surface sites however varied in the surface species chosen for the modelling exercise. In most of these studies following Dzombak and Morel (1990) approach, surface sites (≡SOH) have been considered interacting with metal ions like aquatic ligands, i.e., forming ML_1, ML_2, etc. types of complexes (Rabung et al., 1998; 2000). Backed by recent Synchrotron based X-ray spectroscopic results (Zhang et al., 2004; 2006a; b), some studies considered metal ion as interacting with surface sites primarily in tetradentate manner where metal ion binds to two bridging oxygens and two singly-coordinated oxygens of surface atom polyhedra (Piasecki and Sverjensky, 2008).

Though extensive studies have been focused on the sorption of trivalent lanthanides/ actinides on alumina (Marmier et al., 1997; Rabung et al., 2000; Wang et al., 2000; Stumpf et al., 2001; Rabung et al., 2006), mechanism of sorption under varying metal ion concentration is not yet fully understood. Marmier et al. (1997) modelled Yb(III) sorption on hematite and alumina at low as well as high surface coverage using the same set of mononuclear-monodentate Yb(III) hydrolyzed surface species, $\equiv SOYb(OH)_x^{(2-x)}$, x = 0 - 2. For modelling sorption isotherms of Eu/Am(III) onto γ-alumina, Rabung et al. (2000) partitioned surface sites into "strong" and "weak" types differing in their acidity and metal binding capacity and considered mononuclear-monodentate surface complexation of these sites with metal ions. Metal ion binding on "strong" sites ($\equiv AlOEu^{2+}$) was validated through graphical method and by TRLFS investigations. Rabung et al. (2006) investigated Cm(III) ([Cm(III)] = 2.5×10^{-7} M) sorption on alumina over pH 3.5-13.2 and concluded the occurrence of three surface complexes on the "strong" sites, $\equiv AlOCm(OH)_x^{(2-x)}(H_2O)_{5-x}$, x = 0 – 2, based on the shift in the peak position of fluorescence emission spectra. Interestingly, when Cm(III) was excited indirectly, i.e., energy transfer from solid to the metal ion at λ_{ex} = 355 nm, apart from the 110

μs component observed in direct Cm(III) excitation (λ_{ex} = 396.6 nm), a slow decaying component of 406 ± 203 μs (fraction < 10%) was observed. Results from the different excitation modes visualize the existence of Cm(III) in two different sorption sites at the alumina surface. EXAFS for Gd/Eu(III) sorbed onto γ-Al_2O_3 at pH=6 identified a single oxygen coordination shell with a high degree of disorder indicating inner sphere complexation of metal ions with surface sites though exact speciation could not be delineated even after the application of spectroscopic techniques, viz., TRLFS and EXAFS (Rabung et al., 2006).

Using mononuclear tetradentate species proposed by Zhang et al. (2004; 2006a; b), Piasecki and Sverjensky (2008) modelled La(III) sorption on hematite under the condition of varying surface coverage (Marmier and Fromage, 1999) using mononuclear monodentate and mononuclear tetradentate surface species.

Though these studies do indicate the difference of surface speciation with increasing surface coverage, a clear understanding is yet to be achieved with regard to

- Speciation of trivalent actinides /lanthanide on "weak" site, i.e., speciation appearing on higher surface coverage, and
- Evolution of metal ion surface speciation with increasing surface coverage.

Present study

In the present work, sorption of Am(III)/Eu(III) by γ-alumina has been studied as a function of pH (3-10), ionic strength (0.005-0.1 M) and metal ion concentration (10^{-7}-10^{-4} M). Time resolved fluorescence spectroscopy (TRFS) measurement of Eu(III) (5.0×10^{-5} M) sorbed onto γ-alumina was carried out to reveal the number and nature of the surface species involved sorption process. Structural characterization of surface species formed at higher surface coverage was carried out by the EXAFS study of Eu(III) sorbed onto γ-alumina at pH

6-7. Based on the informations revealed by TRFS and EXAFS measurements regarding surface species, surface complexation modelling of the sorption process was constrained to model the surface coverage of Am/Eu(III) on alumina surface in condition of pH ≤ 7.

4.2.1 Experimental details

4.2.1.1 Sorption experiments

Details of sorption experiment have been discussed in chapter 2 (section 2.1). ^{241}Am radioisotope used in the present work was from the stock solution having concentration 1.8×10^{-8} M and higher metal ion concentration in the experiment was achieved using inactive Eu(III) solution. To study the reversibility of the sorption, desorption experiments were carried out, where, Eu(III) (5.0×10^{-5} M) sorbed on alumina at pH 7.83 was contacted with fresh solutions of 0.1 M $NaClO_4$ at pH 5.8 and pH 3.0 at same mass to volume ratio. 48 hr was provided for the attainment for the desorption equilibrium.

4.2.1.2 Details of spectroscopic experiments

Details of Time resolved fluorescence experiment and X-ray absorption fine structure spectroscopy measurements have been discussed in chapter 2 (sections 2.3 and 2.4).

4.2.1.3 Surface complexation modelling

For modelling of sorption, 2-pK formalism for surface complexation and constant capacitance model for electrostatics were employed in FITEQL V. 4 program. Modelling of the sorption data was restricted up to pH ≤ 7. Constant capacitance value of 1.2 F/m^2 was used in the modelling of sorption data. Protonation / deprotonation constants for surface sites were obtained from the modeling of the potentiometric data (cf. chapter 3) and were kept constant in SCM fitting. Since samples have been prepared under N_2 atmosphere and equilibration was carried out in sealed tubes, carbonate complexation of metal ion was

ignored in the sorption modeling as atmospheric CO_2 is not expected to influence surface reactions in pH range of present study (≤ 7).

4.2.2 Results and discussion

4.2.2.1 Sorption studies

Figure 4.1 shows Am(III) sorption by γ-alumina as a function of pH at varying ionic strength. Percentage sorption was found to increase sharply (from 2 to 100 %) over the pH range 3 to 6. Sorption profile of Am(III) is independent of ionic strength, indicating its complexation with alumina surface sites (≡*AlOH*) in inner sphere mode. Similar observation

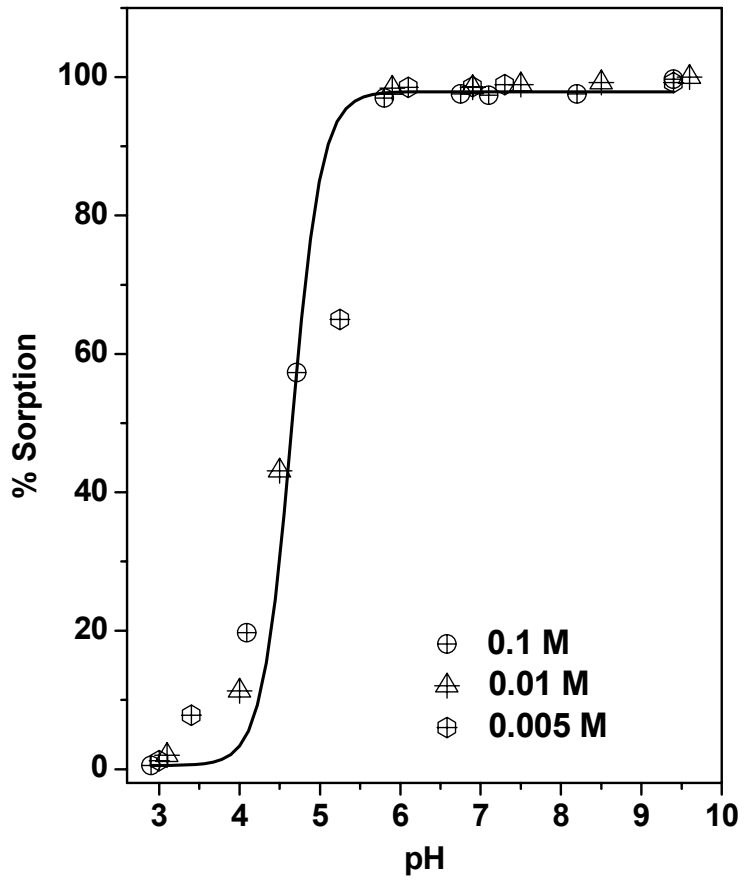

Figure 4.1 Effect of varying ionic strength (0.1 – 0.005 M) on Am(III) (10^{-7} M) sorption on γ-alumina over pH 3 -10. Solid line is eye guide.

has been reported in the sorption of Eu(III) (Rabung et al., 1998) and La(III) (Marmier et al., 1999) on hematite.

Dependence of percentage sorption on varying metal ion concentration over pH 3-10 at 0.1 M ionic strength ($NaClO_4$) is given in figure 4.2. With increasing metal ion concentration the sorption edge shifts to higher pH value in agreement with literature report (Rabung et al., 2003). This is suggestive of structural heterogeneity in Am/Eu(III) binding on alumina surface sites. As the ratio of metal ion concentration to surface sites is very small, the

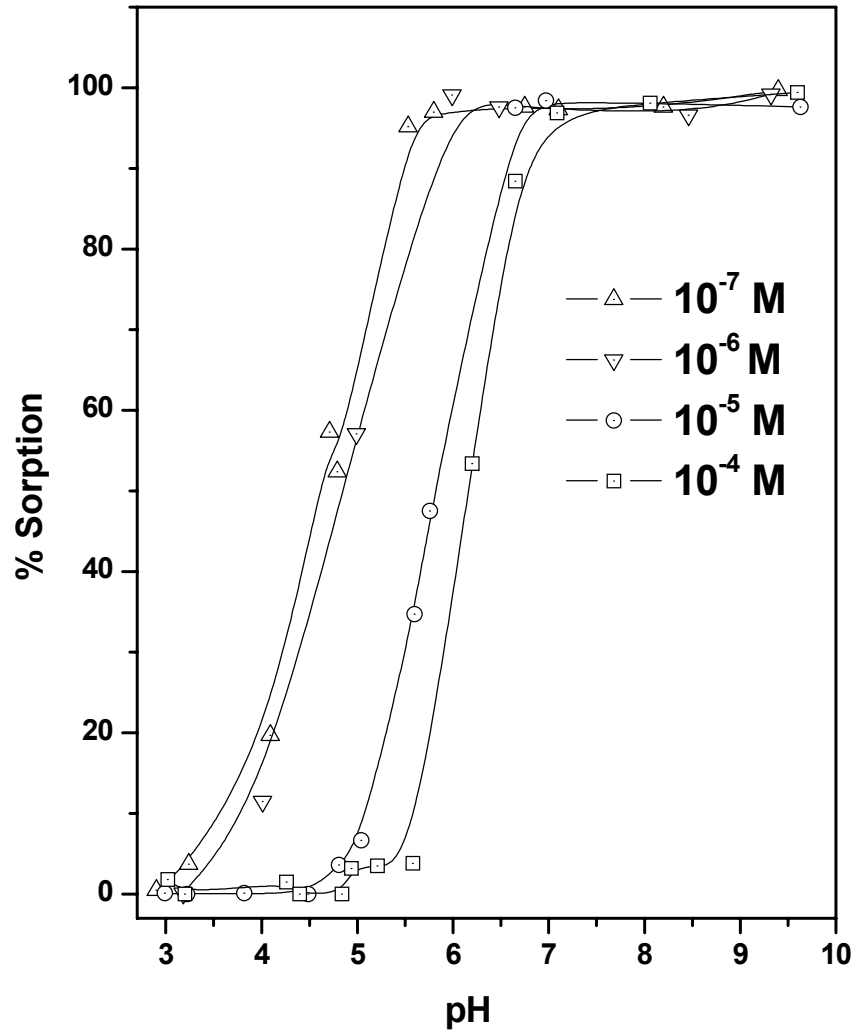

Figure 4.2 Am(III)/Eu(III) sorption on γ-alumina as a function of pH and metal concentration at ionic strength 0.1 M $NaClO_4$.

sorption edge should have remained invariant with pH in case only one type of coordinative behaviour of metal ion exists. Binding of Am(III)/Eu(III) to alumina surface sites, thus can be considered to involve different binding geometries. Metal ion complexation constant to surface sites in different coordinative environment may differ and shift the sorption edge with varying surface coverage.

In the desorption experiment, when the solid phase obtained after Eu(III) equilibration with alumina suspension at pH 7.83, was re-equilibrated with fresh solutions of 0.1 M $NaClO_4$ at pH 5.8 and 3.0, the percentage Eu(III) left on the solid phase (49.8 and 6.1 %, respectively) was found to agree with that (~ 49 and 4 %, respectively) obtained in the sorption experiment suggesting the reversibility of the sorption process. This confirms surface complexation as the sorption mechanism.

4.2.2.2 Characterization of surfaces species

Fluorescence spectroscopy results

Figure 4.3 shows a typical fluorescence decay profile of Eu(III) sorbed on alumina. The best fit (minimum chi-square) of temporal decay data to eq. 2.14 for samples prepared at different pH was obtained in case of two components (1 and 2) fitting. Individual emission spectra for these components over varying pH have been plotted in figure 4.4. No change in the peak positions was observed for both the species. This is expected as the Eu(III) 4f orbital is less exposed to ligand field environment in comparison to Cm(III) and U(VI) 5f orbitals, wherein significant red shift has been observed after surface complexation (Rabung et al., 2006; Froideval et al., 2006).

Intensity ratio (I_{616}/I_{592}) has been used to identify the species corresponding to the different co-ordination environments (Rabung et al., 2000). The 616 nm ($^5D_0 \rightarrow {}^7F_2$) peak in the Eu emission spectra arises in electric dipole assisted transition and is “hypersensitive”,

that is, its intensity changes with the changing ligand field around Eu(III), whereas, 592 nm

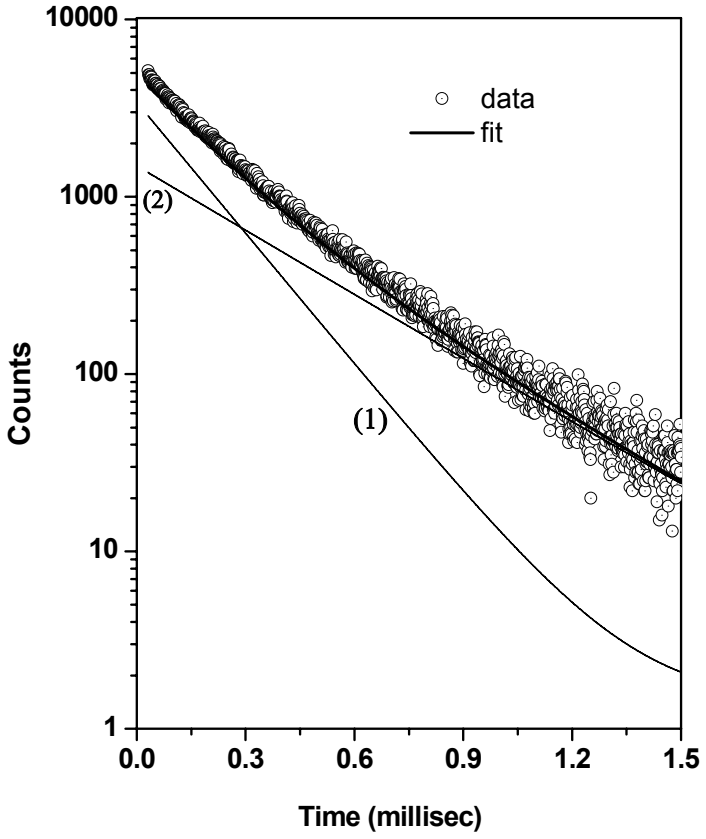

Figure 4.3. Fluorescence decay profile of Eu(III) sorbed onto γ-alumina at pH 6.0. Symbols 1 and 2 represent the two components of the decay profile.

peak, which originates in magnetic dipole transition ($^5D_0 \rightarrow {}^7F_1$), is not sensitive to the changing co-ordination environment. In the present investigation the intensity ratio for the components 1 & 2 changed from 2.03 to 2.63 and 2.85 to 3.06, respectively, with increasing pH (Table 4.1). Variation in the pattern of intensity ratio suggests different binding mechanism/geometry in these two components. The increasing intensity ratio for each component can be attributed to the increasing hydroxylation of the surface sorbed Eu(III) species with pH.

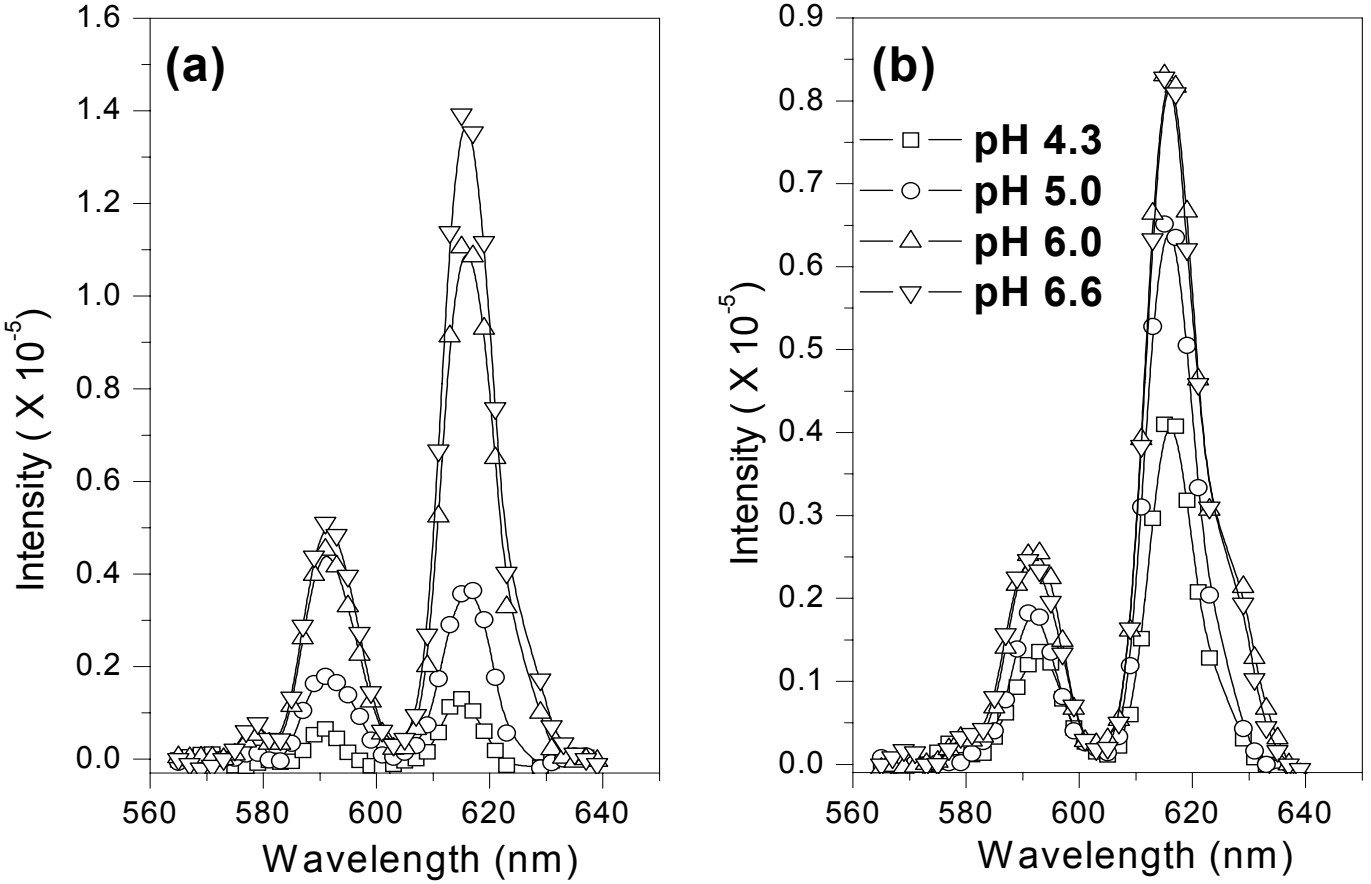

Figure 4.4 Fluorescence emission spectra of Eu(III) species formed on γ-alumina over pH 4 - 7. $[Eu]_{tot} = 5.0 \times 10^{-5}$ M, Strength of alumina suspension = 3 g/l at ionic strength 0.1 M $NaClO_4$. Symbols (□), (○), (Δ), and (∇) stand for pH 4.3, 5.0, 6.0, and 6.6, respectively. Label (a) and (b) stand for lower and higher lifetime, respectively.

Lifetime values corresponding to the two components at different pH have been shown in Table 4.1. The lower lifetime value (τ_1) increases from 114 to 190 μS with increasing pH, while the change is less (from 326 to 367 μS) for the other component (τ_2).

Table 4.1 Fluorescence data for Eu(III) species formed onto γ-alumina over pH 4 - 7 in 0.1 M $NaClO_4$. Intensity ratio corresponds to the ratio of intensities obtained at 616 and 592 nm.

pH	Component 1		Component 2	
	Intensity Ratio	Lifetime (μS)	Intensity Ratio	Lifetime (μS)
4.3	2.03	114	2.85	326
5.0	1.81	153	3.65	375
6.0	2.44	176	3.21	359
6.9	2.63	190	3.06	367

The lower lifetime signifies higher fluorescence quenching modes available, and hence more H_2O/OH^- groups coordinated to Eu(III) (Horrocks et al., 1979). Comparing τ_1 with the lifetime of Eu-aquo species (τ=110 ±10 μs), the component corresponding to τ_1 should have structure like Eu hydrolyzed species, that is, $\equiv AlOEu^{2+}$, $\equiv AlOEu(OH)^{+}$ *and* $\equiv AlOEu(OH)_2$. This result is in agreement with Rabung et al. (2000) and also corroborates the findings obtained for the Cm(III)/γ-alumina system (Stumpf et al. 2001). Considering Horrock's relation ($N_{(H2O)}$ ± 0.5 = 1.07 × (1/τ) - 0.62, τ is in millisecond), the number of H_2O/OH^- present in the second component is 2.5 ± 0.5. Lower number of water molecules for this component indicates multi-denticity of Am(III)/Eu(III) binding on alumina surface. Rabung et al. (2004) obtained a similar number of water molecules (3.2-2.5) in the first hydration sphere of Cm(III) surface species in the TRLFS investigation on different ((012), (104), (018), and (110)) crystallographic planes of α-Al_2O_3. The involvement of a greater number of

surface oxygen atoms in these species was concluded by the observation of a lower binding energy of Cm $5f_{7/2}$ electron in XPS study and a more pronounced red shift of the fluorescence emission spectra in comparison to that observed at (001) plane which shows emission spectra characteristics similar to γ-alumina at lower metal ion concentration (10^{-11}-10^{-12} M). The pattern in the changing intensity ratio and lifetime values for the components thus indicates the formation of species with varied denticity on alumina surface and their hydrolysed species with increasing pH.

Though higher lifetime values have been observed in surface incorporated species of trivalent lanthanides and actinides (Huittienen et al., 2009; Fernandes et al., 2008), surface incorporation is ruled out in the present study on the basis of alumina solubility. In the present study alumina suspensions were first prepared in 0.1 M $NaClO_4$ at pH 6.5 (the pH value where alumina has minimum solubility), and were equilibrated with metal ion at different pH values ranging from 3-10. On both sides of the neutral pH, alumina has higher solubility (Rabung et al., 2006), thereby, precluding the incorporation of Am(III)/Eu(III) in alumina matrix during the present study. Reversibility of sorption-desorption observed in case of Eu(III) desorption study also negates the surface incorporation.

EXAFS Results

To identify metal ion coordination on alumina surface, EXAFS experiments were performed for Eu : γ-Al_2O_3 sorption samples prepared at pH 6.18 and 7.15. As peaks in EXAFS R-space data correspond to backscatterer-shells surrounding the probe atom, metric analysis of the spectra could yield the inter-atomic distance (R) and coordination number of those neighbours (N) and thus establish the structure of the species. The k^3 weighted Eu-L_3 edge EXAFS spectra for Eu-sorption samples and their corresponding Fourier Transforms (FT) are shown in figure 4.5.

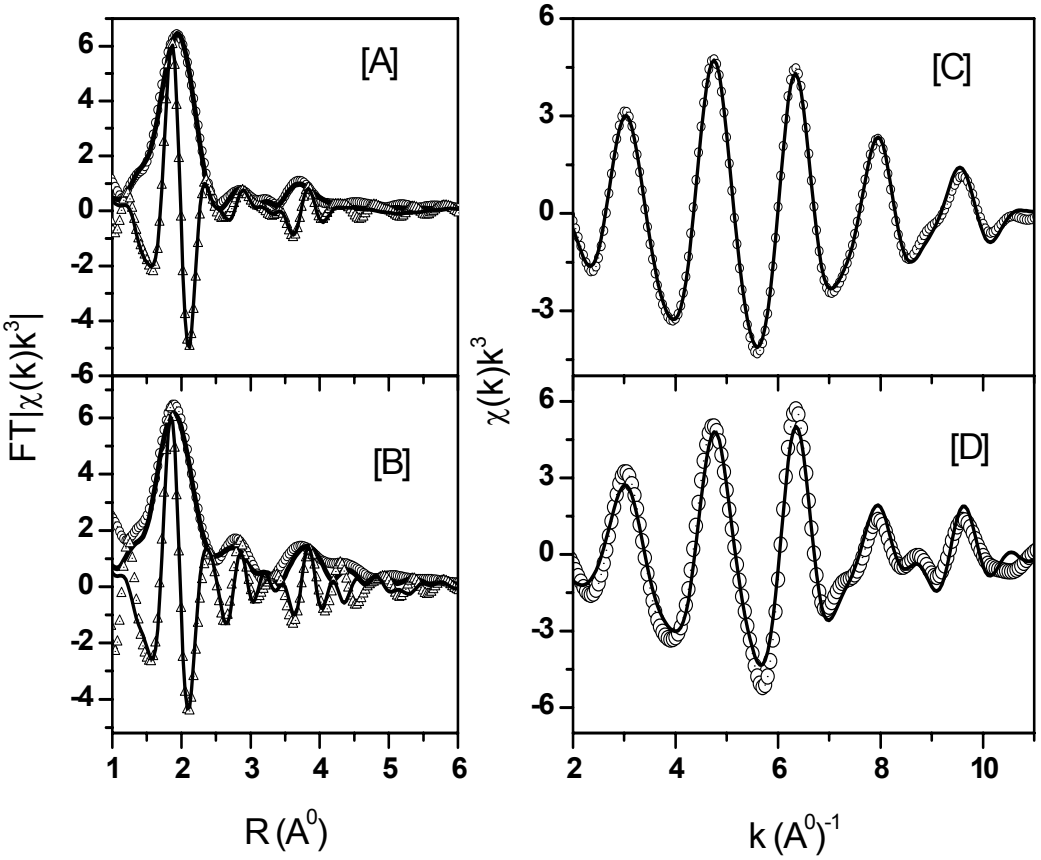

Figure 4.5. Right: k^3-weighted Eu L_{III} edge filtered EXAFS oscillations and the best fit. Left: Experimental and simulated moduli and imaginary parts of the Fourier transform for sorption samples. Symbols [A] and [C] stands for sorption sample made at pH 7.15 while [B] and [D] are for sample made at pH 6.18. The solid line in the plots represents the best fit and symbols (o, Δ) are for experimental data.

On visual inspection the peak intensity at ~ 3.2 Å (R+ΔR) decreased for pH 7.15 sample in comparison to pH 6.18 sample whereas a peak at ~ 3.4 Å starts to appear in higher pH samples spectra. The peak at ~ 3.4 Å could be due to the presence of a backscatterer shell at this distance or it may form as an artifact of Fourier transformation. Back Fourier transform of the pH 6.18 spectra in 2.5-3.2, and 3.2-4.3 Å radial distribution window yields a maximum intensity at ~ 7 $Å^{-1}$, suggesting a light atom such as Al. The maximum intensity position in

the sample of the pH 7.15 in these two R-space windows, however, shifts to lower and higher k, respectively, confirming the presence of some other scatter in the 2.5 - 4.2 Å window.

Fitting of the experimental spectra to the EXAFS equation has been done in R-space. First Eu-O shell fitting was performed separately within 1.2 - 2.5 Å window. 2.5 – 4.2 Å data was back transformed and fitting was carried out in k-space using multiple shells, Eu-Al and Eu-Eu. Evaluation of Eu-O-O multiple scattering shell at R ~ 3.89 Å (Schlegel et al., 2004) did not produce a meaningful fit. Finally both fits were optimized using 1.2-4.2 Å R- space data to yield an optimal solution.

Results of the fit are summarized in Table 4.2. A comparison of the structural parameters for the first shell, Eu-O, of the sorption samples reveals that Eu-O distance is 2.39 ± 0.02 Å for all the samples. No splitting of the Eu-O coordination sphere upon binding to alumina surface was observed. However, higher Debye Waller factor, σ^2, indicates the variability in the nature of the oxygen atoms. This may arise as a result of Eu coordination by different oxygen atoms present in surface hydroxyl group (≡*AlOH*), *OH*, and H_2O.

Table 4.2 EXAFS Samples details and metric results of the spectral analysis

Sample pH	$\Gamma_{(Eu\ Sorbed)}$, ($\mu mol/m^2$)	Shells	R(Å) (±0.02 Å)	$N \times S_0^2$ (±1.5)	σ^2 ($Å^2$)	ΔE(eV)	R-factor*
pH 7.15	0.472	Eu-O	2.41	7.4	0.009	1.59	0.007
		Eu-Al	3.22	2.4	0. 018		
		Eu-Eu	3.45	0.9	0.018		
		Eu-Al	4.23	3.2	0.011		
pH 6.18	0.208	Eu-O	2.39	7.7	0.010	7.32	0.001
		Eu-Al	3.23	2.1	0.015		
		Eu-Al	4.07	3.4	0.006		

**Residual factor, R-factor, is a measure of goodness of fit of the modelled data with respect to the experimental data.*

Small differences in Eu-O bonds on binding with these groups, however, cannot be resolved with the bond length resolution (0.16 Å) achieved in the present analysis ($\Delta R \approx \pi/2k_{max}$). Within the experimental error, N (7.5-7.7) is invariant for both the sorption samples.

Next neighbor shells for Eu sorbed species should consist of aluminium. Possible interaction modes of Eu on AlO_6 octahedra are (A) monodentate species, (B) bidentate edge sharing species, and (C) bidentate corner sharing species. A face sharing tridentate binding of Eu on AlO_6 octahedra is energetically unfavourable (Randall et al., 1999). The range of expected Eu-Al distances for different binding modes based on the Al-O and O-O distances in α–Al_2O_3 ($R_{Al\text{-}O}$: 1.85-1.97 Å, $R_{O\text{-}O}$: 2.52-2.86 Å) (Zhou et al., 1991) and the Eu-O bond length obtained in our first shell analysis is given below. Angles considered for the Al-O-Eu bond length calculation are between 120-180^0.

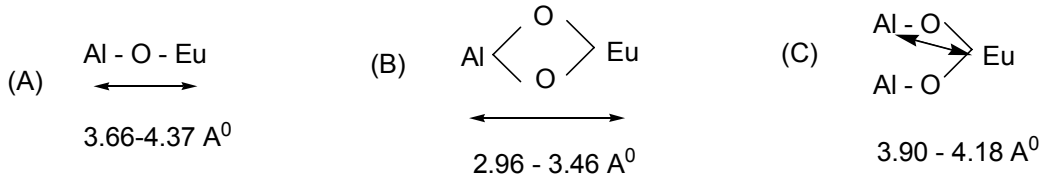

Both the samples show an Al shell at ~ 3.22 ± 0.02 Å. This distance falls in the range of edge-sharing bidentate binding. The appearance of another Al shell at R = 4.1- 4.2 Å indicates monodentate binding. The presence of a Eu-Eu shell at 3.45 ± 0.01 Å, as in case of the pH 7.15 sample, indicates the onset of formation of a Eu precipitated phase. This shell is absent in the spectral fit for sample of pH 6.18. Similar bidenticity have been observed by Dardenne et al. (2001) for Lu sorbed on amorphous hydrous Ferric oxide (HFO) at pH ≥ 5.5. Below pH 5.5 monodentate binding has been observed in surface speciation.

4.2.2.3 Surface Complexation Modeling

Model fit of Am(III)/Eu(III) sorption over varying pH and metal ion concentration plotted along with their species distribution is shown in figure 4.6. Choice of the species for the

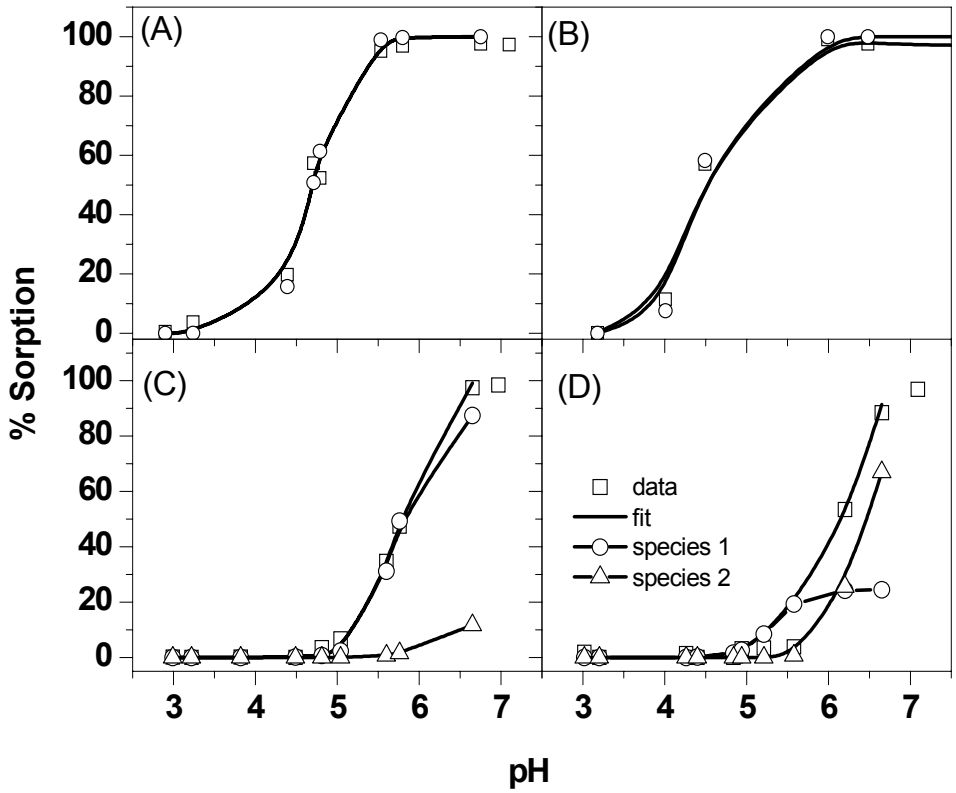

Figure 4.6 FITEQL generated plots for the evolution of Am(III)/Eu(III) surface species over varying metal concentration and pH. Label (A), (B), (C), and (D) stand for 10^{-7}, 10^{-6}, 10^{-5} and 10^{-4} M metal ion concentration conditions, respectively. Species 1 and 2 represent the monodentate species ($\equiv AlOAm^{2+}$) and bidentate species ($(\equiv AlO^{-})_2Am^{+}$), respectively.

optimization procedure is monodentate and edge sharing bidentate Am(III) species (A and B in the above drawing), $\equiv Al\text{-}O\text{-}Am^{2+}$ and $(\equiv Al\text{-}O^{-})_2Am^{+}$ and their hydrolyzed forms. However, to obtain the best possible convergence in the optimization procedure, only the non-hydrolyzed species have been considered in the fitting procedure. Errors on the percentage sorption values, calculated by propagating statistical error of the γ-counting data, was found to be < 2% and hence neglected in the fitting. Formation constant of the species employed in SCM fits is given in table 4.3.

Table 4.3 Optimized surface complexation constants for Am(III)/Eu(III) species formed on alumina surface.

[Am(III)] (mol/l)	Log K $\{\equiv AlOAm^{2+}\}$	Log K $\{(\equiv AlO^{-})_2Am^{+}\}$	WSOS/DF
1.0×10^{-7}	2.72 ± 0.18	-	1.92×10^{-5}
1.0×10^{-6}	2.15 ± 0.17	-	5.90×10^{-4}
1.0×10^{-5}	1.97 ± 0.28	-5.01 ± 3.03	0.05
1.0×10^{-4}	2.02 ± 0.21	-4.96 ± 0.06	6.94

The log K for monodentate species was found to be in the range of 2.0 - 2.2 while the same for bidentate species is close to -5.0. Similar formation constants have been observed for Am(III) monodentate surface speciation with ≡*Al-OH* sites (Rabung et al., 2000) and Lu(III) bidentate species onto ferrihydrite (Dardenne et al., 2001). The log K (- 0.82) value reported by Rabung et al. (2000) for Eu(III) speciation at the "weak" site, however, differs from that found in the present study. Change in log K value is attributed to selection of different binding geometry in two studies. Rabung et al. (2000) considered the formation of monodentate binding at both strong and weak sites while in the present study, with the TRFS and XAFS informations bidenticity at weak site was considered more appropriate. Speciation data (figure 4.6) indicates that while the mononuclear surface species is the predominant surface species for Am(III)/Eu(III) at lower metal ion concentrations (10^{-7}-10^{-6} M), the bidentate surface species starts to compete with monodentate speciation substantially after pH 5.5 at 1.0×10^{-5} M and becomes the predominant surface species of Am(III)/Eu(III) on alumina surface at 1.0×10^{-4} M.

4.2.3 Conclusion

Sorption of Am(III)/Eu(III) by γ-alumina increases with pH (3-10) and is independent of ionic strength, indicating inner sphere complexation of metal ions with alumina surface

sites. With increasing metal ion concentration the sorption edge shifts to higher pH values, suggesting heterogeneity in metal ion coordination at alumina surface sites. The existence of two surface species having different denticity on alumina surface is shown by TRFS. Based on EXAFS results, the two species are (a) mononuclear monodentate $\equiv AlOAm^{2+}$, and (b) mononuclear edge sharing bidentate, $(\equiv AlO^{-})_2Am^{+}$. SCM of the sorption data for pH ≤ 7 using these two species shows the predominance of the bidentate speciation at higher metal ion concentration.

4.3 XAFS study of Eu(III) sorption on silica and alumina

Silica (SiO_2) and alumina (Al_2O_3) are important oxide minerals in the geological environment. Apart from their role in radionuclide retention and migration, investigation on such solids may reveal the reactivity of clay minerals. Clay minerals contain layers of silicon and aluminium oxides and bonding on the sites attributed to oxide surface is parallel to that found on pure oxide surfaces (Tertre et al., 2006). These solids are structurally different substrates. Si atoms are tetrahedrally surrounded by oxygen atoms in silica, whereas Al is present in both the tetrahedral as well as octahedral sites of the close-packed arrangement of oxygen atoms in alumina. Surface site silanol (≡SiOH) in silica is, therefore, attached to a tetrahedron and aluminol (≡AlOH) site in alumina is attached either to a tetrahedron or an octahedron, which may cause significant change in the surface reactivity of these two solids towards metal ions and, in turn, may change the surface speciation of metal ions (Cheah, et al., 1998).

Recently, synchrotron based X-ray absorption fine structure (XAFS) spectroscopic studies have been successfully applied in delineating surface speciation of metal ions on solid surfaces. Characteristics metric informations form XAFS (identification, oxidation state, number, and bond lengths of the neighbouring atoms around the probe atom) enable the determination of structure of the surface species (Cheah et al., 1998; Manceau et al., 1999; Trainor et al., 2000; Ha et al., 2009).

Literature update on XAFS investigation on silica and alumina surfaces

Very few literature studies have probed speciation of trivalent lanthanides/actinides in sorption on silica and alumina surfaces using XAFS.

In EXAFS study of Nd and Lu sorption on silica (Schlegel et al., 2011), no effect of pH on surface speciation was found in the pH range of 6 to 9, with the formation of edge sharing surface complex of Nd/Lu on silica tetrahedra. In another EXAFS study for the mechanism of

Eu retention on calcium silicate hydrates, even in the metal concentration and pH range amenable to precipitation there was no evidence of $Eu(OH)_3(s)$ on the solid surface (Schlegel et al., 2004). Fourier transforms of EXAFS spectra of Eu for both adsorption and precipitation samples exhibited comparable structural features, pointing to similar crystallographic environments. EXAFS investigation of Nd- and Lu- sorbed on layered silicate, hectorite ($[Mg_{2.77}Li_{0.66}]Si_4O_{10}(OH)_2$), however, shows distinct spectral dissimilarities when compared with spectral features observed for silica (Schlegel et al., 2011).

Rabung et al. (2006) carried out EXAFS investigation on alumina surface using Gd and Lu as probe atom. The study identified a single oxygen coordination shell with a high degree of disorder. Authors thereby concluded mononuclear monodentate speciation on the surface, and shells beyond the first neighbour could not be delineated in this study. Dardenne et al. (2001) observed monodentate Lu sorbed species on hematite (iron oxide/hydroxides are isomorphous to alumina) at pH 8, while edge sharing bidentate binding of Lu was obtained on amorphous 2-line hydrous ferric oxide above pH 5.5.

In view of geological importance of silica and alumina substrates, it is necessary that speciation of trivalent lanthanides/actinides on these surface under conditions ranging from adsorption to precipitation should be understood on the molecular level.

Present Study

Eu(III) sorption onto amorphous silica (am-SiO_2) and γ-alumina (γ-Al_2O_3) has been examined in near neutral pH conditions (6-8) with X-ray absorption fine structure spectroscopy. Eu(III) has been chosen as an analogue for various long-lived trivalent lanthanides and actinides. Absorption spectra were collected for samples equilibrated with Eu(III) solutions under- and over- saturated with respect to solid Eu-hydroxide with an aim to elucidate the role of pH and mineral substrate in influencing the local atomic coordination and binding of trivalent lanthanides/actinides on naturally occurring mineral oxides.

4.3.1 Experimental details

Details on sample preparation and data analysis have been discussed in chapter 2, section 2.4.

4.3.2 Results and discussion

4.3.2.1 Batch sorption experiment

Eu(III) sorption on silica and alumina (figure 4.7) rises sharply over pH 6-7 range, starting from ~ 5 % at pH 4 to quantitative sorption at pH 7. Sorption profile is sharper in case of alumina in comparison to silica. This agrees with the literature report suggesting

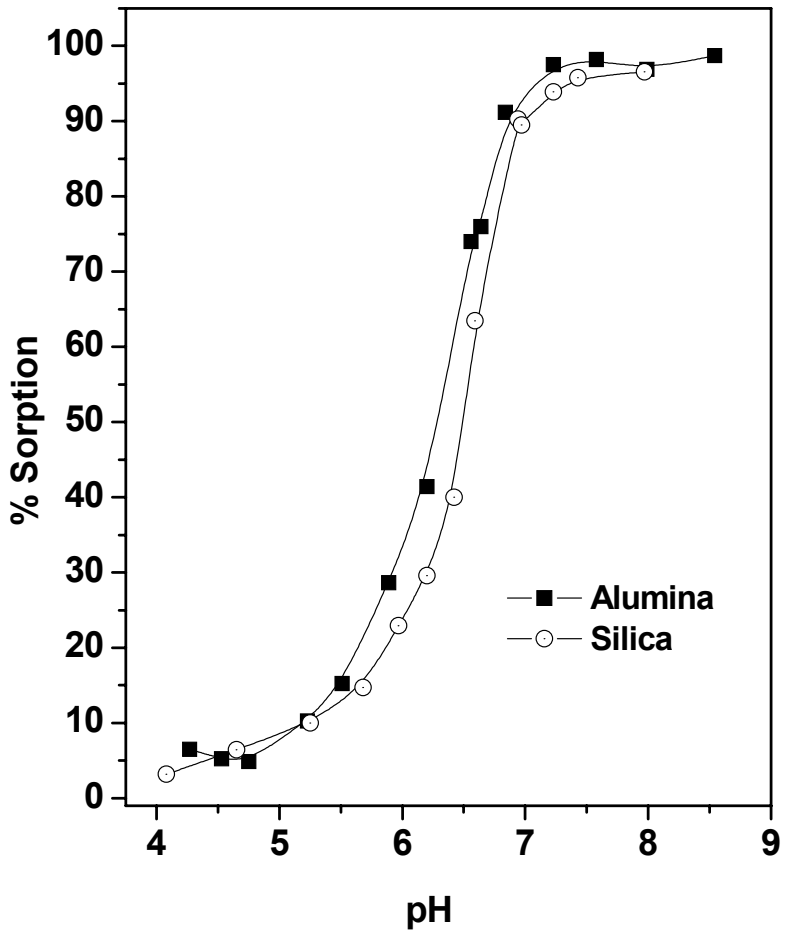

Figure 4.7 Eu(III) sorption onto am-SiO_2 and γ-Al_2O_3 as a function of pH.

higher sorption ability of alumina (Kowal-Fouchard et al., 2004). Table 4.4 lists Eu sorption density on silica and alumina under the studied pH conditions.

Table 4.4 Eu(III) sorption on silica and alumina

Solid	pH	% Sorption	$\Gamma_{(Eu\ Sorbed),}$ ($\mu mol/m^2$)
am-Silica	6.08	26.4	0.144
	7.05	91.2	0.506
	8.02	96.4	0.536
γ-Alumina	6.18	42.8	0.208
	7.15	95.7	0.472
	8.17	97.4	0.480

Sorption process may follow different mechanisms ranging from adsorption to surface precipitation. A preliminary assessment about the possible mode of Eu(III) binding on silica and alumina indicates Eu binding on silica/alumina in monodentate and/or bidentate manner in case of surface adsorption, while the precipitation of Eu with hydroxyl ions, dissolved silicates and aluminates may occur in case of surface precipitation. Figure 4.8 shows the variation of $\log([Eu]_{disso})$ vs. pH while considering solubility of $Eu(OH)_3$ in the pH range. The dotted line represents for the initial Eu(III) concentration (10^{-4} M) and the symbols are for the final concentration of Eu(III) left in the supernatant after equilibration in the XAFS sorption samples. Europium hydroxide solubility calculation was carried out at fixed ionic strength of 0.1 M $NaClO_4$ using the formation constant given in Yun et al. (2001) for different hydroxide species. Eu(III) solubility in case of both the solids follows the same trend. At pH ~ 6 it is in under-saturated state with Eu(III) concentration two orders of magnitude below the solubility limit. It falls just below the solubility limit at pH ~ 7 while it is in oversaturated state at pH ~ 8. However, as the silica and alumina have significant

solubility over the pH range (figure 4.9) the possibility of precipitation of Eu-silicates or Eu-aluminates in the sorption samples cannot be ruled out. In fact, silicate formation has been observed in various sorption studies on silica at higher surface coverage (O'Day et al., 1996)

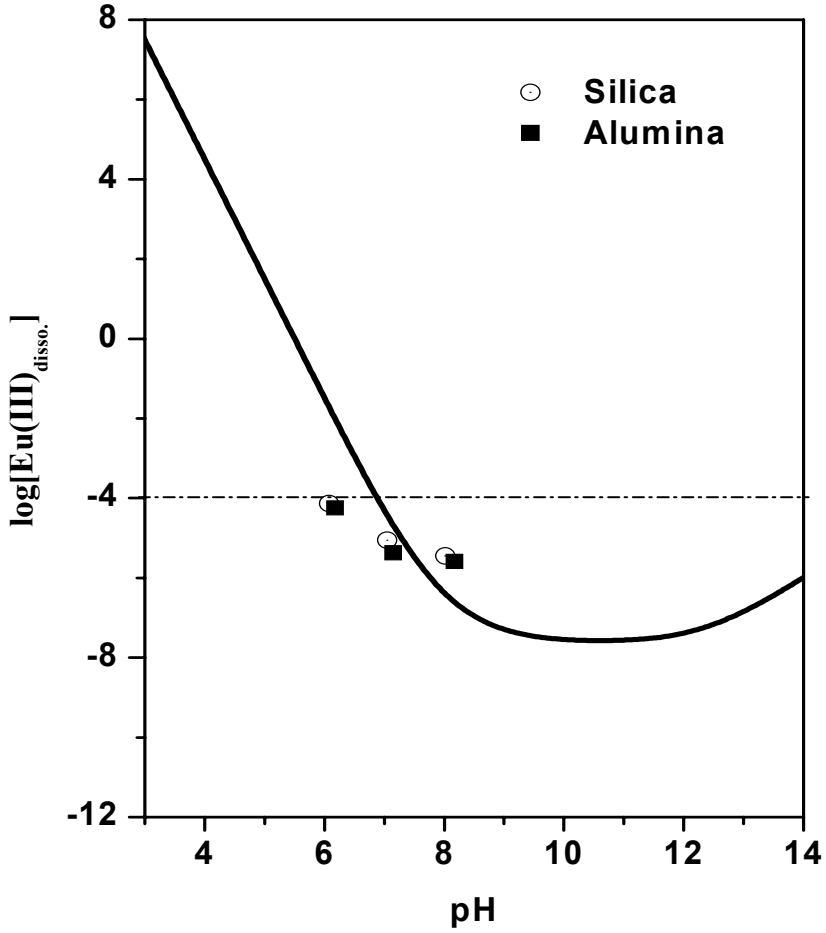

Figure 4.8 Calculated $Eu(OH)_3$ solubility curve as a function of pH. The different species contributing to the solubility of europium hydroxide include, Eu^{3+}, $Eu(OH)^{2+}$, $Eu(OH)_2^{+}$, $Eu(OH)_3(aq.)$, $Eu(OH)^{-}_4$.

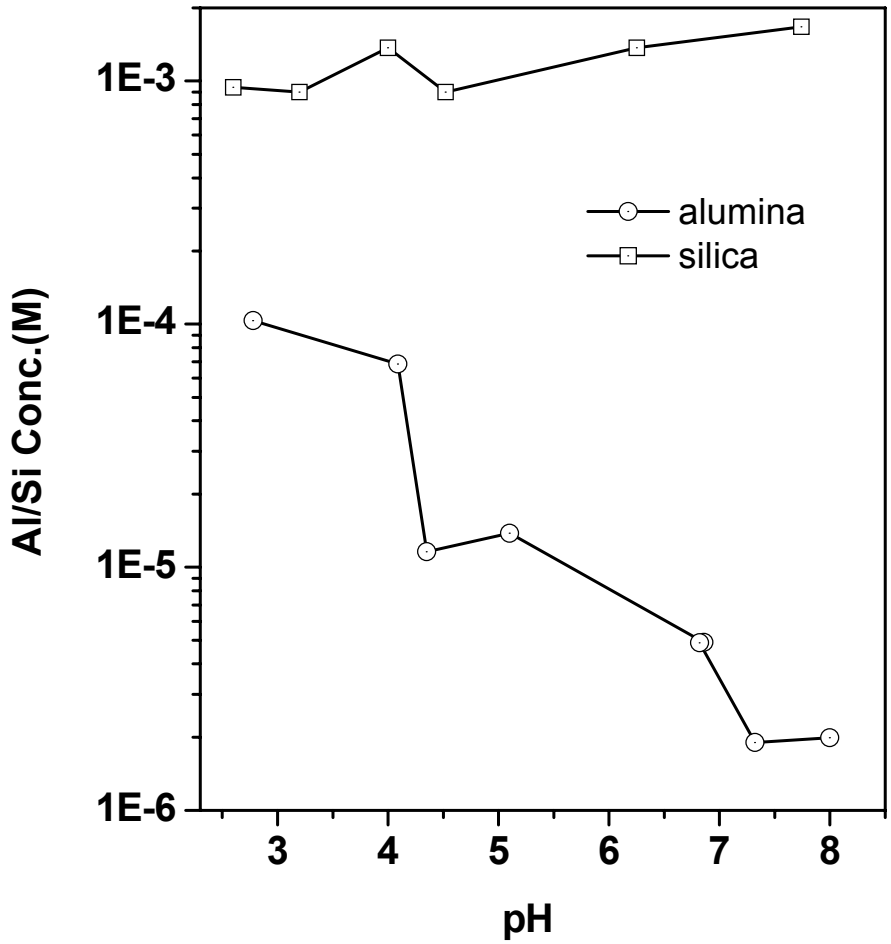

Figure 4.9 Solubility of silica and alumina (3 g/l suspension) measured over pH 3 – 8 in 0.1 M $NaClO_4$ medium.

4.3.2.2 XANES measurement

XANES spectra of all the reference solids and sorption samples fall at the same position (figure 4.10). Position of X-ray absorption edge at ~ 6982 eV compares well with that for trivalent Eu in solids and is located at significantly higher energy than the maximum of X-ray absorption edge for divalent Eu (~ 6973 eV) (Yoshida et al., 2000). This indicates the existence of +3 oxidation state for Eu in all the sorption and reference samples.

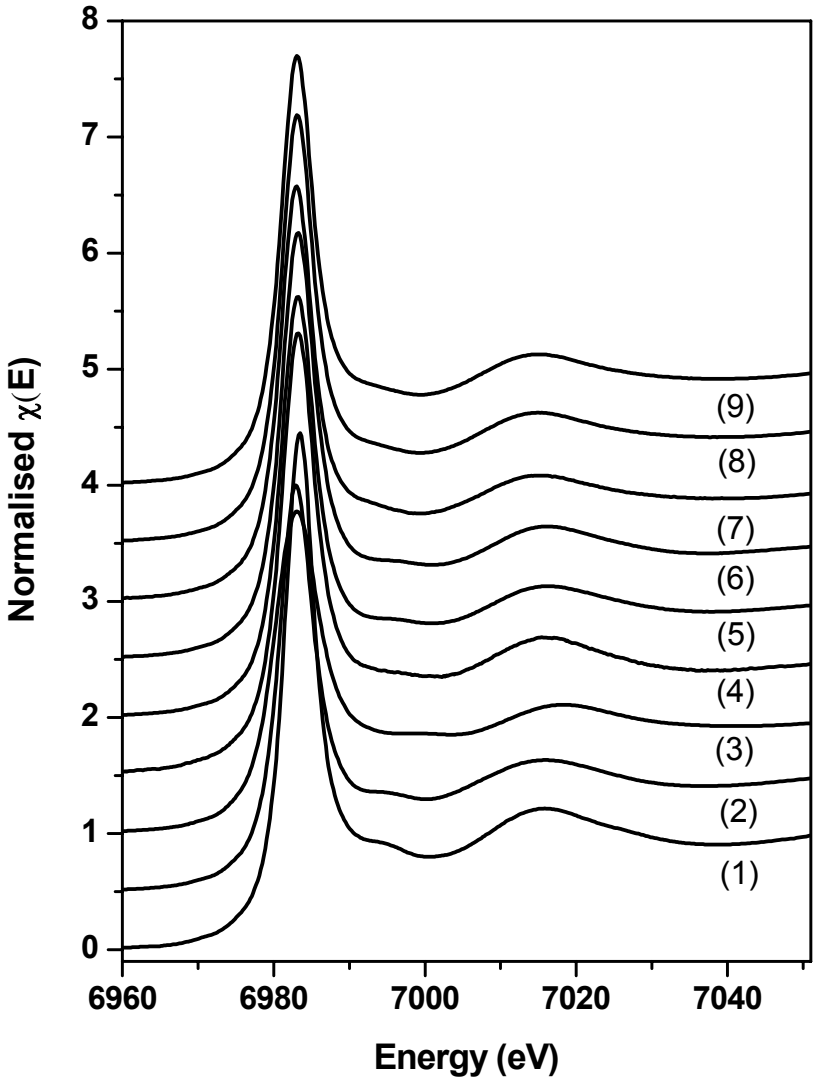

Figure 4.10 XANES spectra of Eu(III) reference and sorption samples. (1) Eu(aqua), (2) $Eu(OH)_3$ (solid), (3) Eu_2O_3 (solid),(4) Eu-silica-pH 6.08, (5) Eu-silica-pH 8.02, (6) Eu-silica-pH 7.05, (7) Eu-alumina-pH 6.18, (8) Eu-alumina-pH 7.10, (9) Eu-alumina-pH 8.17.

4.3.2.3 EXAFS measurements

Reference samples

EXAFS spectra of the reference samples (figure 4.11) show increasing structural complexity from Eu(aq) to Eu_2O_3. Eu(aq) spectrum has a monotonically decreasing beat pattern beyond k = 3.0 $Å^{-1}$, characteristic of the presence of a single neighbouring shell. Oscillating patterns in the k-space spectra of two other reference samples clearly indicate the presence of many shells. Table 4.5 lists the required shells to model the EXAFS spectra of these reference samples along with the quantitative estimates for the parameters of each shell, found in the fitting of the Fourier transform of the EXAFS spectra (figure 4.11b). Symbols R, N and σ^2 carry conventional meaning (cf. Chapter 2, section 2.4). ΔE, R_f stand for energy shift, and residual factor ($= \sum_k (k^3\chi_{\exp} - k^3\chi_{calc}) / \sum_k (k^3\chi_{\exp})$), respectively, in the EXAFS

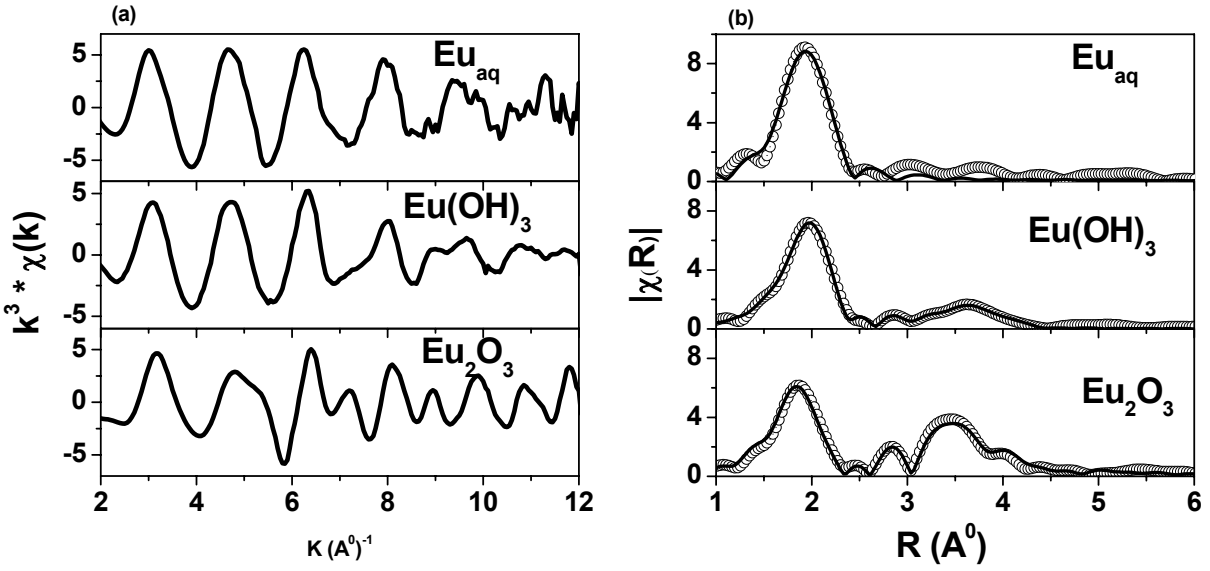

Fig. 4.11 (a) k^3 weighted Eu-L_{III} EXAFS spectra of Eu(III) reference samples. (b) Experimental (open symbol) and simulated (solid line) moduli of the Fourier transforms for the reference samples.

equation. The residual factor measures the quality of the fitted model with respect to the experimental data. Parenthetic data shows the estimated standard deviation on the main value.

Table 4.5 Structural parameters from EXAFS analysis of Eu(III) reference solids

Sample	path	R	N	σ^2	ΔE(eV)	R_f
Eu(aq)	Eu-O	2.420 (0.002)	9.0*	0.008(0.001)	0.9	0.03
$Eu(OH)_3$(s)	Eu-O	2.432(0.007)	7.7(0.6)	0.010(0.001)	3.1	0.01
	Eu-Eu	3.672(0.004)	1.7(0.6)	0.007(0.001)	3.4	
	Eu-O-O	3.918(0.004)	30.6(0.6)	0.013(0.008)		
	Eu-O	3.944(0.003)	2.5(0.6)	0.013(0.008)		
	Eu-Eu	4.090(0.006)	5.1(0.6)	0.014(0.002)	0.40	
	Eu-Eu-O	3.993(0.007)	10.3(0.6)	0.010(0.005)		
	Eu-O	4.114(0.007)	5.1(0.6)	0.010(0.005)		
Eu_2O_3(s)	Eu-O	2.340(0.014)	6.0*	0.011(0.001)	0.72	0.11
	Eu-Eu	3.601(0.018)	6.0(0.1)	0.009	0.71	
	Eu-Eu	4.071(0.001)	6.0(0.1)	0.010(0.005)		
	Eu-O	4.235(0.004)	6.0(0.1)	0.010(0.005)		
	Eu-Eu-O	4.334(0.001)	12.0(0.1)	0.010(0.005)		

**: values are fixed during the fitting.*

Sorption samples

EXAFS spectra of Eu(III) sorbed onto silica and alumina (figure 4.12 (a)) appear similar in beat pattern to the Eu(aq) and $Eu(OH)_3$, though not exactly same. Below 6.3 $Å^{-1}$, at which the maxima in the oscillation pattern was observed, all the sorption samples, Eu(aq) and $Eu(OH)_3$ have similar features exhibiting Eu-O as the shell responsible for this feature. Oscillations in the 9-10 $Å^{-1}$ range for the sorption samples appear at higher k than that in case of Eu(aq) and are different from that for $Eu(OH)_3$. The difference in the EXAFS spectra of sorption samples

from that of $Eu(OH)_3$, in the k range of 9-10 $Å^{-1}$ suggests the absence of surface precipitation of Eu(III) in the former at all the pH values, despite the over-saturation conditions at pH=8.

Figure 4.12 (b) shows the EXAFS data in R- space. The solid lines in figures represent the modelled data. Figure 4.12 (c) represents the back-Fourier transformed data of figure 4.12 (b) over R window 1.2 - 4.2 Å. The first shell in the spectra appearing at R ~ 1.8 Å compares well with the Eu-O shell of the Eu- reference samples confirming the Eu-O as the first shell of the Eu-sorption product on the surfaces of silica and alumina.

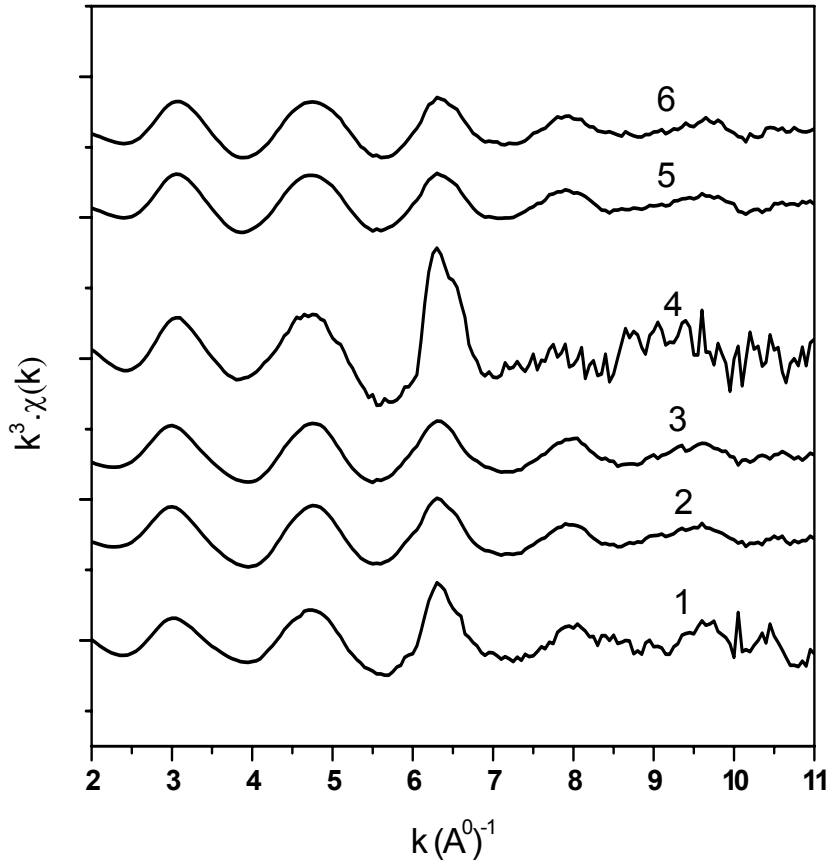

Figure 4.12 (a) k^3 weighted Eu-L_{III} EXAFS Spectra of Eu(III) sorption samples. Numbers 1-3 stand for Eu sorption on alumina at pH 6 to 8, respectively and spectra numbered 4 to 6 are for Eu sorbed onto silica at pH 6-8.

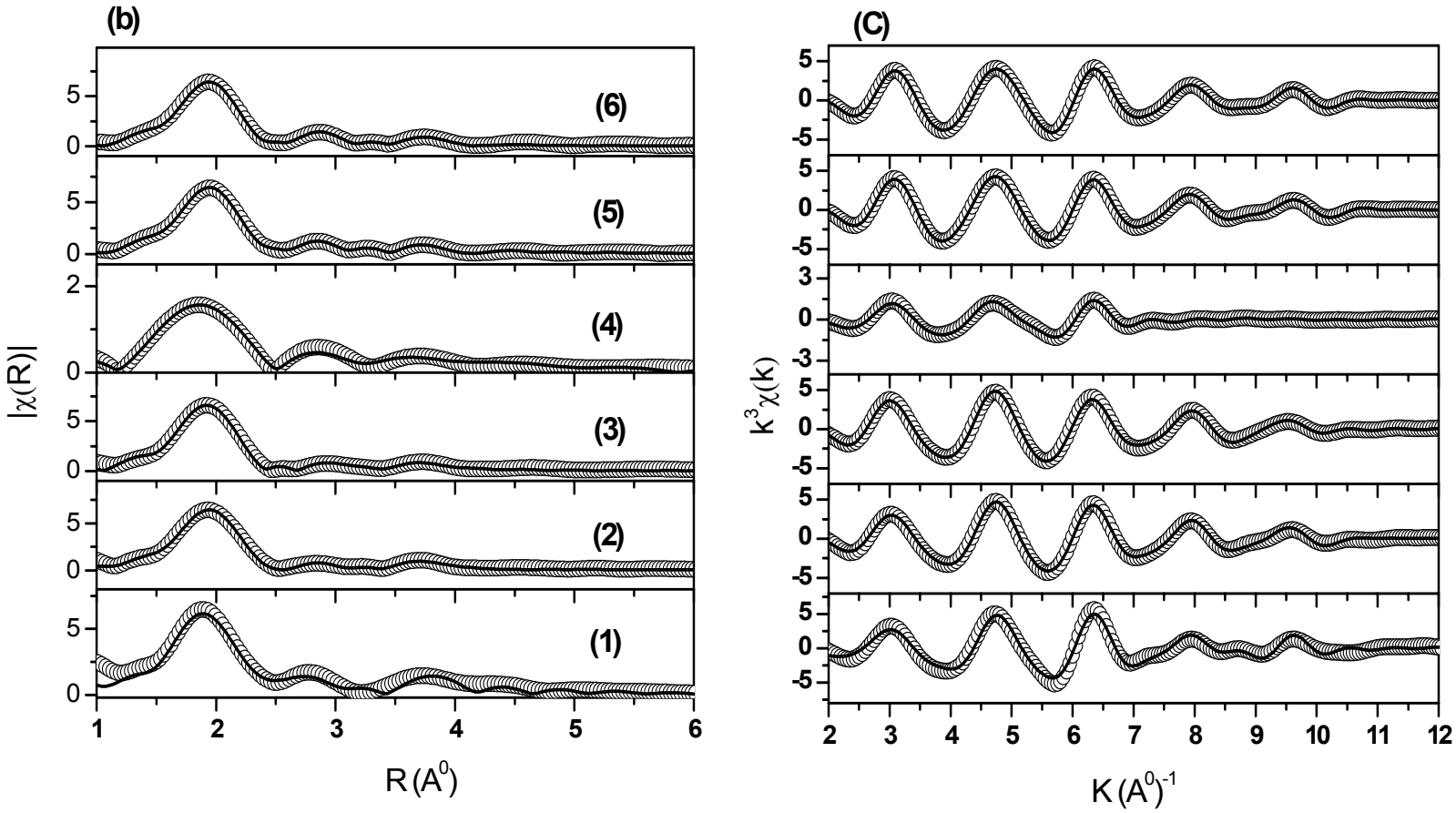

Figure 4.12 (b) FT magnitude of EXAFS spectra. Open symbol is for the experimental data while the solid line is the fitting line. (c) Experimental (open symbol) and modeled (solid line) Fourier filtered $K^3.\chi(k)$ Contributions for the next-neighboures backscattering shells in R range 1.2-4.2 Å.

Next prominent peak in the sorption samples is at ~ 2.8 Å (phase uncorrected) which is absent in Eu(aq.) and matches with a peak in $Eu(OH)_3$ and Eu_2O_3 spectra. This peak is due to Eu-Eu shell in the reference samples, but was fitted only with Eu-Si/Al shells in the sorption samples (Table 4.6). Similarly the peak in the sorption samples at ~3.7 Å, though matches with $Eu(OH)_3$, could be fitted only considering the Eu-Si/Al shells.

First shell fitting

The FT peak at 1.8 Å for all the sorption samples was modelled by assuming a single oxygen shell in R-space over 1.2-2.5 Å. The fits yielded N_O value as 7.1 ± 0.4, and R_{Eu-O} distances 2.41 ± 0.01 Å (Table 4.6). The R_{Eu-O} distance is longer than R_{Eu-O} = 2.34 Å for hexadentate Eu in Eu_2O_3, and marginally shorter than R_{Eu-O} = 2.42 Å for 9-cordinated Eu in water (Eu(aq)). First shell coordination for lanthanides decreases from 9 to 8 as we move from La to Lu and in a recent study it has been shown that Eu(III) actually exists as a mixture of both 8- and 9-fold coordinated form in Eu(III) aqua ions (Marmidee et al., 2010). Taking into consideration the uncertainty associated with the analysis for first shell (10% for N value), this means Eu is hepta to octa coordinated in the sorption products. As expected, R_{Eu-O} = 2.41 Å and N_O value compare well with the coordination of Eu substituted on calcium site in calcium silicate hydrate (Schlegel et al., 2004) and Gd sorbed on γ-alumina (Rabung et al., 2006). The similarity of this shell for both the substrate and all the pH values indicates the similarity of primary interaction mechanism of Eu on these two substrates.

Higher shell fitting (Eu-Si/Al)

FT features over 2.5 - 4.2 Å indicate mainly two peaks. However, back transformation of higher pH spectra presents a beat pattern maximizing at three k values (~ 3, 6.5, and 9 $Å^{-1}$)

Table 4.6 Results of the quantitative analysis of EXAFS spectra of Eu(III) sorption samples

sample/ pH	Eu-O			Eu-Si/Al			Eu-Eu			Eu-Si/Al		
	N	R	σ^2	N	R	σ^2	N	R	σ^2	N	R	σ^2
Silica 6.08	7.1	2.41	0.008	2.2	3.24	0.011				4.0	4.01	0.007
	(0.1)	(0.03)	(0.005)	(0.1)	(0.04)	(0.007)				(0.01)	(0.04)	(0.001)
Silica 7.05	6.9	2.41	0.011	2.0	3.27	0.008	1.6	4.02	0.02	3.8	4.01	0.014
	(0.1)	(0.03)	(0.002)	(0.1)	(0.02)	(0.010)	(0.1)	(0.11)	(0.008)	(0.05)	(0.01)	(0.003)
Silica 8.02	6.8	2.40	0.009	1.2	3.19	0.008	3.7	4.00	0.015	2.2	4.02	0.007
	(0.5)	(0.005)	(0.001)	(0.1)	(0.02)	(0.004)	(0.02)	(0.04)	(0.008)	(0.1)	(0.02)	(0.003)
Alumina 6.18	7.7	2.39	0.010	2.1	3.23	0.015				3.4	4.07	0.006
	(0.6)	(0.030)	(0.005)	(0.1)	(0.07)	(0.009)				(0.04)	(0.04)	(0.001)
Alumina 7.15	7.3	2.41	0.009	2.4	3.22	0.018	0.9	3.45*	0.018	3.2	4.03	0.011
	(0.1)	(0.01)	(0.001)	(0.4)	(0.08)	(0.008)	(0.03)		(0.01)	(0.07)	(0.02)	(0.003)
Alumina 8.17	6.7	2.41	0.009	3.6	3.34	0.017	2.5	3.53	0.018	2.4	4.02	0.009
	(0.2)	(0.10)	(0.001)	(0.1)	(0.11)	(0.002)	(0.2)	(0.04)	(0.008)	(0.1)	(0.08)	(0.001)

*Values given in the parentheses, below the main value, are estimated standard deviation on the main value obtained in the least square fitting routine. *: values kept fixed in the fitting.*

with the beat pattern intensity at ~9 $Å^{-1}$ substantially reduced in case of alumina than silica. This suggests a complex structural arrangement in the sorption products. Due to this complexity, the approach used here was to propose different structurally reasonable silicate/aluminate clusters around the sorbed Eu as the initial fit model and then to adjust the parameters to get a good match of the back transformed k data. Evaluation of $Eu(OH)_3$ as the fitting model produced no sensible sets of parameters for the best fit case. Inclusion of a Eu shell was found necessary for modelling EXAFS spectra of higher pH values, especially to model the small peak like feature at ~3.5 Å and the peak at ~ 4 Å.

The best fit model was found with two Si/Al shells at ~ 3.22 and 4.01 Å and a Eu backscatterer shell at 4.00 Å for silica (3.45-3.53 Å for alumina) at higher pH values (7-8) (Table 4.6). N_{Si} for Si shell at ~3.22 Å decreases with pH while N_{Al} for Al shell at 3.22 Å increases with pH. Considering Eu-Al/Si distances in all possible coordination geometry on alumina/silica surface (cf. appendix 3), ~3.22 Å shell relates to Eu bonded to Si or Al in edge sharing manner and ~4 Å shell corresponds to corner sharing binding of Eu to Si/Al polyhedra. The relative trend for number of coordinating Si/Al atoms at ~ 3.22 Å shell, thus, suggests that while the corner sharing mode of interaction is more preferred for silica, Eu binds to alumina surface predominantly in edge sharing manner. Similar conclusion was arrived at in the XAFS study of Cu(II) sorption on amorphous silica and γ- alumina at lower surface coverage (Cheah et al., 1998).

Higher shell fitting (Eu-Eu)

For Eu shell, N_{Eu} increases with pH for both silica and alumina, with the enhancement being more significant in silica than alumina. Higher N_{Eu} value for silica can be attributed to its weaker sorption capacity (compared to alumina) and higher dissolution tendency, resulting in co-precipitation of Eu with the dissolved silica species.

High $N_{Si/Al}$ value at 4 Å shell for the sorption samples at pH 6 indicates the formation of some small multinuclear atomic cluster. This atomic cluster consists of Eu bound in monodentate manner to many oxygen atoms present at the corner of silica or alumina polyhedra. At higher pH, many such atomic clusters may come together forming Eu-Eu bonds and thereby resulting in bigger multinuclear complex.

Multinuclear sorption product formation on oxide surfaces, at higher surface coverage, has been observed as norm rather than exception (Charlet and Manceau,1992; Towle et al., 1997; Rabung et al., 2000; Trainor et al., 2000; Ha et al., 2009). Eu forming multinuclear surface species on silica surfaces at higher surface coverage has been reported in studies involving batch sorption (Takahashi et al., 1998) and fluorescence investigations (Kar et al., 2011). Very few studies examine the sorption products of trivalent lanthanides/actinides on alumina surface at higher surface coverage. At lower surface coverage, rare earth ions (Lu & Gd) exhibit monodentate binding on γ-alumina (Rabung et al., 2006) while fluorescence and EXAFS based characterization of sorbed lutetium species onto synthetic hydrous ferric oxide at pH ≥ 5.5 exhibits edge shared binding in surface complex formation. Fe-oxides/hydroxides are isomorphous to aluminium oxides/hydroxides and sorption products ranging from surface adsorption to surface precipitation have been observed with the increasing Zn(II) sorption density on hematite (Ha et al., 2009).

4.3.3 Conclusion

The present study investigates Eu(III) sorption products on silica and alumina surfaces under varying pH conditions corresponding to under-saturation to over-saturation with respect to $Eu(OH)_3$ formation. The surface charge characteristics and solubility of the two solids are quite different. XANES spectra indicate the presence of Eu in +3 oxidation state for all sorption products. Quantitative results for the modeling of the EXAFS data indicate

similar binding geometry of Eu on both amorphous silica and γ-alumina. Eu binds in edge as well corner sharing mode for both the solids, though the formation pattern of these two types of binding differs. Silica surface prefers corner sharing binding mechanism while edge sharing binding is more favoured in the sorption product onto alumina surface. At pH ~ 6, Eu forms sorption species involving corner sharing and edge sharing mononuclear binding whereas EXAFS spectra at higher pH values indicate the formation of atomic cluster containing Eu. At higher pH values, the number of coordinating Eu atoms is more for silica than alumina indicating the effect of sorption capacity and dissolution characteristics on the sorption product. Our results demonstrate that variation in characteristics of the solids affects the mode of Eu sorption, and pH plays an important role in the formation of different sorption products.

4.4 Pu(IV) sorption on mineral oxides

Plutonium has long lived radioisotopes such as ^{239}Pu (24110 yrs) and ^{240}Pu (6561 yrs), which dominate the α-activity of spent nuclear fuel. These are mainly α-decaying isotopes and carry environmental concern due to strong and nearly irreversible interaction with bone and liver cells of mankind (Durbin, 2010). In addition, Pu shows complex chemistry in the groundwater chemical condition (Choppin, 2006). Variable oxidation states of Pu, ranging from III to VI, have been observed in seawater to dilute salt solutions (Morse et al., 1991). Pu(IV) forms strong hydroxide complexes and precipitates as $Pu(OH)_4(s)$ (log K_{sp} = -58.7 ± 0.9) in neutral pH conditions (Choppin and Stout, 1989; Kim et al., 1989). Aqueous phase solubility of Pu is thus primarily governed by plutonium oxide/hydroxide solid phase. The redox potentials for Pu couples in different oxidation states lie relatively close to each other (E^0 ~1 V) (Degueldre et al., 2009). Higher pH and oxidizing conditions of the aquatic system thus favour the formation of plutonium in higher oxidation states, Pu(V) and Pu(VI), while reducing Eh values at lower pH produces Pu(III) (Silva and Nitsche, 1995). pH and Eh of ground water at a location is decided by its geochemistry and can alter the oxidation state of Pu thereby effecting oxidation state dependent sorption behaviour of Pu on mineral surfaces (Degueldre et al., 2009). System pH also greatly affects Pu hydrolysis and complexation (Rai, 1984), both of which may in turn influence the geochemical behaviour of Pu.

Literature update on Pu sorption on oxide surfaces

Previous studies have shown high affinity of Pu(IV) for solid phases such as iron oxides, magnesium hydroxide, and silica (Powell et al., 2005; Farr et al., 2000; Lu et al., 2003; Righetto et al., 1991). Sorption studies of higher (V and VI) oxidation state of Pu on mineral oxides have also indicated surface meditated oxidation state transformation to Pu(IV) with different kinetic rates (Powell et al., 2004, 2006). For a redox sensitive element like Pu, change in the sorption behaviour can happen when Pu oxidation state changes either in the

aqueous phase or on the solid surface during sorption process. Time dependent oxidation of PuO_2^+ to Pu(VI) and subsequent reduction to Pu(IV) have been observed on MnO_2 surface (Powell et al., 2006). In the long term transport study conducted in sediment from the Savannah river site, Pu mobility was found underestimated by a factor of 3.5 on the assumption that all Pu exists as Pu(IV) (Kaplan et al., 2006a). Among the colloidal particles investigated for Pu sorption, extensive studies has been devoted to redox sensitive solids such as iron and manganese oxides (Powell et al., 2004, 2005, 2006; Lu et al., 2003). Relatively less information is available in the literature with regard to oxidation state characterization of Pu on silica, alumina or clay surfaces even though it is important for the near-field behaviour of Pu.

Sanchez et al. (1985) observed significant difference in sorption behaviour of Pu(IV) and Pu(V) on goethite and, based on the shift of Pu(V) pH-sorption edge with time to lower pH values and redox speciation, proposed reduction of Pu(V) to Pu(IV) on the goethite surface. In a comparative adsorption-reduction study of Pu(V) on hematite and goethite, reduction to Pu(IV) was obtained with the adsorption on hematite as the rate-limiting step (Powell et al., 2005). In contrast, Pu(V) adsorption on goethite was found to occur faster than its reduction to Pu(IV). Fraction of oxidation states (IV, V and VI) of plutonium in the aqueous and solid phase showed the dependence on pH and nature of the solid surface. X-ray absorption fine structure measured at the Pu L_{III} edge showed that Pu(VI) was reduced (Pu(IV) and Pu(V)) in contact with manganite (MnOOH) and hausmannite (Mn_3O_4) with higher fraction of Pu(IV) formed on Mn_3O_4 (Shaughnessy et al., 2003). In Pu(V) sorption on red subsurface sandy-clay-loam sediment, Pu_{aq} was found in V ($\geq$ 94%) and VI ($\leq$6%) oxidation states in contrast to the IV state of sorbed Pu (Kaplan et al., 2006b). The desorption studies conducted with the sediment in contact with Pu for 24 years, showed similar oxidation state distribution and the solubility of the sorbed Pu was found parallel to that of PuO_2(am.).

Pu(V) sorption on silica was found to be slower than that on hematite colloids, though, desorption was faster (Lu et al., 2003). This has been attributed to the lack of efficient electron donor sites in the silica surface leading to less efficient reduction of Pu(V). X-ray absorption spectroscopic investigation of Pu(V) sorbed on different clays and mineral oxides surfaces indicated IV as the oxidation state of surface sorbed Pu and concluded the disproportionation in the aqueous phase as against the surface mediated reduction for slower rate of adsorption and faster desorption from silica and clay surfaces (Kersting et al., 2003). In the microscopic study of plutonium nanocolloids formed on mineral oxides, Powell et al. indicated the formation of 2-5 nm sized PuO_2 and Pu_4O_7 nanocolloids on silica (α-SiO_2) and goethite (α-FeOOH) and attributed slower desorption rate of Pu from goethite to the favorable structural alignment of Pu_4O_7 nanocolloids with the goethite surface (Powell et al., 2011). Such studies on alumina are unambiguously lacking in the literature.

Present study

The objective of this study was to evaluate the impact of pH and the nature of solid surface, on concentration and speciation of Pu in aqueous phase as well as on silica and alumina surfaces using sorption, desorption and kinetic studies. To perform the experiments with lower metal ion concentration (~10^{-9} M), higher specific activity radioisotope of Pu, namely, ^{238}Pu has been used. At nanomolar plutonium concentration, Pu speciation by spectroscopic method was not feasible, hence, solvent extraction based analysis has been carried out to determine oxidation state of Pu in aqueous phase and on solid surface. The two solids used are the main components of the various aluminosilicates found in nature and the role of these solids towards Pu(IV) sorptions/desorption could help in making better prediction of the source term for Pu migration in geosphere.

4.4.1 Experimental details

4.4.1.1 Materials

The details of the source and characterization of silica and alumina have been discussed in chapter 3. AR grade thenoyl trifluoro acetone (TTA) and bis (ethyl hexyl) phosphoric acid (HDEHP) used in the experiment were procured from Lancaster. Freshly prepared TTA solution was used in the experiment as TTA is photosensitive. Solvents (xylene and heptane, both AR grade) used in the extraction experiments were obtained from BDH. Aqua Light liquid scintillation cocktail (Hidex, Finland) was used for Liquid scintillation counting (LSC, Electronics Corporation of India Ltd.). Combination type pH electrode connected with M/s. Lab India pH meter (pico model) was used in the pH measurement and Combination type Pt-Ag/AgCl (Metrohm) redox electrode was used for Eh measurements. Calibration of the pH meter was carried out using pH 4.0, 7.0, and 9.0 buffers and Eh electrode standardization was checked by Metrohm redox standard. ^{238}Pu, used as a radiotracer for plutonium, was obtained from Fuel Chemistry Division, BARC. Pu-stock ([Pu] = 2.5×10^{-7} M) was prepared in 1 M HNO_3 medium and the isotopic purity of the stock was checked by alpha spectrometry (Canberra). Oxidation state of Pu in the stock solution was found to be IV (~98%) by TTA/Xylene based solvent extraction procedure (Morss et al. 2010).

4.4.1.2 Sorption experiments and analysis of sorption kinetics

50 µl of the Pu(IV) stock solution (~1643 Bq) was added to silica and alumina suspensions (5g/l and 4.5 g/l, respectively to have equal surface area) prepared in 0.1 M $NaClO_4$ and pH was adjusted over the range 2-9 using NaOH and $HClO_4$. Prior to metal ion addition, silica/alumina solids were equilibrated overnight with 0.1 M $NaClO_4$ to ensure hydroxylation of the surface sites. All the sorption/ desorption/ leaching experiments were carried out in 50 ml polypropylene tubes under ambient condition (25 ^{0}C). Sorption of Pu on the wall of these tubes was found to be very less (~2-3% at higher pH values), but was considered in all the experiments. In the kinetic experiments, aliquots were taken at various

intervals of time while in the sorption experiment, an aliquot of the suspension was taken at the attainment of the steady state condition (48 hrs). pH (± 0.1) values in the kinetic experiments were ~ 3.2, 6.2, and 8.5. Samples were rotated in a shaker (model Rotospin, Tarsons) in top-down manner at 50 rpm during the period of equilibration. Aliquots were checked for pH and Eh, centrifuged for phase separation at 16000 rpm for 45 min (High speed centrifuge, Sigma) and 1 ml of the supernatant was mixed with 5 ml of Aqua Light scintillator to measure ^{238}Pu alpha activity by liquid scintillation counting. Percentage Pu sorption was calculated by the difference of the Pu activity initially added and that present in the supernatant after equilibration. Error on the sorption and kinetic data has been calculated by propagating the statistical uncertainty of the LSC counts as detailed in chapter 2.

4.4.1.3 Desorption and leaching experiments

For desorption experiment, solid phase of the sorption experiment (carried out for 48 hrs) was contacted with the fresh 0.1 M $NaClO_4$ solution of the pH value same as that in the sorption experiment. After the 48 hrs equilibration in the top-down shaker, pH was checked and after centrifugation, 1 ml of the supernatant was assayed for alpha activity to get the Pu amount desorbed at the respective pH value. In the leaching experiment, sorption samples at pH ~7-8, equilibrated for 48 hrs and that equilibrated for 16 months, were contacted with pH 1.5 $HClO_4$ solution for 48 hrs. The leached ^{238}Pu activity was determined by LSC counting.

4.4.1.4 Oxidation state analysis

Pu oxidation state distribution in the supernatant of the kinetic experiments was determined using a combined centrifugation and solvent extraction technique. This technique was initially employed by Keeney-Kennicutt and Morse (1985) and subsequently modified by Morgenstern and Choppin (2002) and Powell et al. (2004). Additional modification to this methodology has been made to make it suitable for the present study. The technique permits the determination of oxidation state in solid as well as supernatant phase.

Schematic of the methodology followed for the present work is shown in figure 4.13. Briefly, at the end of decided time interval, the suspension was centrifuged and 1 ml of the

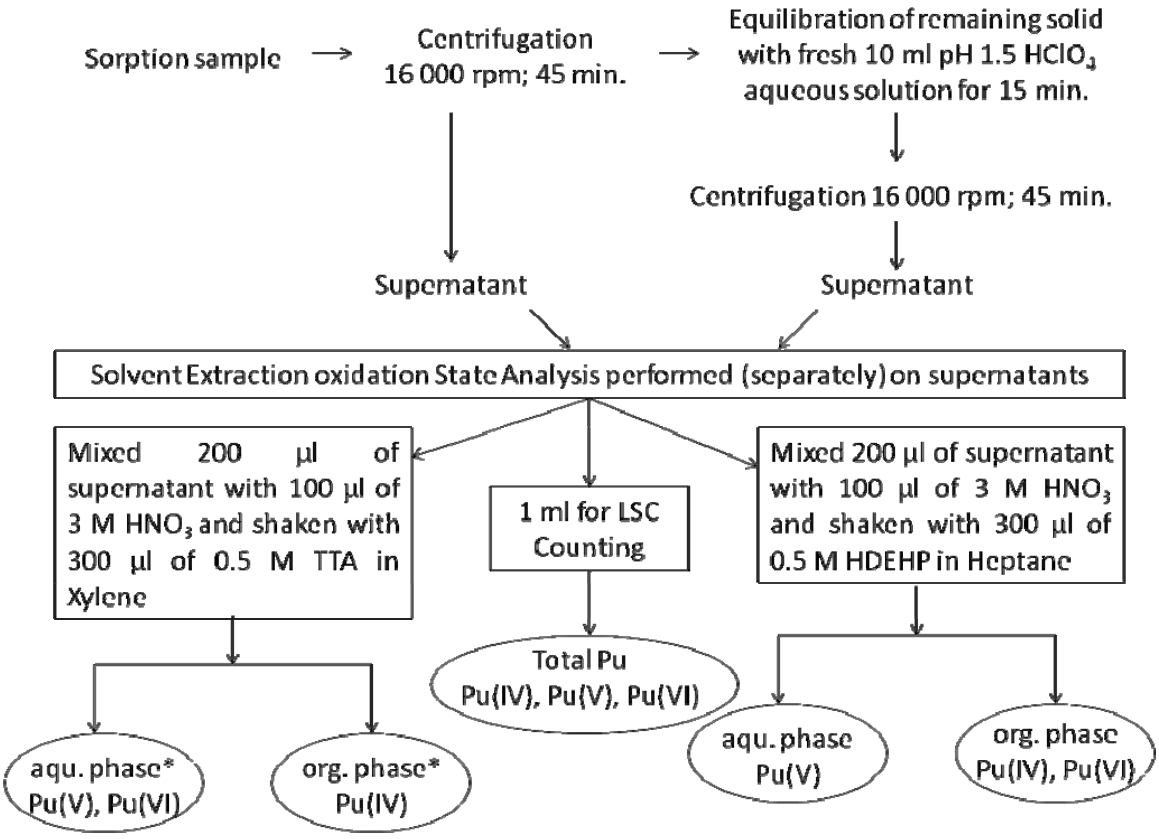

Figure 4.13 Schematic for Pu oxidation state analysis. Abbreviations aqu. and org. stand for the aqueous and organic phase.

supernatant was counted for Pu content. 200 µl of the supernatant was mixed with 100 µl of 3 M HNO_3 in two separate polypropylene tubes to make 300 µl of 1 M HNO_3 aqueous phase for use in the solvent extraction experiments. Different organic phases, namely 0.5 M TTA in Xylene and 0.5 M HDEHP in heptane were used in parallel solvent extraction procedures, to determine Pu(IV) and Pu(IV+VI) respectively.

The volume ratio of organic to aqueous phase was kept as 1:1. 150 µl of organic and aqueous phases was mixed separately with 5 ml of scintillator to find the activity in organic

phase and to check the mass balance, respectively. Pu extracted in TTA phase is in IV oxidation state while that extracted in HDEHP phase accounts for Pu(IV) + Pu(VI). Though the present methodology can be extended to include Pu(III), it has not been done in view of the instability of Pu(III) in oxic environment at pH above 2 (Olsson, 2006). The difference between the alpha activity in TTA and HDEHP phases gives Pu(VI) fraction while the difference of alpha activity between the total and HDEHP phase corresponds to Pu(V) fraction. Kinetic control on the oxidation state change enables this methodology to be applied for oxidation state determination, which has also been validated previously (Powell et al., 2004; Olsson, 2006).

For the oxidation state analysis of sorbed Pu, the solid phase obtained after the equilibration and centrifugation of the sorption samples was suspended in 10 ml of pH 1.5 $HClO_4$ solution and equilibrated for 15 min. The equilibration time was kept short to avoid the oxidation of leached out Pu. Determination of the oxidation state in the leached solution was then carried out as per the scheme of figure 4.13. Integrity of the oxidation state of sorbed Pu in similar leaching and analysis method has been observed in literature (Powell et al., 2004).

4.4.2 Results and discussion

4.4.2.1 Sorption experiment

Figure 4.14 gives the percentage sorption of Pu on silica and alumina surfaces as a function of pH. Significantly higher sorption was observed at all pH values for both the solids, starting from ~ 60 -70 % at pH 2-3 and it reaches quantitative sorption value by pH 7. However, there is a marked difference in their sorption profiles. At lower pH values upto ~ 5.5 Pu(IV) sorption by silica is higher than that on alumina whereas after this pH both the surfaces show similar sorption characteristics. To extrapolate this information for clay

substrates, Pu(IV) sorption at lower pH values should be governed by silica sites whereas both silica as well as alumina sites should contribute equally at higher pH values. Kersting et al. successfully modeled Pu(IV) sorption on aluminosilicate involving silica sites at lower pH values and participation of silica and alumina sites at higher pH values (Kersting et al., 2003).

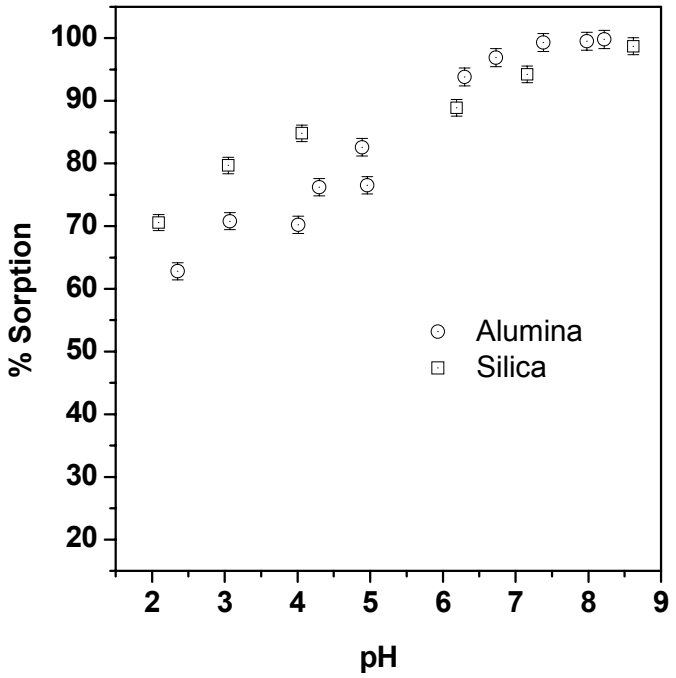

Figure 4.14 Sorption of Pu(IV) on silica and alumina. Experimental condition: 5 g/l Silica (4.5 g/l alumina) suspensions in 0.1 M $NaClO_4$ over pH 2-9 with [Pu] =1.22 × 10^{-9} M.

Mass to volume ratio used for silica and alumina suspensions in the experiments ensures similar surface area. The observed variation in the Pu percentage sorption on silica and alumina surfaces can occur either due to different interaction ability of Pu(IV) with these surfaces or due to different pattern of change in Pu-oxidation state in the oxide suspensions. Figure 4.15 shows the Eh measurement in experimental conditions ranging from pure background electrolyte to the silica/alumina suspensions and Pu equilibrated suspensions. As

there is no difference in the Eh value in these conditions, this clearly indicates the absence of any role of Eh in defining the sorption process.

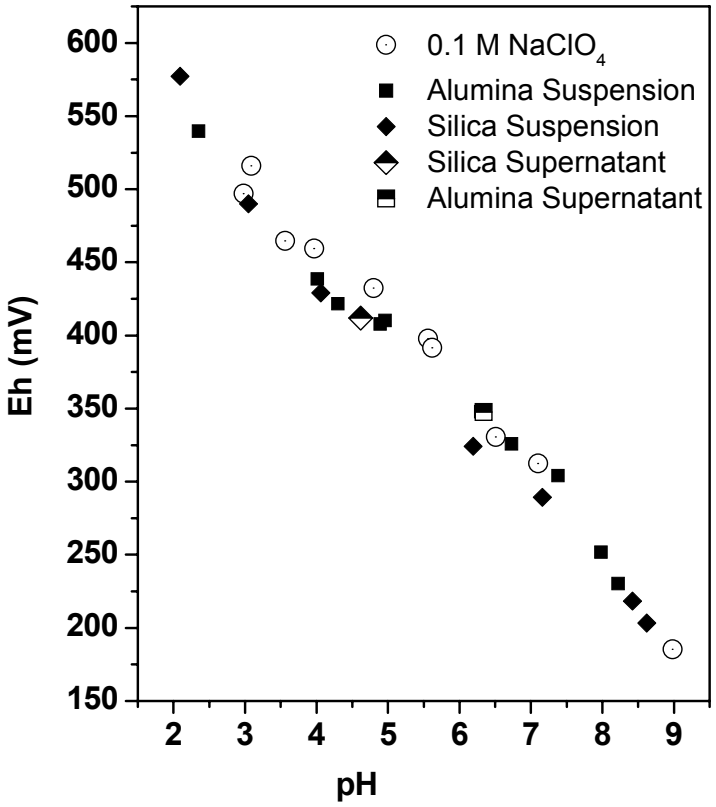

Figure 4.15 Eh measurement in different experimental conditions; Background electrolyte 0.1 M $NaClO_4$, silica/alumina suspensions prepared in 0.1 M $NaClO_4$ (labeled as supernatant), silica/alumina suspensions in 0.1 M $NaClO_4$ medium equilibrated with Pu at pH 2-9 for 48 hrs (suspension).

Eh-pH diagram (figure 4.16) of Pu indicates the existence of IV as the oxidation state under experimental condition of the sorption experiment. Silica has negatively charged surface over the studied pH range while alumina is positively charged (PZC < 2.3 and ~ 8.9 for silica and alumina, respectively, cf. chapter 3). Favourable electrostatic interaction between negatively charged silica surface and positively charged Pu(IV) species can thus be attributed to produce marginally higher sorption in case of silica at lower pH values.

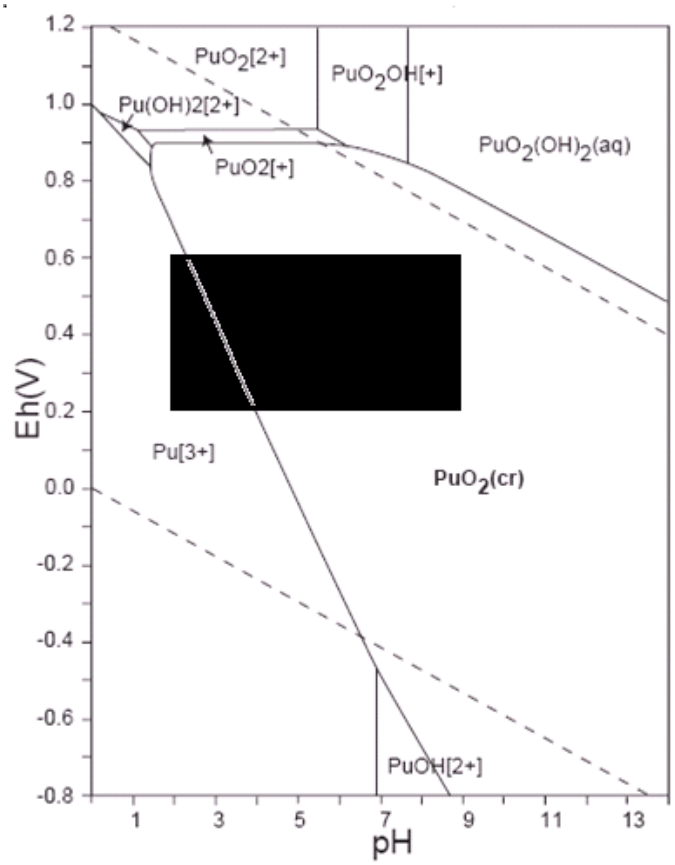

Figure 4.16 Eh-PH diagram of Pu aqueous speciation ([Pu] =10^{-10} M). Black coloured box in the plot represent Eh and pH range of the present experimental conditions.

4.4.2.2 Kinetic Experiment

As Pu has been added to the sorption systems in IV oxidation state, the kinetics should be faster in line with its higher complexing ability. Figure 4.17 shows the kinetics of sorption of Pu on silica and alumina at three different pH values. At higher pH values (~ 6 and 8.5), 80 - 100% of sorption has been observed in the first few minutes and the steady state was attained in 24 hrs. At lower pH (3.1 - 3.2) Pu sorption approaches the steady state value of ~70%. Difference in the steady state sorption value is attributed to the increasing complexing ability of Pu(IV) with increasing pH.

Kinetic profile of Pu(IV) sorption on both the surfaces can be interpreted in terms of two processes: fast sorption followed by a relatively slow process leading to steady state. The fast sorption step is in good agreement with the Th(IV) sorption kinetics on silica in the present study (figure 4.17) and the sorption kinetics on hematite (Romanchuk et al., 2011). Slow attainment of the steady state condition in the kinetic experiment could be either due to redox transformation reactions of added Pu(IV) or some slow process involving Pu(IV) occurring on the surface following the fast sorption step. Constancy of the Eh value precludes any redox transformation (figure 4.16). Assuming pseudo first order kinetics for the slow component, the rate constant at lower pH (~3.1 - 3.2) was found to be 4.17×10^{-5} s^{-1} for alumina as against 2.06×10^{-5} s^{-1} for silica. For the metal concentration (4.25×10^{-10} M) similar to the present study, Romanchuk et al. (2011) observed a faster sorption step followed by the slow process of rate constant 3.62×10^{-5} s^{-1} at pH 6 in Pu(IV) sorption on iron oxide (hematite). In the present study, the fast and the slow step could be attributed to the sorption of Pu(IV) monomeric species and the formation of polymeric species from sorbed monomeric species, respectively.

4.4.2.3 Desorption and leaching experiments

To further check the surface polymerization as the mechanism involved in the slow attainment of the steady state, desorption of sorbed Pu from silica and alumina surfaces has been carried out and the results are shown in figure 4.18. The desorption of Pu from both the silica as well as alumina surfaces follows the same trend (log [Pu] = - 0.17*pH - 0.96) which is much lower than that in the case of dissolution of Pu(V) from PuO_2(am) in 0.4 M $NaClO_4$ (figure 4.18) (Rai et al., 2001). This clearly indicates the absence of Pu on solid surfaces as PuO_2(am)

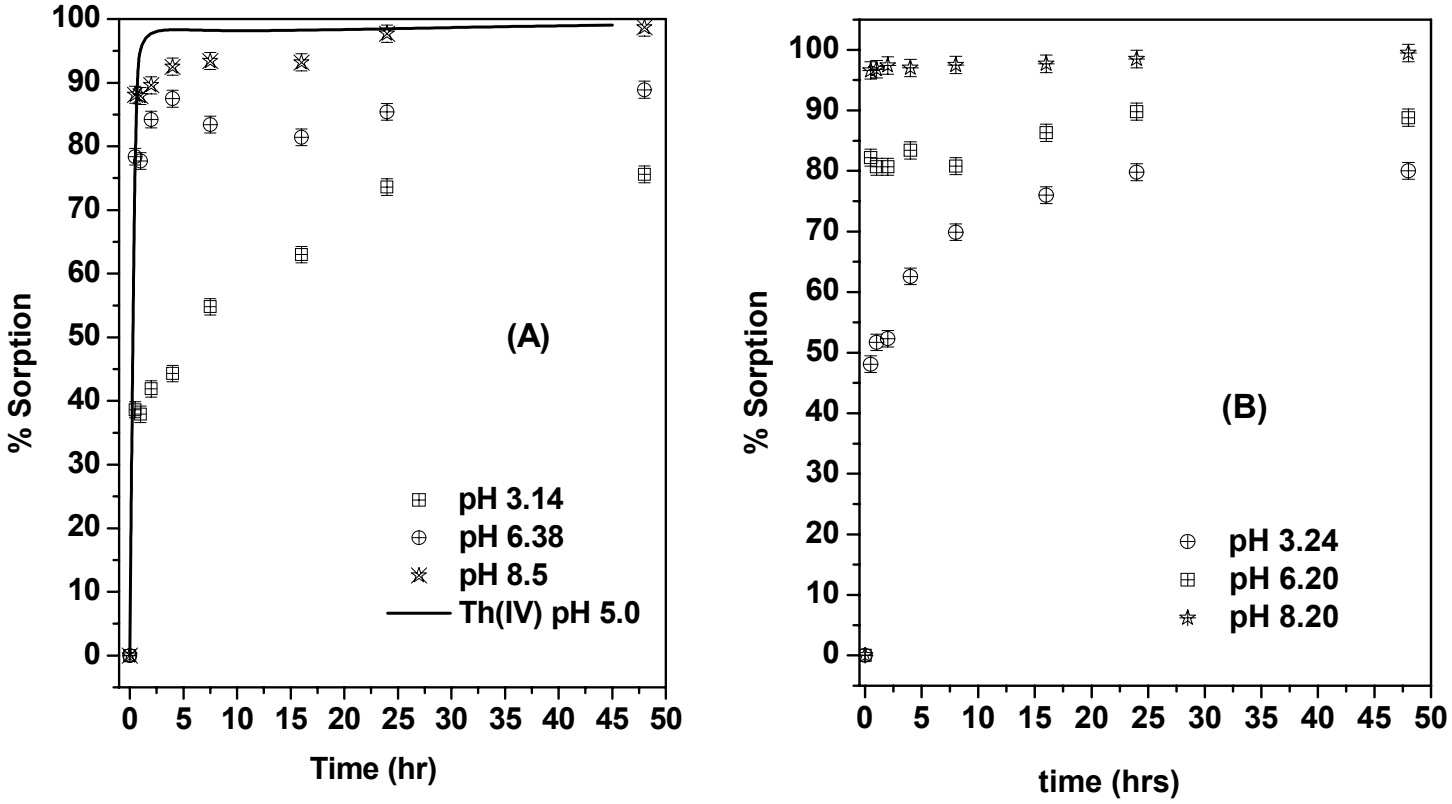

Figure 4.17 Kinetics of sorption of Pu ([Pu] =1.22 × 10^{-9} M) on silica (A) (5g/l) and alumina (B) (4.5 g/l) at pH values ~3.2, 6.2, and 8.5 and constant ionic strength (0.1 M $NaClO_4$). Solid line shows the kinetics of Th(IV) ([Th] =8.70 × 10^{-10} M) sorption on silica (5 g/l) at pH 5.0 in 0.1 M $NaClO_4$ medium.

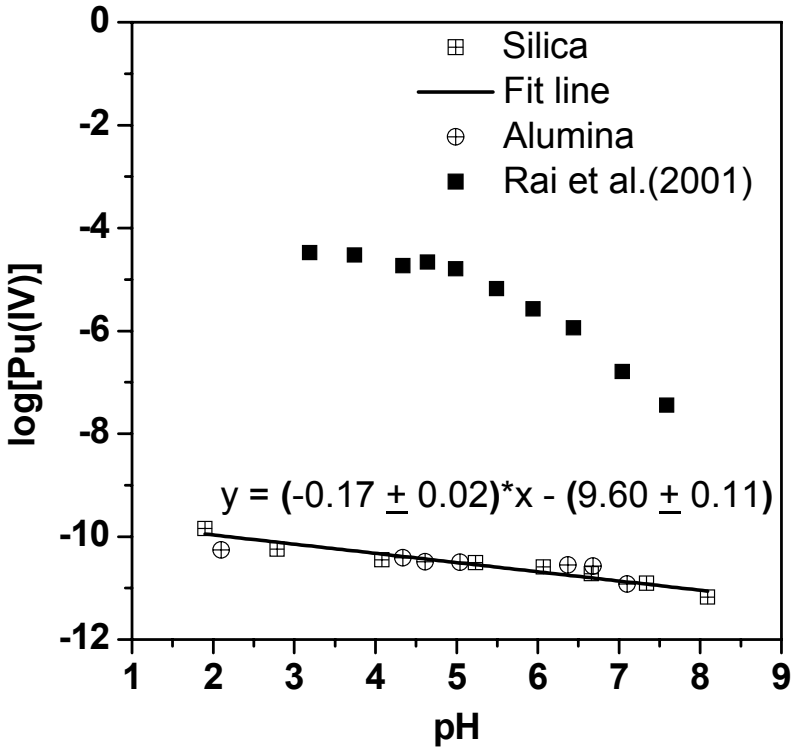

Figure 4.18 Pu desorption from silica and alumina surfaces over pH 2-8. The solid line represents the fit to the experimental data of [Pu(IV)] vs. pH. The solid symbol is for the desorption of Pu(V) from PuO_2(am) precipitate in 0.4 M $NaClO_4$.

Oxidation state distribution study of Pu sorbed at pH 6.20, obtained following the scheme shown in figure 4.13, indicates ~96% of Pu as Pu(IV). The polymeric species involved in the slow step of the kinetic profile may thus be in the form of small Pu clusters formed with either hydroxides or dissolved silicate/aluminate in view of significant silica and alumina dissolution in the studied pH range (figure 4.9). As the Pu concentration in the experiment is very small, Pu-silicate/aluminate precipitation is not possible and therefore formation of small oxide/hydroxide clusters is the only option left for the surface speciation. Pu concentration used in the present study (~10^{-9} M) is near the aqueous solubility limit. As the concentration of surface sites (~ 10^{-3} M) (table 3.2) available for Pu sorption is many orders

of magnitude higher than the metal ions, mononuclear species formation becomes the most probable interface reaction. However, in view of the low solubility product of $Pu(OH)_4$ (am), these mononuclear species may convert into small Pu oxide/ hydroxide clusters on surfaces. These small clusters might finally result into PuO_2 phase with time and to check this possibility, leaching experiment was carried out with the silica and alumina samples which had been equilibrated with Pu(IV) for 48 hours and 16 months. No difference was observed in the concentration of Pu(IV) leached from these two type of samples (figure 4.19). These results establish small Pu(IV) oxide/ hydroxide species as the surface speciation of Pu(IV) in steady state condition on both the surfaces.

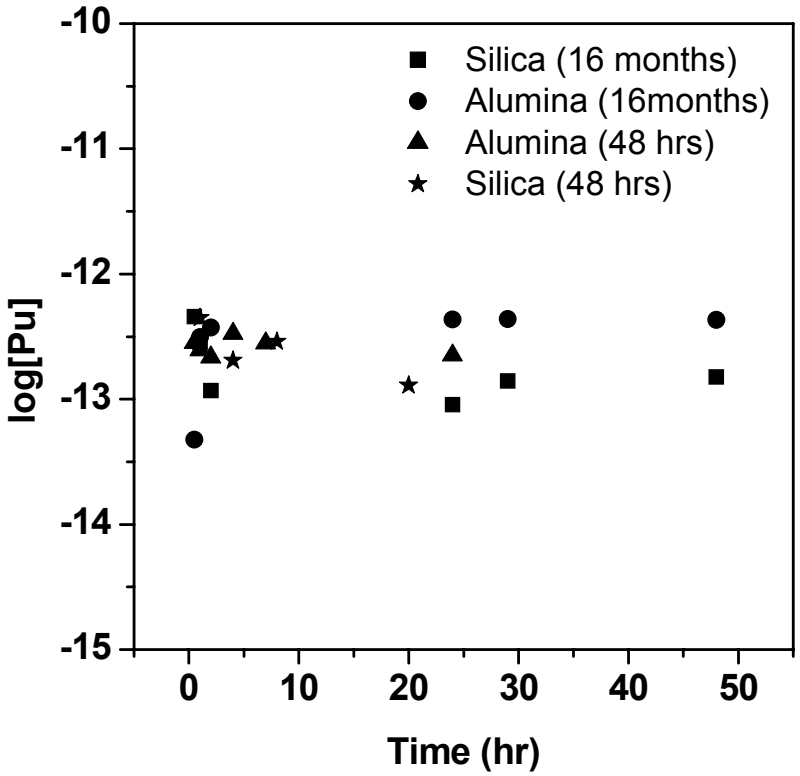

Figure 4.19 Pu leaching from solid surfaces of fresh (48 hrs) as well as long time (16 months) equilibrated sorption samples, with pH 1.5 $HClO_4$ solution.

4.4.2.4 Oxidation state distribution in the supernatant

To check for the oxidation state transformation in the aqueous phase during the kinetic experiment, TTA and HDEHP based solvent extraction methods have been used to determine the fraction of Pu(IV), Pu(V) and Pu(VI) present in the supernatant of silica and alumina suspensions at different time intervals. The oxidation state profiles are shown in figure 4.20. There is a marked difference in oxidation state distribution of Pu in the two suspensions. In silica suspension Pu(V) is in competition with Pu(IV) and with increasing time and pH, Pu(V) becomes the dominant oxidation state. In alumina suspension, on the other hand, instead of Pu(V), Pu(VI) is in competition with Pu(IV) at lower pH value (3.24) and becomes the major oxidation state with increasing time. At higher pH values, the Pu(IV) fraction decreases to nearly insignificant value and Pu(V) becomes the second dominant oxidation state, after Pu(VI), in the supernatant.

Redox transformation of Pu(IV) in the literature has been explained by its disproportionation (Morss et al., 2010),

$$2\ Pu^{4+} + 2\ H_2O \rightleftarrows Pu^{3+} + PuO_2^{+} + 4\ H^{+} \qquad (4.1)$$

followed by the disproportionation of Pu(V) or the reaction of intermediate Pu(V) with Pu(IV) yielding Pu(III) and Pu(VI) which results in the total reaction:

$$3\ Pu^{4+} + 2\ H_2O \rightleftarrows 2\ Pu^{3+} + PuO_2^{2+} + 4\ H^{+} \qquad (4.2)$$

Olsson et al. (2006) observed the oxidation of Pu(III) to Pu(IV) at different pH under aerobic conditions. Existence of different oxidation states of Pu in silica and alumina supernatants can be explained in light of these redox reactions. In silica supernatant at lower pH (~3.2), the oxidation state of IV and V for Pu is readily explained as per eq. 4.1. At higher pH, this reaction gets favoured, which, when coupled with the high sorption ability of Pu(IV) at higher pH, results in the dominance of Pu(V) in the supernatant. In the present study, kinetic

rate of sorption has been found higher for alumina compared to silica (cf. section 4.3.2.2) and because disproportionation is a concentration dependent reaction (Morss et al., 2010), higher concentration of Pu(V) in interfacial region of alumina-water causes its disproportionation leading to formation of Pu(VI). Calculations by Romanchuk et al. (2011) showed local concentration of 1×10^{-5} M in 1 nm layer near the hematite surface considering 1×10^{-10} M Pu concentration sorbing at 99% in 10 m^2/L hematite suspension, enabling disproportionation reaction. At higher pH values, where Pu(IV) sorption is higher, Pu speciation in the alumina supernatant is thus dominated by Pu(VI) followed by Pu(V).

4.4.3 Conclusion

Strong sorption for Pu(IV) on silica and alumina under pH (2-9) conditions has been demonstrated with marginally higher sorption for silica at lower pH values and has been attributed to negatively charged surface of silica. Kinetics of the sorption process on both the surfaces indicate fast sorption of Pu monomeric species followed by the slow step involving the formation of polymeric species as the mechanism of the sorption process. Desorption and leaching studies on the sorbed Pu negate the existence of PuO_2(am.) phase and confirm the existence of small polymeric Pu oxide/hydroxide species as the surface speciation. In the present study main difference between the two surfaces appears towards the oxidation state of the Pu present in the supernatant: Pu(V) is the speciation of unsorbed Pu in silica suspension while Pu(VI) competes with Pu(V) as the oxidation states of Pu in alumina suspensions. Higher interfacial sorption of Pu(V) in case of alumina causes its disproportionation to produce Pu(VI) in the supernatant.

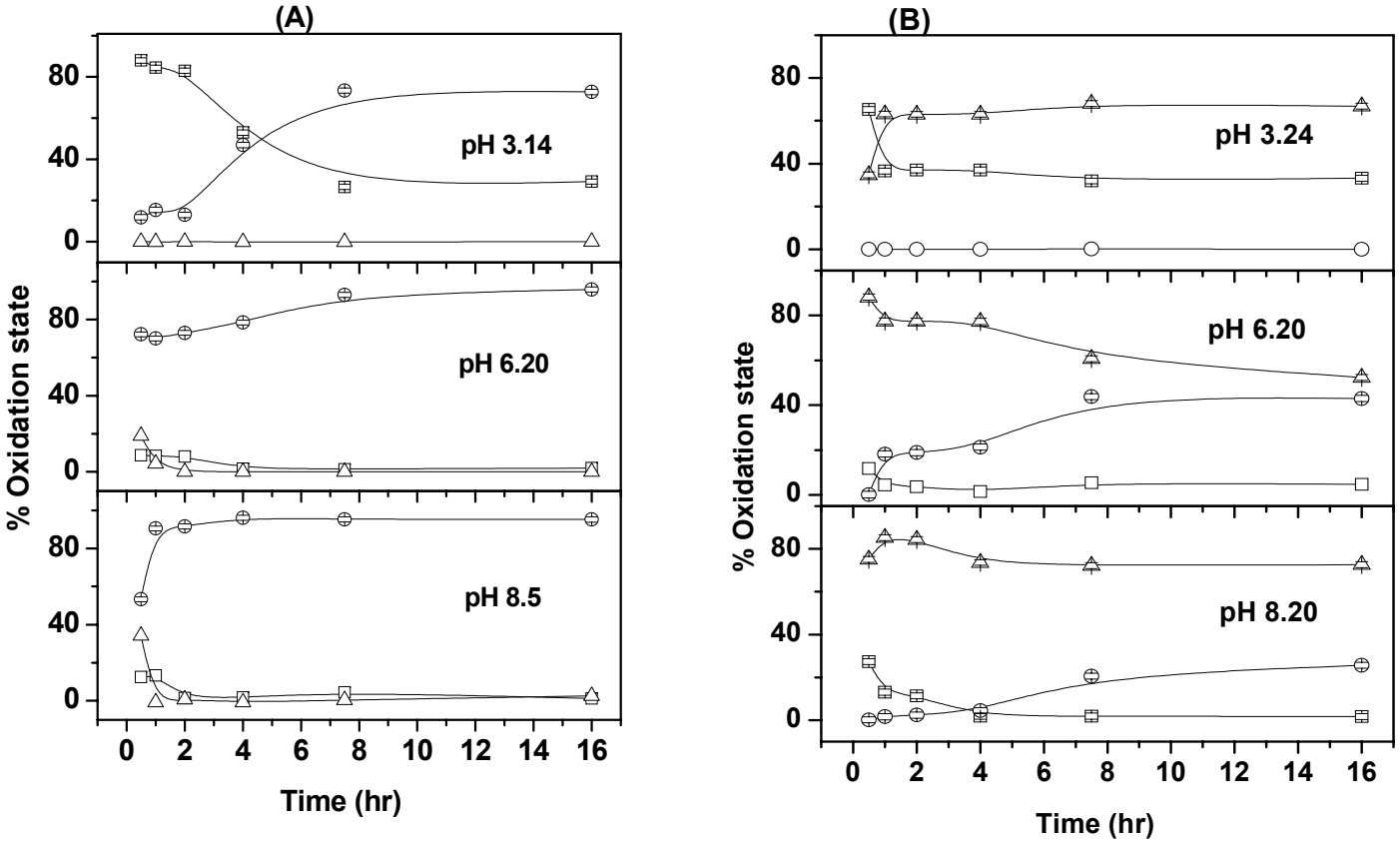

Figure 4.20 Oxidation state distribution of Pu in the supernatant of silica (A) and Alumina (B) kinetic samples at pH ~3.2, 6.2, and 8.5. Symbols (□), (O), and (Δ) stand for Pu(IV), Pu(V), and Pu(VI), respectively. Errors < 1% have not been shown.

4.5 Summary of the experimental results

Studies of the present chapter demonstrate the role of solid surfaces playing an important role in deciding the sorption product. Structural and compositional characteristics of the solids define how metal ions interact with surface sites and evolve into new surface phase. Pu sorption experiment suggests the requirement of consideration of higher oxidation state of Pu in their hydro-geochemical behaviour. Molecular level insight of the interfacial sorption reaction in terms of the type of binding and evolving surface species is thus requisite for robust description of radionuclide transport in geosphere.

Chapter 5

Sorption of trivalent actinides on smectite rich natural clay

5.1 Introduction

Since the publication of the seminal papers on surface complexation (SC) concept by Stumm and Schindeler (Stumm et al., 1970; Schindeler and Gamsjager, 1972; Hohl and Stumm, 1976), a voluminous literature describing sorption behaviour of various metal ions and long lived radionuclides on pure phase mineral surfaces such as oxides, sulphides, carbonates, etc. has appeared. Developing chemical models for sorption in natural system is, however, beset with uncertainties regarding basic tenets (cf. Chapter 2) of SC models. One of the complexities of natural sorption systems is identifying the mineralogical composition in the near surface region of sediment. Heterogeneous compositions make choice of surface functional groups difficult. Composition of aqueous solutions is not easily controlled in experiments with such sediment. Groundwater/porewater is a complex salt solution (Silva and Nitsche, 1992) and evolution of pH-Eh of such a water is governed by its interactions with clay component (Bradbury and Baeyens, 2009). This makes it more difficult to determine "intrinsic" stability constants of molecular scale reactions for sediment surfaces than in the case of single mineral phases suspended in simple electrolyte solutions. The quantification of coulombic correction factors for the electrical double layer on the surfaces of particles is equally complex. Interacting double layers of heterogeneous particles (Prieve and Ruckenstein, 1978), the formation of surface coatings (Davis and Gloor, 1981; Coston et al., 1995; Dähn et al., 2002) due to coprecipitation, and the competitive adsorption of many different ions cause significant changes in the electrical properties of mineral – water interfaces. As a result, the surface charge and electrical potential of the surfaces of solids and sediments are much more difficult to quantify than in the case of pure mineral phases commonly used in laboratory investigations.

Strategies for modelling sorption in natural systems

Sorbents

A number of approaches to model radionuclide interactions with complex geological materials have been advocated. Two broad types of strategies have been suggested: "top-down" and "bottom-up" (Altmann, 2001). In the "top-down" strategy, the behaviour of the complex system is modelled on the basis of bulk system parameters (e.g., surface area and cation exchange capacity of the geological substrates). In this approach, no attempt is made to quantify the relative importance of constituent mineral phases, such as clays, oxides or humic materials. Basic assumption in this approach is that surface composition of the mineral assemblage is inherently too complex to be quantified in terms of the contributions of individual phases to sorption.

In the alternative "bottom-up" strategy, one identifies all significant components of the natural sorbent and attempt to systematically understand and model the interactions of each component with the metal ion of interest. It is assumed in this approach that the wet surface of the complex mineral assemblage is composed of a mixture of one or more mineral phases whose surface properties are known from independent studies of individual phases. This involves detail study of both the mineralogy of the solid phase and the chemistry of the aqueous phase. Inevitably some simplifications are required in this approach, because the number of potential interactions is unlimited. However, this strategy is more fundamental and appears more applicable than the top down method as it necessarily relates to specific geological materials and groundwater chemistry.

Davis et al. (1998) observed that both the approaches predict well Zn^{2+} sorption on a sediment collected from an aquifer, but concluded that the "bottom-up" approach (component additivity approach) is better than the "top-down" approach (generalized composite approach) as the latter does not utilize conclusions drawn about actual surface speciation from spectroscopic investigations and lacks transferability to other mineral assemblages.

Groundwater/Porewater

To deal with the complex hydrochemistry of natural system, a scoping calculation can be separately carried out to determine the effect of aquatic chemical composition on the solubility and speciation of sorbing metal ions (Duro et al., 2000). In situation of significant effect of a component, modelling protocol specific to that component need to be developed and integrated into the sorption model (Bachmaf et al., 2008, Joseph et al., 2011). For example, humic acid has been found to complex the metal ions significantly in aquatic environment (Lenhart et al., 1999) and its presence needs to be taken into account in the SCM procedure for sorption system in natural system.

Surface electrostatics

Surface charge distribution of natural sorbent is difficult to quantify unlike oxide surfaces. For example, clayey sorbent carries pH independent charge due to isomorphous substitution within clay lattice. It also varies with the degree of compaction of sorbents (Muller and Wang, 2012). Models for surface charge used in literature vary from purely non-electrostatic (charge not distributed into solution), to explicit double layer models such as constant capacitance model, diffuse double layer model, etc. Nonelectrostatic (e.g., "2-site surface complexation and cation exchange (2SPNE/CE)" (Bradbury and Baeyens, 2002)) and CCM models (Guo et al., 2009) have been extensively applied for modelling sorption on clayey sorbents (Hartmann et al., 2008; Bradbury and Baeyens, 2011).

Literature update on sorption of trivalent actinides in natural system

Kinetics of Am(III) sorption on smectite rich natural clay minerals have, in general, been found to be fast (Lujaniene et al., 2012). Model calculations of Eu(III) sorption on the mixture of smectite and illite clays suggest increasing sorption with increasing content of smectite in the mixture (Lützenkirchen, 2012). In the modelling of adsorption-desorption of Eu(III) on Na-bentonite, reversibility has been observed over pH 4-8 (Guo et al., 2009).

Degree of microscopic reversibility has, however, been found to decrease with pH (Coppin et al., 2002). These and other similar observations for other radionuclides, such as Cs(I), Sr(II), Pu(IV), etc., have been explained mechanistically by considering two distinct processes of sorption occurring on clay surfaces, viz., ion exchange and surface complexation (Reiller and Bradbury, 2006, Reiller, 2008, 2007). Formation of outer sphere complex on the ion exchange sites at lower pH values follows fast exchange while reversibility at higher pH values is obstructed by the formation of inner-sphere complexes. Strong competition of monovalent background cations to sorbing Am(III) on montmorillonite at lower pH values further indicates the prevalent existence of cation exchange mechanism (Bradbury et al., 2005). Sharp increase in Am(III) sorption over a narrow pH range and insensitivity of sorption to varying ionic strength at higher pH values, in the same study, indicates the existence of more than one mechanism for sorption process. Formation of two types of surface complexes has been found in the combined Time Resolved Laser Fluorescence Spectroscopy (TRLFS) and Extended X-ray Absorption Fine structure Spectroscopy (EXAFS) study of the sorption of trivalent actinides onto smectite (Stumpf et al., 2001, 2004, Tertre et al., 2006).

Lanthanides' sorption on smectite clays was found to decrease with increasing Ca(II) concentration in the solution (Galunin et al., 2010). This has been explained in terms of the Ca(II)-Ln(III) competition, which causes displacement of the lanthanides to edge sites leading to the observed decrease in K_d value. On the other hand, in the experimental and modelling study of sorption on montmorillonite, this competition by divalent metal ions has been reported selective in favour of Eu(III) (Bradbury et al., 2005).

Groundwater or pore water contains many anions, such as, sulphate, silicate, phosphate, organic molecules etc., which complex the metal ions and thus affect their uptake on clay surfaces (Reiller, et al., 2012). Carbonate is ubiquitous in ground waters and, in absence of

any explicit source such as calcite mineral, may come from atmospheric CO_2. Owing to the formation of carbonate species at higher pH values, it may change the metal ion uptake behaviour (Guo et al., 2009). Significant dip in Eu(III) sorption has been observed at pH > 8 in presence of atmospheric carbon dioxide in comparison to that in absence of CO_2. On the contrary, Hartmann et al. (2008) observed similar results in Eu(III) sorption on Opalinus clay and Callovo-Oxfordian clay at pH > 7 in Ar atmosphere and aerobic conditions. Recently, the complexing properties of organic matter extracted from natural clay, toward curium has been investigated (Claret et al., 2005, Courdouan et al., 2008). Asymmetric flow field - flow fractionation method applied to the interaction of bentonite colloids with Eu in presence of humic acid showed Eu(III) preferential speciation with humic colloids (Bouby et al., 2011).

Natural clay samples are mostly multiphasic minerals and the overlapping sorption behaviour of different phases can modify the sorption behaviour of a metal ion on such substrates in comparison to that in the pure clay phase case. Effect of minor phase of the clay sample on Eu(III)/Cm(III) sorption has been investigated by Hartmann et al., (2008) on Opalinus clay and Callovo-Oxfordian clay using TRLFS and surface complexation modelling. Results of this study conclude the surface speciation of Eu(III) to be linked to the main phase of the clay mineral and negates the role of minor components, calcite and quartz, in Eu(III) uptake. Similar observation was made in the "bottom-up" approach of Eu(III) sorption modelling on MX-80 bentonite (Bradbury et al., 2011). Contradicting these results, significant Am(III) speciation was found in the minor phase (at the carbonate sites) in the sorption from natural ground water to three Smectite clay minerals varying in the content of carbonate and iron minerals (Lujaniene et al., 2012).

Present study

Owing to significant retention capability and low water permeability, clay minerals have been proposed as a component of the engineered barrier around the vitrified nuclear waste form in their deep-underground geological repositories. Smectite rich natural clay has been selected for evaluation of its suitability in Indian deep-underground geological repository program (Bajpai, 2008). The present study aims at developing a sorption model for Am(III)/Eu(III) interaction with the smectite rich clay in granitic ground water, using sorption experiments and surface complexation modelling. Mineralogical analysis of the clay sample and chemical compositional analysis of the granitic groundwater have been carried out. To identify the minerals present in the clay and controlling the sorption process, adsorption isotherm of Eu(III) was carried out on montmorillonite - kaolinite clay mixture having 0-20 wt% kaolinite. Effect of experimental parameters, such as, pH, ionic strength, cation and anions present in granitic groundwater, on Am(III) sorption was further investigated to develop the sorption model for the natural clay. Surface complexation model developed in ground water conditions was finally calibrated on the adsorption isotherms data of Eu(III) in natural sediment-granitic groundwater combination.

5.2 Materials and methods

5.2.1 Materials

All the chemicals used in experiments were of analytical grade. Clay samples have been collected from the Western India and used after minor dressing at the site. Origin, dressing details and physical, thermal and mechanical characterization details of the clay has been discussed by Pente (2009). Clay lumps were crushed and passed through 0.2 μm sieve. Filtered clay was heated upto 120 ^{0}C. The crushed and filtered clay was characterized for mineralogical and chemical composition and used in sorption experiment. Crushed clay has been observed to have same sorption sites as intact clay (Van Loon et al., 2009). For the

purpose of the present study, clay sample was analyzed for (a) major, minor and trace elements by X-ray Fluorescence method, (b) chemical analyses for organic as well as inorganic carbon content by total organic carbon (TOC) analyser, (c) whole rock analyses using lithium borate fusion process and ICP-AES analysis, (d) mineral identification by X-ray Diffraction method, and (e) surface area by BET analysis. Granitic ground water was collected from an underground experimental facility located at a depth of 205 m in granitic rocks in Karnataka, India and was analyzed for pH value and its composition using ion chromatography and TOC analyser.

5.2.2 Adsorption isotherm and Batch sorption experiments

All the experiments were carried out in polypropylene tubes at room temperature (25 ± 2 ^{0}C) in ambient atmosphere. Na/Ca-equilibrated clays were prepared by equilibration of the clays in 1.0 M NaCl or $CaCl_2$ medium overnight followed by phase separation and washing with Millipore water. Clays were then dried and used in the experiments. Clay suspensions were prepared at concentration of 0.5 g/l in 0.1 M NaCl except mentioned otherwise. Clay suspensions were equilibrated with the supernatant overnight before metal ion addition and pH adjustment. pH of the suspension was adjusted with the addition of HCl and NaOH. Sorption experiments were carried out using ^{241}Am, except for the sorption isotherm experiments, wherein its chemical analogue, ^{154}Eu was used. Assay of gamma activity was carried out using a well type shielded (3" × 3") NaI(Tl) gamma detector coupled to a 2048 channel analyser. Inactive Eu(III) was used along with ^{154}Eu to achieve the requisite Eu concentration in the isotherm experiment. Suspensions were equilibrated for 48 hours based on the kinetic experiment and subsequently centrifuged at 16 500 rpm for 45 min. for phase separation. The distribution coefficient (K_d, mL/g) was calculated as:

$$K_d = \frac{A_0 - A_{eq}}{A_{eq}} \times \frac{V}{m} \qquad (5.1)$$

where, A_0 is the initial metal ion concentration in the suspension, A_{eq} is the metal ion concentration left in the supernatant after equilibration, V is the volume of the suspension in millilitre, and m is the mass of the clay in gram.

Sets of replicate sampling and measurement indicated uncertainty of ± 0.2 log unit in the log K_d values at lower pH values while it increases with pH to ± 0.5 log unit at highest pH value. To ensure that the decrease in the metal ion concentration is due to sorption by clay and not due to sorption on the container walls, suspensions were carefully removed from the tubes and after washing with water, refilled with 1.0 M HNO_3 for overnight equilibration. At the end of the reaction time, acid solution was assayed for desorbed activity. The wall sorption was found to be negligible (~2 % at higher pH values) and hence was not considered while calculating the metal ion sorption onto the clay.

5.2.3 Modelling of sorption data on natural clay

Sorption isotherm data have been modelled considering montmorillonite as the sorbent for metal ions. The approach followed for the surface complexation modelling of the sorption data is based mainly on Bradbury and Baeyens' model "2-site surface complexation and cation exchange (2SPNE/CE)" (Bradbury and Baeyens, 2002). The present modelling assumes two types of sites for montmorillonite surface, one ($\equiv X^-$) carrying permanently negative charge and participating in ion exchange reaction with sorbing metal ions while the other ($\equiv SOH$) type situated along the edges of the clay platelets, undergoes protonation / deprotonation reactions and binds the metal ions in inner sphere complexation reactions. The approach adopted in the present study for defining of cation exchange in terms of equilibrium constant is different from that based on selectivity coefficient employed in 2SPNE/CE model. Cation exchange reaction of Am(III) on Na-montmorillonite can, thus, be written as:

$$3 \equiv XNa + Am^{3+} \Leftrightarrow \equiv X_3Am + 3Na^+ \qquad (5.2)$$

For the amphoteric clay site (≡SOH) assumptions regarding site types, capacity and protolysis constants are similar to 2SPNE/CE model. However, the capacity for ≡SOH sites has been scaled down to 90% of that used for montmorillonite in 2SPNE/CE model, to account for the weight fraction of montmorillonite in the clay. On the other hand, the ion exchange capacity determined in the present study has been used for cation exchange sites. As per the convention of the 2SPNE/CE model, no electrostatic term has been used in the present study. The charge contributed by the permanent negatively charged ion exchange sites remains constant over the pH values and is much more than the charge contributed by amphoteric sites (~7% of the former), hence, an explicit electrostatic term was not included in the modelling. Bradbury and Baeyens (2006, 2002) have successfully modelled the sorption of Eu(III)/Am(III) on montmorillonite without an electrostatic term in the 2SPNE/CE model. Fitting of the data was carried out using FITEQL software (version 4) (Herbelin and Westall, 1999). Sorption data was optimized in part for cation exchange and surface complexation reactions separately and finally optimized values for surface complexation constant were obtained using whole of the data set and keeping the cation exchange reaction constants fixed.

5.3 Results and discussion

5.3.1 Clay and groundwater characterization

Physicochemical characterization of the clay samples along with mineralogical analysis is shown in table 5.1. The water content was determined to be 10.1 wt %. Cation exchange capacity (CEC) of the clay sample was determined using Cu(II)-trien method (Meier and Kahr, 1999) and was found comparable to the montmorillonite CEC reported in literature (80-100 meq/100g). Table 5.1 shows montmorillonite as the major mineral phase present in the clay (figure 5.1).

Table 5.1 Physicochemical characterization of clay sample

Characteristics	Value
Surface area (N_2-BET method) (m^2g^{-1})	79.6
Pore volume (cc/g)	0.087
Cation exchange capacity (meq/100 g)	76
Total carbon content	< 0.05%
Total organic carbon	< 0.05%
Composition (by X-ray diffraction) (wt %)	Montmorillonite (~ 90), Kaolinite (~ 10), Silica (Trace)

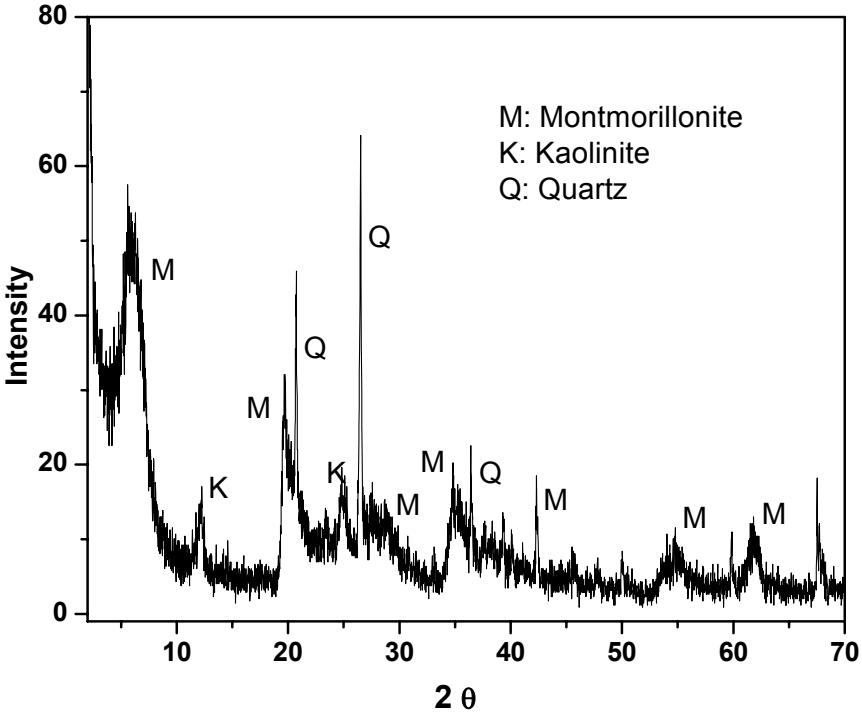

Figure 5.1 X-ray diffraction profile of the clay sample.

For chemical analysis (table 5.2) of the clay sample, clay was fused with $LiBO_2$ and dissolved in HNO_3 and then analysed by ICP-AES. The loss of ignition (LOI) value is 8.0%.

Table 5.2 Chemical composition of the clay sample expressed as weight % of major element after ignition.

	SiO_2	TiO_2	Al_2O_3	Fe_2O_3	MnO	MgO	CaO	Na_2O	K_2O	P_2O_5
wt %	48.80	1.50	18.42	6.50	0.02	1.82	0.08	2.58	0.89	0.10

Granitic groundwater pH is slightly alkaline (8.2) due to its carbonate content with Na^+, Ca^{2+}, F^-,Cl^- constituting the major ionic composition.

Table 5.3 chemical composition of granitic groundwater

Element	Composition (M)
Anions	
F^-	8.9E-05
Cl^-	5.7E-03
NO_3^-	2.9E-04
SO_4^{2-}	1.1E-03
Cations	
Li^+	2.9E-06
Na^+	8.0E-03
K^+	9.0E-04
Mg^{2+}	8.8E-04
Ca^{2+}	2.6E-04
Sr^{2+}	5.7E-06
Zn^{2+}	2.6E-06
Inorganic Carbon (ppm)	44.07
Organic carbon (ppm)	7.03

5.3.2 Adsorption isotherm of Eu(III) on Montmorillonite - Kaolinite mixtures

Eu(III) distribution between solid and liquid phases at pH 6.04 in the three clay suspensions having 0-20 wt% of kaolinite in montmorillonite-kaolinite clay mixture is presented in figure 5.2. Isotherm data for Eu(III) overlap for all the three compositions indicating montmorillonite as the main sorbent for Eu(III). For comparison, an adsorption isotherm of Eu(III) on Na-montmorillonite at pH 6, [$NaClO_4$] = 0.1 M and m/V = 0.5 g/l

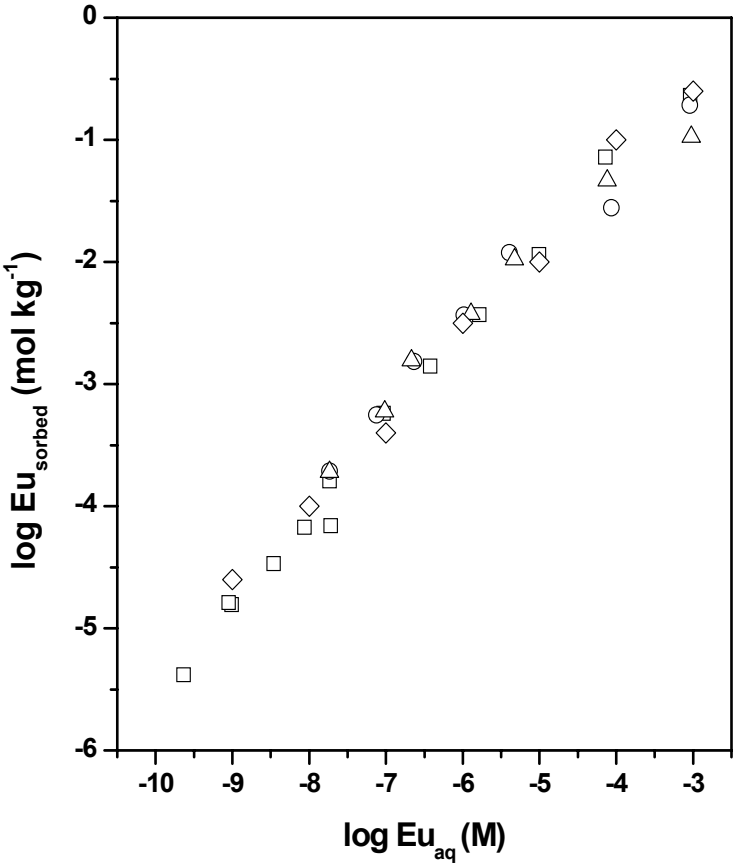

Figure 5.2 Effect of Kaolinite composition (wt %) on Eu(III) sorption on Montmorillonite: (□): 0 %, (○):10 %, (Δ): 20 %. [Eu(III)] = 10^{-3}-10^{-7} M, [NaCl] = 0.1 M, m/V = 0.5 g/l and pH = 6.04 ± 0.15. Symbol (◊) is for Eu(III) sorption on Na-montmorillonite at pH 6.0 and 0.1 M $NaClO_4$ from Bradbury and Baeyens (2002).

reported by Bradbury and Baeyens (2002) is also presented in figure 5.2. This isotherm merges entirely with the data of the present work establishing the reproducibility of the result and montmorillonite as the controlling sorbent in the clay mixture.

Kaolinite and montmorillonite are distinguished by the wide difference in their ion exchange capacity and hence the presence of kaolinite in smectite clay could affect the sorption capacity of smectites. In the sorption study of lanthanides on kaolinite and Na-montmorillonite, the measured K_d was influenced by the nature of clay at low ionic strength (0.025 M) (Coppin et al., 2002). In the present study insignificant role of kaolinite fraction in Eu(III) sorption thus clearly indicates the high ion exchange capacity of montmorillonite governing the sorption at lower pH values while the amphoteric edge sites (silanol and aluminol sites) of both the clays decide the sorption profile at higher pH values as described below. Adopting a "bottom-up" approach for complex mineral/groundwater systems, Bradbury et al. (2011) successfully modelled Eu(III) sorption isotherm on MX-80 (75 wt% montmorillonite) and Opalinus clay (illite + smectite: 40 wt%) using the sorption models developed for montmorillonite and illite and site capacities scaled down to the respective 2:1 clay mineral content in the natural clay. In view of these results and isotherm data of the present work, the smectite rich natural clay (containing ~ 90 wt % montmorillonite), can be considered to have montmorillonite as the main sorbent for metal ions.

5.3.3 Effect of pH and ionic strength on Am(III) sorption on Clay

pH dependent sorption of Am(III) on natural clay at [Am(III)] = 6.0×10^{-9} M in 0.1 M NaCl medium is shown in figure 5.3. With the varying ionic strength (0.01-0.1 M), the sorption edge of Am(III) exhibits significant change. As evident from figure 5.3, sorption edges show three distinct parts: (i) at lower pH values (< 4), the sorption of Am(III) increases slowly with pH; (ii) in the pH range 4-7, the slope of the Am(III) adsorption edge increases sharply; and (iii) above pH 7.5, the sorption of Am(III) remains nearly constant with pH.

With decreasing ionic strength in the suspension, the percentage sorption increases at lower pH values, while that at higher pH values remains unaffected. Similar pH and ionic strength effects have been observed for Am(III)/Eu(III) sorption on montmorillonite (Bradbury and Baeyens, 2006, Coppin et al., 2002) and Eu(III) sorption on bentonite clay (Guo et al., 2009).

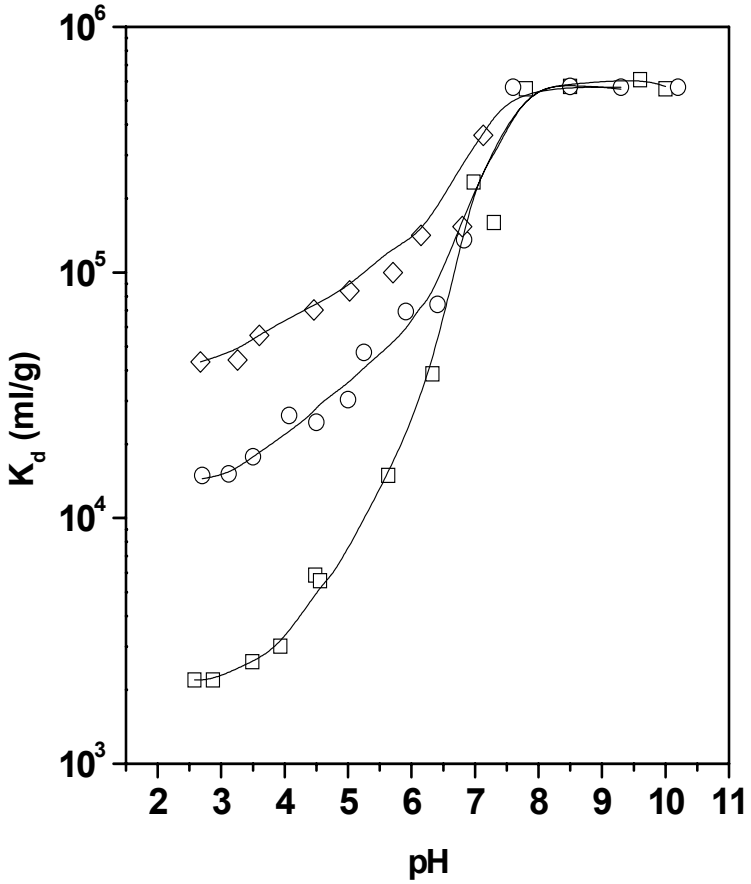

Figure 5.3 pH sorption edge of Am(III) on Na-equilibrated natural clay in 0.1 M NaCl medium and effect of ionic strength on Am(III) sorption under m/V = 0.5 g/l and [Am(III)] = 6.0 × 10^{-9} M conditions. Symbols (□), (○) and (◊) stand for 0.1, 0.05 and 0.01 M NaCl.

The results presented in figure 5.3 can be easily understood by taking into consideration the surface chemistry of the smectite clays. Smectite surface is characterized by two types of surface sites: ion exchange sites which are primarily responsible for high cation exchange capacity of clays and edge or "broken" sites which constitute aluminol and silanol groups.

Increasing sorption of metal ions with decreasing ionic strength at low pH values infer the formation of outer-sphere surface complex of Am(III) on the natural clay surface. This suggests that montmorillonite surface at lower pH values is dominated by ion exchange surface sites. Increase in the ionic strength causes saturation of surface sites with background electrolyte cations leading to decreased sorption of Am(III). Unlike this non-specific sorption, Am(III) sorption on edge sites are pH dependent as these sites get progressively ionized with pH causing enhanced sorption. The near constant profile of sorption edge below pH < 4, thus, seems to arise primarily by the participation of the ion exchange site and the increasing slope of the sorption edge above pH 4 may have the contribution of both the types of sorption sites.

Presence of atmospheric carbon dioxide can cause carbonate ions in the suspension, which may retain the metal ions in the aqueous phase by making anionic species and thereby leading to decreased sorption. Coppin et al. (2002) did not observe any difference in lanthanides sorption on smectite and kaolinite when the sorption was carried out in aerobic atmosphere and argon atmosphere. However, Significant decrease in the Eu(III) sorption on bentonite was observed in presence of atmospheric carbon dioxide at pH > 7 (Guo et al., 2009). In the present study no dip in Am(III) sorption was observed at higher pH values indicating the insignificant effect of atmospheric carbon dioxide.

The solid lines corresponding to the sorption data (figure 5.3) indicate the surface complexation modeling results. Mean optimized values for the surface reaction constants are given in table 5.3. Complexation constants of the species formed at edge sites compare well with those obtained using 2SPNE/CE model for Am(III) sorption on Na-montmorillonite (Bradbury and Baeyens, 2006). As the formulation of the cation exchange reaction in the present exercise differs from that in 2SPNE/CE model, the values obtained are also very different. However, the log K values of the Am^{3+}-Na^{+} and Na^{+}-H^{+} exchange reactions agree

well with those reported in the modelling study of Eu sorption on Na-bentonite (Guo et al., 2009). Similar magnitude of constants could be traced to similar formalism for cation exchange reactions in two studies.

Table 5.4 Summary of the site types, site capacities, protolysis and surface complexation reactions and constants for Am(III)/Eu(III) sorption on natural clay mineral. [1]: Guo et al., 2009. [2]: Bradbury and Baeyens, 2002.

Site type	Site capacity	
$\equiv X^-$	0.76 eq/kg	
$\equiv S^S OH$	1.8×10^{-2} mol /kg	
$\equiv S^{W1} OH$	3.6×10^{-2} mol /kg	
Aqueous solution/solid equilibrium	log K_{int}	Values/Reference
$\equiv XNa + H^+ \Leftrightarrow \equiv XH + Na^+$	0.80	0.79 [1]
$\equiv S^S OH + H^+ \Leftrightarrow \equiv S^S OH_2^+$	4.5	[2]
$\equiv S^S OH \Leftrightarrow \equiv S^S O^- + H^+$	-7.9	[2]
$\equiv S^{W1} OH + H^+ \Leftrightarrow \equiv S^{W1} OH_2^+$	4.5	[2]
$\equiv S^{W1} OH \Leftrightarrow \equiv S^{W1} O^- + H^+$	-7.9	[2]
Surface complexation reactions of Am/Eu(III)		
$3 (\equiv XNa) + Eu^{3+} \Leftrightarrow X_3Eu + Na^+$	1.3	1.3
$\equiv S^S OH + Eu^{3+} \Leftrightarrow \equiv S^S OEu^{2+} + H^+$	1.87	1.3 [1], 1.8[2]
$\equiv S^S OH + Eu^{3+} \Leftrightarrow \equiv S^S OEu(OH)^+ + 2H^+$	-5.4	-5.4[2]
$\equiv S^S OH + Eu^{3+} \Leftrightarrow \equiv S^S OEu(OH)_2 + 3H^+$	-20.2	-22.1 [2]
$\equiv S^{W1} OH + Eu^{3+} \Leftrightarrow S^{W1} OEu^{2+} + H^+$	-0.3	-2 [1], -0.5[2]

5.3.4 Effect of Ca(II) concentration on Am(III) sorption by Clay

Competition of Ca(II) to Am(III) sorption on natural clay is shown in figure 5.4 (A) and (B). Figure 5.4 (A) shows the sorption of Am(III) at pH 7.1 over the Ca(II) concentration of 0.005 - 0.1 M. Sorption of Am(III) by the clay remains constant over the studied Ca(II) concentration range which concludes the non-competitiveness of Ca(II) against Am(III) for sorption sites on clay at pH=7.1. Similar observation was made in the experimental and modelling studies of sorption competition on montmorillonite by Bradbury and Baeyens (2005). The agreement between the observation of the present work and that of literature (Bradbury and Baeyens, 2005) again establishes montmorillonite as the main sorbent in the natural clay mineral.

Am(III) sorption on Ca-equilibrated natural clay over pH 3-10 in 0.0335 M $CaCl_2$ medium is shown in figure 5.4 (B). The sorption edge follows the general pattern of Am(III) sorption on Na-equilibrated clays (figure 5.2); it exhibits the three regions of K_d, that is, almost pH independent K_d at lower pH values (pH < 4) followed by sharp variation of K_d in the intermediate pH range and constant K_d values at higher pH values. However, the transitions between these ranges are not as sharp as that in the case of Na-equilibrated clay. These observations can be rationalized by considering the Am(III) – Ca(II) exchange at ion exchange sites of clay at lower pH values and Am(III) sorption on edge sites at higher pHs where Ca(II) does not compete with Am(III). As the increased ionic charge of Ca(II) leads to stronger binding with the ion exchange site in comparison of Na(I), movement of Am(III) to ion exchange site is less favoured on Ca(II)-equilibrated clay in comparison Na-equilibrated clay and hence the transition is not sharp. Comparison of selectivity coefficient (K_c) for Eu(III)-Ca(II) and Eu(III)-Na(I) exchanges (13 and 30, respectively at I = 0, Bradbury and Baeyens, 2002) at montmorillonite surface further corroborate these conclusions. These

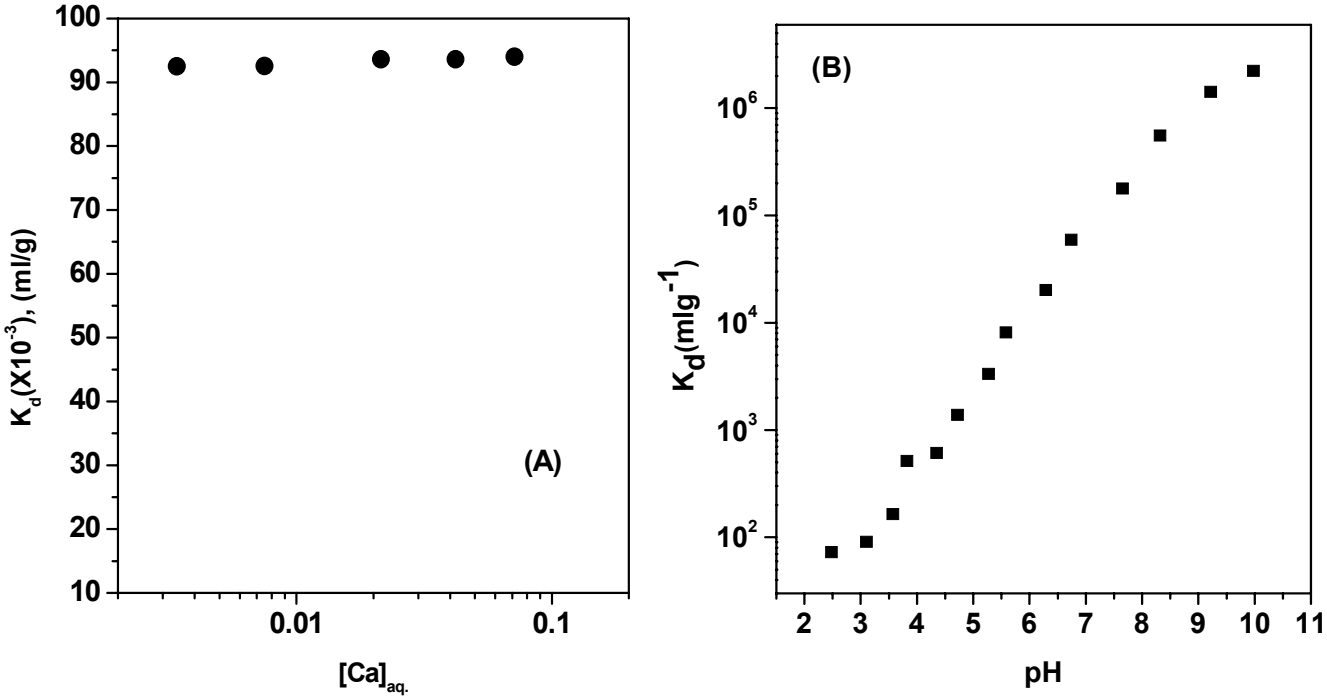

Figure 5.4 (A) Effect of Ca(II) concentration on K_d value for Am(III) sorption; pH 7.1 ± 0.1, [NaCl] = 0.1 M, m/V = 0.5 g/l. (B) Am(III) sorption edge on Ca-equilibrated natural clay in 0.0335 M $CaCl_2$ medium. m/V = 0.5 g/l. [Am(III)] = 6.0×10^{-9} M.

values infer lesser sorption of Am(III) on ion exchange sites of Ca(II)-equilibrated clay than that of Na(I)-equilibrated clay and this has indeed been observed in the present study (figure 5. 4 (B)).

5.3.5 Effect of anions on Am(III) sorption by Clay

Granitic ground water contains chloride (Cl^-), nitrate (NO_3^-) and sulphate (SO_3^{2-}) as the main anions and their effect on Am(III) sorption by clay over pH 2-10 in 0.1 M ionic strength has been studied. The results are presented in figure 5.5 (A). All the three anions do not affect the Am(III) sorption, except at the lower pH values (< 6) in the sulphate medium. These observations can be correlated to Am(III) aqueous speciation in the studied background electrolyte media. Am(III) exists predominantly as Am^{3+} in pH range 2-7 in the chloride and nitrate medium while speciation in the sulphate medium includes $Am(SO_4)^+$ and $Am(SO_4)_2^-$ along with Am^{3+} (figure 5.5 (B)). In the higher pH range the speciation remains the same in all the three anionic media and is dominated by the hydrolyzed species of Am(III), namely, $Am(OH)^{2+}$ and $Am(OH)_2^+$. Formation of singly charged Am(III) species and anionic species in the sulphate medium causes lesser electrostatic attraction of Am(III) to clay surfaces leading to decreased sorption at lower pH values.

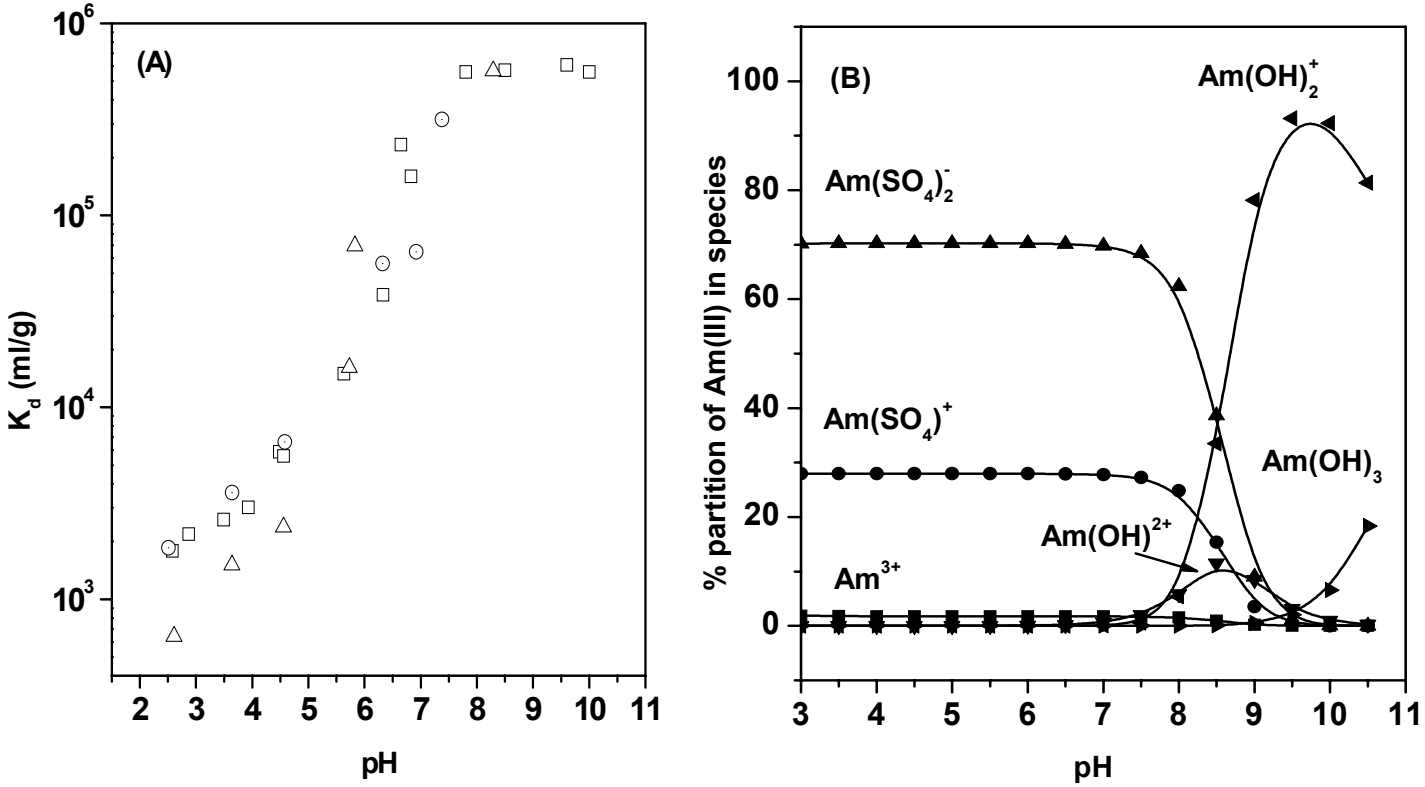

Figure 5.5. (A) pH-sorption edge of Am(III) in presence of different anions on Na-equilibrated natural clay. [Am] = 6.0 ×10^{-9} M, Symbols □, ○ and Δ stand for 0.1 M NaCl, 0.1 M $NaNO_3$, and 0.035 M Na_2SO_4, respectively. m/V = 0.5 g/l. (B) Am(III) speciation diagram in 0.035 M Na_2SO_4 medium made using MINTEQ A2 program. log K values for the species have been taken from Silva et al. (1995).

5.3.6 Eu(III) sorption on natural clay in granite ground water

Adsorption isotherm of Eu(III) on natural clay in granitic ground water has been shown as figure 5.6. Based on the conclusions drawn from the effect of pH, ionic strength, cation and anions, the model developed for natural clay was applied for sorption in granitic ground water. The solid line in figure 5.6 represents the model prediction with the optimized values of surface reactions. Model based simulation of experimental data is satisfactory for $\log[Eu]_{aq.} < -5$ while deviation from the experimental data was observed at higher metal ion concentrations. Inclusion of carbonate species $\equiv YOEuCO_3$ did not improve the fitting. The option of addition of one more surface site in the modelling could not be exercised owing to

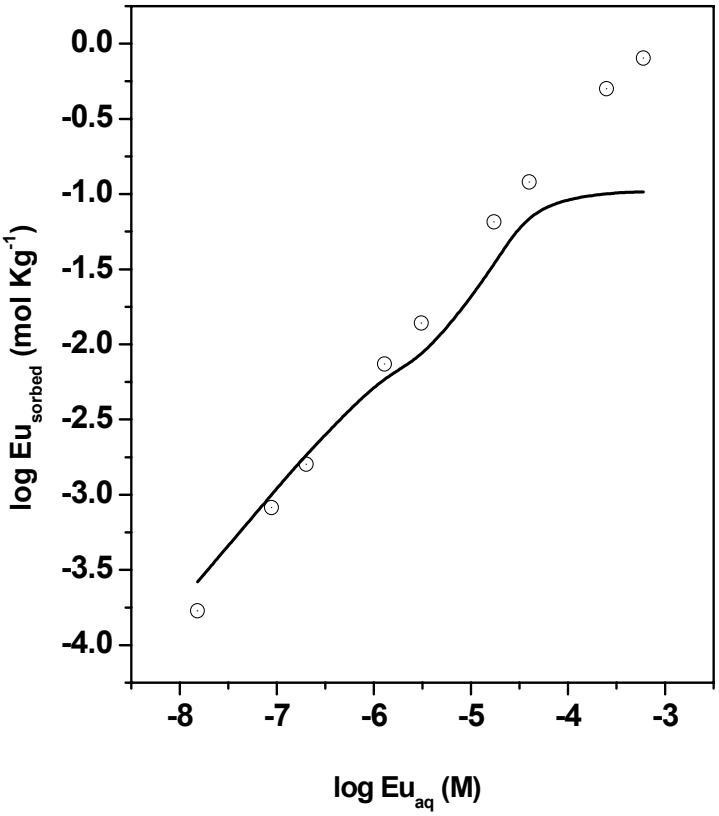

Figure 5.6 Adsorption isotherm of Eu(III) on natural clay in granitic ground water at pH 6.1 ± 0.1. [Eu(III)] = 10^{-3}-10^{-7} M. m/V = 0.5 g/l.

the limitation of number of surfaces species in FITEQL to only two amphoteric sites ($\equiv S^{S}OH$ and $\equiv S^{W1}OH$). At the highest Eu(III) concentration, the surface sites concentration will be lower than the metal ion concentration and hence surface precipitation may also take place.

5.4 Conclusion

A model has been proposed to simulate Am(III) sorption on multiphasic natural clay which is rich in smectite content. Experimental data of Am(III) sorption on montmorillonite - kaolinite clay mixtures established montmorillonite as the main sorbent for metal ions. Sorption studies at varying pH and ionic strength indicated ion exchange and surface complexation as the main mechanisms for Am(III) sorption at lower and higher pH, respectively. Simulation of sorption edges with the model based on ion exchange and surface complexation sites correctly predicted the sorption behaviour. Am(III) sorption by the clay remains unaffected in the presence of Ca(II) and anions (chloride, nitrate and sulphate) at higher pH values. However, at lower pH values the sorption is decreased in presence of sulphate ions. Thermodynamic model developed for clay in simple electrolyte media correctly predicted the sorption behaviour of Eu(III) for natural clay-groundwater combination in condition of metal ion concentration lower than 0.01 mM (pH 6.1). The model underestimates the sorption at higher metal ion concentrations, which could be due to onset of surface precipitation reactions.

Chapter 6

Summary and Conclusions

As part of the dissertation work, batch sorption study, molecular level spectroscopic techniques, linear additive and surface complexation modelling were used to investigate sorption behaviour of actinides and long lived fission products on oxide surfaces and Smectite rich natural clay. Aspects delineated in these studies were (1) effect of humic acid (HA) on sorption of fission products by mineral oxides, (2) role of surface reactivity in guiding the speciation of tri- and tetra valent actinides at oxide-water interface, and (3) modelling of sorption of trivalent actinides on smectite rich natural clay. The major findings and conclusions from this work are summarized below.

1. A batch sorption study over pH 3-10 and ionic strength 0.05- 0.1 M $NaClO_4$ indicated insignificant retention of Cs(I) by silica surface till pH ~ 7, which increased at higher pH values and attained a value ~30% at pH 10. Sorption percentage of Cs(I) dramatically increased in lower pH region in presence of HA, but there was no effect on sorption percentage above pH 7. Silica is negatively charged over the studied pH range and sorption of HA was found to lessen the surface charge. Charge characteristics thus failed to account for increased sorption in the ternary system of Cs(I)-HA-silica. As HA interacts very weakly with Cs ($\log \beta = -1.86 \pm 0.23$) in aqueous medium and silica does not show sorption capacity for Cs(I) at lower pH values, the sorption characteristics at lower pH values is thus attributed to modification of the silica surface sites upon their interaction with HA. Linear additive modelling of sorption in ternary system revealed higher binding capability of surface sorbed HA than that present in the aqueous phase. HA sorbed strongly on silica surface over lower pHs and its sorption decreased with increasing pH. There was no change in the sorption of HA on silica when ionic strength was varied from 0.05 to 0.1 M. Sorption of Cs(I) in HA equilibrated silica suspension, however, decreased with increased ionic

strength. This indicated the binding of Cs(I) in outer sphere complexation to the swarm of HA charge present on silica surface.

2. Tc(IV) sorption on alumina surface over pH 4 – 10 was also small (~ 20 %) but increased to quantitative sorption value at lower pH values (5 -7) in presence of HA. Sorption profile was in agreement with the typical effect of enhanced sorption at lower pH values and suppressed sorption at higher pH values in comparison to that of binary, Tc(IV) – alumina system. Linear additive modelling reproduced the sorption characteristics of ternary system (Tc(IV)-HA-alumina) with enhanced metal binding capacity of surface sorbed HA. Surface complexation modelling of the ternary system carried out to reveal the surface speciation indicated the formation of ligand bridged type 1 ternary complex of Tc(IV) on alumina surface. **These studies suggest metal - HA interaction as governing factor in the sorption of metal ions in ternary systems.**

3. Am(III) sorption on γ-alumina over varying pH and ionic strength indicated stronger sorption due to inner sphere complexation of metal ions with alumina surface sites. pH - sorption edge was found shifting to higher pH values with increasing metal ion concentration (10^{-7}-10^{-4} M). Life time data obtained in the fluorescence spectroscopic investigation with lanthanide analogue, Eu(III), revealed the existence of two types of binding of metal ions with surface sites, that is, formation of two surface species. Extended X-ray absorption fine structure spectroscopy (EXAFS) investigation confirmed the two surface complexes with different coordination geometries around Eu(III). Further, the onset of surface precipitation of Eu(III) was observed at pH 7. Surface complexation modelling of Am(III)/Eu(III) sorption under varying metal ion concentration condition at pH ≤ 7 revealed the evolution of surface species with varying surface coverage; mononuclear-monodentate species is the predominant

species at 10^{-7}-10^{-6} M, while at 10^{-5} M, and above pH 5.5, mononuclear-bidentate surface species starts to compete with monodentate speciation, and becomes the predominant surface species of Am(III)/Eu(III) on alumina surface at 10^{-4} M.

4. X-ray absorption spectroscopic investigation of Eu(III) sorbed by silica and alumina was carried out. At pH 7 – 8 the data indicated the absence of $Eu(OH)_3$ as surface speciation and showed coprecipitation of metal ions with dissolved species of alumina. Though the binding pattern of Eu(III) on both silica and alumina surfaces was found to be similar in the pH range of 6 – 8 there was a distinct difference in binding characteristics. Alumina prefers edge sharing metal ion binding over silica where corner sharing mode is more predominant. **These findings are of significant environmental relevance, as attachment of metal ions on solid substrates decides the surface speciation and thereby dissolution and fate of metal ions in aquatic environment.**

5. Pu(IV) sorption on silica and alumina over pH 2-10 showed strong binding capacity on both the substrates in concurrence with the strong complexing nature of hard Lewis acid, such as, Pu(IV), with hard Lewis base (oxygen atom of surface sites, ≡SOH). Kinetics of sorption of Pu(IV) on both the solids was found to follow similar pattern, namely, a fast step over small time followed by a slow step, though the rate of slow step was found to be higher for alumina surface. Comparison of kinetic rate constants observed in the present study and those in literature suggests that the slow step involves polymerization of surface sorbed Pu. Oxidation state analysis of surface sorbed Pu showed it in the form of Pu(IV). Dissolution study for surface Pu(IV) negated the formation of PuO_2(am.). Pu(IV) on silica and alumina surfaces may thus be present as small Pu (hydr)oxide clusters though there may exist difference in their exact stiochiometry and structure. Main difference regarding the role of these surfaces

was, however, observed in the oxidation state of Pu in the supernatants of oxide suspensions after equilibrium. The unsorbed Pu in silica suspension was found to be present as Pu(V), while in the case of alumina, it was present as a mixture of Pu(VI) and Pu(V). Higher sorption kinetics of Pu(IV) in case of alumina compared to silica causes disproportionation of Pu(V) to form Pu(VI) in the supernatant. **The study emphasizes the consideration of redox speciation of Pu during its migration in geosphere.**

6. Am(III) sorption on smectite rich natural clay, under varying conditions of pH and ionic strength, indicated the predominance of ion exchange mechanism at lower pH values while surface complexation dominated the sorption mechanism with increasing pH. Major phase of the clay sediment, montmorillonite, was found to govern the sorption behaviour of the clay with no effect of the minor phase kaolinite. Presence of cations, such as, Ca(II), as well as anions (Cl^-, NO_3^-, SO_4^{2-}) does not affect Am(III) sorption on clay in granitic ground water pH and ionic strength conditions. However, the profile of Am(III) sorption to Ca(II)-equilibrated clay is quite different from that for Na-equilibrated clay corroborating weaker exchange of Ca(II)-Am(III) in comparison to Na(I)-Am(III). Surface complexation model, developed for natural clay in simple electrolytes by including ion exchange site and amphoteric sites present at edges of montmorillonite, simulates well the sorption profiles at varying pH and ionic strength. Thermodynamic sorption model was finally applied to explain the Eu(III) sorption isotherm with granitic ground water at pH 6.1. The model was found to simulate the sorption well at lower metal ion concentration while there was deviation at higher metal ion concentration. **Description of sorption process in natural system in the framework of SCM thus promises to provide a realistic assessment of the risk posed by migrating radionuclides in environment.**

Appendix 1

Program written in BASIC language and run on GWBASIC COMPILER

```
10    REM PROGRAM TO CALCUALTE THE PERCENTAGE SORPTION
20    INPUT "ENTER THE FILE NAME: ",A$
30    FILEIN$= A$+".IN"
40    FILEOUT$=A$+".OUT"
50    OPEN "I", #1, FILEIN$
60    OPEN "O", #2, FILEOUT$
70    INPUT#1, NDAT
80    FOR I=1 TO NDAT
90    INPUT#1, PH, A0, BKG1, A, BKG2
100   CORRA0= (A0-BKG1)
110   CORRA= (A-BKG2)
120   PERSORP=((CORRA0-CORRA)/(CORRA0)*100
130   FACT1= ((SQR(A0+A+BKG1+BKG2))/(CORRA0-CORRA))^2
140   FACT2= ((SQR(A0+BKG1))/CORRA0)^2
150   ERRFACT=SQR(FACT1+FACT2)
160   ERRSORP=PERSORP*ERRFACT
170   PRINT PH, PERSORP, ERRSORP
180   PRINT#2, PH, PERSORP, ERRSORP
190   NEXT I
200   STOP
210   END
```

Appendix 2

Table: Screen "II. Species" in FITEQL for the Tc(IV)-HA-alumina system

Components→ Species↓	Log K	x-PSI	TcO^{2+}	XOH	HL_1	HL_2	HL_3	Tc(ads)	H[+]
H[+]	0	0	0	0	0	0	0	0	1
OH[-]	-13.800	0	0	0	0	0	0	0	-1
TcO[2+]	0	0	1	0	0	0	0	1	0
TcO(OH)[+]	-1.140	0	1	0	0	0	0	1	-1
$TcO(OH)_2$	-3.300	0	1	0	0	0	0	1	-2
HL_1	0	0	0	0	1	0	0	0	0
HL_2	0	0	0	0	0	1	0	0	0
HL_3	0	0	0	0	0	0	1	0	0
L_1	-3.602	0	0	0	1	0	0	0	-1
L_2	-5.885	0	0	0	0	1	0	0	-1
L_3	-8.118	0	0	0	0	0	1	0	-1
XOH	0	0	0	1	0	0	0	0	0
XO[-]	-9.100	-1	0	1	0	0	0	0	-1
XOH_2[+]	7.292	1	0	1	0	0	0	0	1
$TcOL_1$	-5.00	0	1	0	1	0	0	1	-1
XOL_1TcO	6.500	0	1	1	1	0	0	1	-2
$XOHHL_1$	4.439	0	0	1	1	0	0	0	0

Appendix 3

Possible geometries for Eu binding onto amorphous silica and γ-alumina surfaces

Eu can bind on the silica surface in (1) corner-sharing monodentate mode, (2) edge sharing monodentate mode, (3) corner sharing bidentate bridging mode, and (4) tetrahedral face sharing tridentate mode (figure 1S). Assuming individual SiO_4 tetrahedra in am-SiO_2 similar in size to the tetrahedra of quartz (α-SiO_2), O-O edge distances of SiO_4 tetrahedra range from 2.58 to 2.67 Å in am-SiO_2 (Cheah et al., 1998). Considering O-O edge distance of silica tetrahedra and the Eu-O distance obtained in the EXAFS analysis for the sorption samples, Eu-Si distance would be ~3.28 to 4.18 Å in corner sharing monodentate binding, ~2.88 to 3.08 Å in edge-shared, bidentate binding and distance will be in the range of 3.68 to 4.18 Å when monomeric Eu binds to the silica surface in a corner-shared, bridging bidentate mode. A tridentate binding of Eu on silica surface will cause considerable strain because of the mismatch between the O-O bond distances in Eu-O polyhedra and Si-O tetrahedra and hence was not included in the present calculation. Distances in case of corner sharing binding mode are higher compared to the edge sharing mode as the corner sharing mode offers flexibility of placement of Eu polyhedra with respect to the silica tetrahedra. Bond angle considered in the bond distance calculation of Eu – Si corner sharing monodentate bonding, ranges from 120^0 to 180^0; angle lower than 120^0 will be sterically hindered. First Si shell at ~3.2 Å compares with the range of edge shared bidentate binding while the higher shell at 4.0 Å lies in the range of corner sharing binding mode. However, it cannot be ascertained whether it is for the bridging bidentate coordination geometry or the monodentate binding. Nevertheless, the higher N_{Si} value for this shell suggests formation of multinuclear surface sorption product where the existence of either or both binding mode cannot be ruled out. For example, the most thermodynamically stable silicate phase - disilicates - of rare earth ions exhibit both types of binding on silica tetrahedral (SiO_4) (Fleet and Liu, 2004).

Similar calculation in case of γ-alumina yielded the following values: ~3.40 to 4.40 Å for corner-shared monodentate binding, 3.30 to 3.40 Å for edge-shared bidentate bonding to the Al-octahedra, ~2.70 Å for edge-shared bidentate bonding to the Al-tetrahedra (AlO_4), 3.81 to 4.31 Å for Eu vicinal binding to the apices of two nearby Al octahedra (AlO_6) (i.e, bridging mode) (figure 2S). Bond distance determination is based on O-O edge distances (2.69-2.90 Å) of AlO_6 octahedra in γ-Al_2O_3 (Cheah et al., 1998) and Eu-O distance determined in the first shell analysis of the alumina sorption samples. Comparing the distances obtained for two Al backscatter shells with the distances calculated for different interaction modes at alumina surface, it indicates edge shared bidentate binding for shorter distance while the binding is corner sharing for the 4 Å backscatter shell.

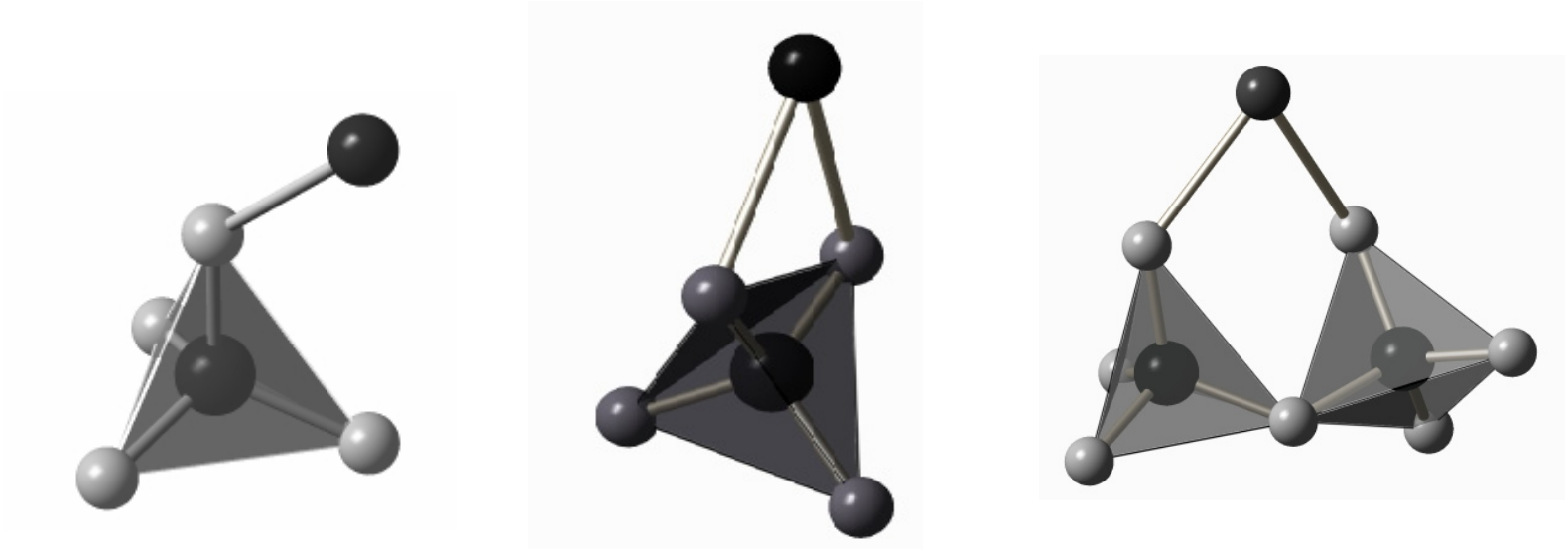

Corner-shared monodentate binding:

Eu-Si distance = 3.28 – 4.18 Å

Edge-shared Bidentate binding:

Eu-Si distance = 2.88 – 3.08 Å

Corner-shared Bridging Bidentate binding:

Eu-Si distance = 3.68 – 4.18 Å

Figure 1S. Schematic for the possible binding modes of Eu(III) on SiO_4 tetrahedra and the resulting Eu-Si distances.

(a)

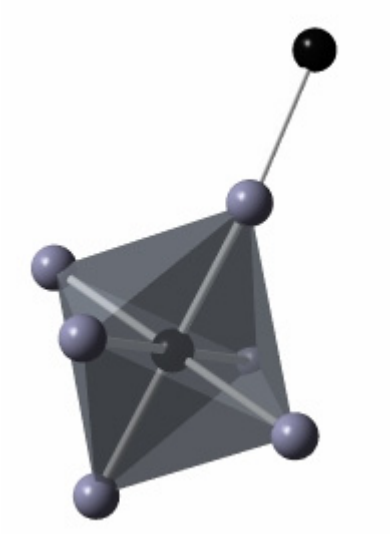

Corner sharing monodentate binding

Eu-Al distance = 3.40 – 4.40 Å

(b)

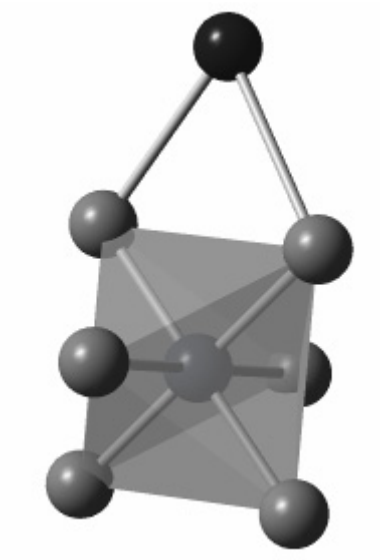

Edge-shared Bidentate binding:

Eu-Al distance = 3.30 – 3.40 Å

(c)

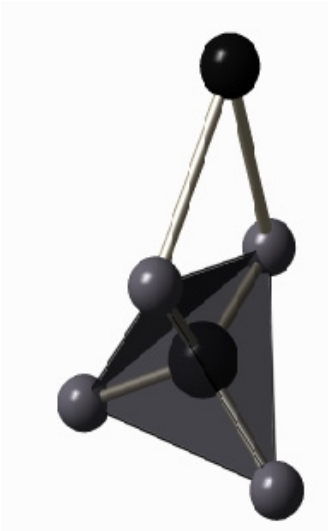

Edge-shared Bidentate binding:

Eu-Al distance = ~ 2.70 Å

(d)

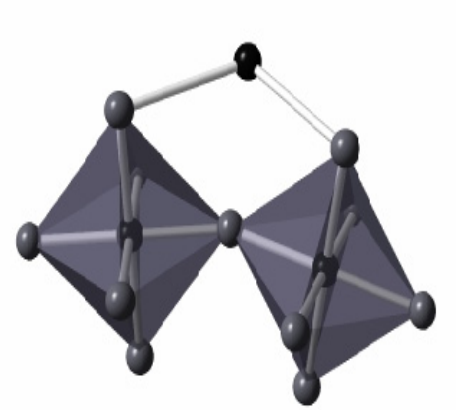

Corner-shared Bridging Bidentate binding:

Eu-Al distance = 3.81 – 4.31 Å

Figure 2S. Schematic for the possible binding modes of Eu(III) on Aluminium octahedra and tetrahedra, and the resulting Eu-Al distances on alumina surface.

References

A

Altmann, S. (2001) Using chemical thermodynamic models for guiding radioelement K_d investigations for performance assessment. A status report. *OECD, Nuclear Energy Agency*.

Andre´, C., Choppin, G. R. (2000) Reduction of Pu(V) by humic acid. *Radiochim. Acta* **88**, 613-616.

Artinger, A., Buckau, G., Zeh, P., Geraedts, K., Vancluysen, J., Maes, A., Kim, J. I. (2003) Humic colloid mediated transport of tetravalent actinides and technetium. *Radiochim. Acta* **91**, 743 – 750.

Alacacio, T. E., Hesterberg, D., Chou, J. W., Martin, J. D., Beauchemin, S., Sayers, D., E. (2001) Molecular scale characteristics of Cu(II) bonding in goethite-humate complexes. *Geochim. Cosmochim. Acta* **65**, 1355 - 1366.

B

Bachmaf, S., Planer-Friedrich, M., Merkel, B. J. (2008) Effect of sulphate, carbonate, and phosphate on the uranium(VI) sorption behaviour onto bentonite. *Radiochim. Acta.* **96**, 359 - 366.

Bajpai, R. K. (2008) Characterization of Natural Barriers of Deep Geological Repositories for High-level Radioactive Wastes in India. *Indian Nuclear Society News*, **5 (4)**, 40 - 47.

Banwart, S. A. (1997) Aqueous speciation at the interface between geological solids and groundwater. *In*: *Modelling in Aquatic Chemistry*. (Eds.) Grenthe, I., Puigdomenech. OECD.

Bargar, J. R., Towle, S. N., Brown, G. E., Jr., Parks, G. A. (1997) XAFS and bond valence determination of the structures and compositions of surface functional groups and Pb(II) and Co(II) sorption products on single-crystal α-Al_2O_3. *J. Colloid Interface Sci.* **185**, 473 - 492.

Berger, G., Cadore, E., Schott, J., Dove, P. M. (1994) Dissolution rate of quartz in lead and sodium electrolyte solutions between 25 and 300 ^{0}C: Effect of the nature of surface complexes and reaction affinity. *Geochim. Cosmochim. Acta* **58**, 541 – 551.

Bradbury, M. H., Baeyens, B. (2002) Sorption of Eu on Na- and Ca-montmorillonites: Experimental investigations and modelling with cation exchange and surface complexation. *Geochim. Cosmochim. Acta* **66**, 2325 - 2334.

Bradbury, M. H., Baeyens, B. (2005) Experimental measurements and modelling of sorption competition of montmorillonite. *Geochim. Cosmochim. Acta* **69**, 4187 - 4197.

Bradbury, M. H., Baeyens, B. (2006) Modelling sorption data for the actinides Am(III), Np(V) and Pa(V) on montmorillonite. *Radiochim. Acta* **94**, 619 - 625.

Bradbury, M. H., Baeyens, B. (2009) Experimental and modelling studies on the pH buffering of MX-80 bentonite porewater. *Appl. Geochem.* **24**, 419 - 425.

Bradbury, M. H., Baeyens, B. (2011) Predictive sorption modelling of Ni(II), Co(II), Eu(III), Th(IV) and U(VI) on MX-80 bentonite and Opalinus clay: A “bottom-up” approach. *Appl. Clay Sci.* **52**, 27-33.

Brown, Jr., G. E., Henrich, V. E., Casey, W. H., Clark, D. L., Eggleston, C., felmy, A., Goodman, D. W., Gratzel, M., McCarthy, M. I., Nealson, K. H., Sverjensky, D. A., Toney, M. F., Zachara, J. M. (1999) Metal oxide surfaces and their interactions with aqueous solutions and microbial organisms. *Chem. Rev.* **99**, 77 – 174.

Bruggeman, C., Liu, D. J., Maes, N. (2010) Influence of boom clay organic matter on the adsorption of Eu^{3+} by illite – geochemical modelling using the component additivity approach. *Radiochim. Acta* **98**, 597 – 605.

Bruno, J., Montoya, V. (2012) From aqueous solution to solid solutions: A process oriented review of the work performed within the FUNMIG project. *Appl. Geochem.* **27**, 444 - 452.

Bryan, N. D., Abrahamsen, L., Evans, N., Warwick, P., Buckau, G., Weng, L., Van Riemsdijk, W. H. (2012) The effects of humic substances on the transport of radionuclides: recent improvements in the prediction of behaviour and the understanding of mechanisms. *Appl. Geochem.* **27**, 378 - 389.

Bouby, M., Geckeis, H., Lutzenkirchen, J., Mihai, S., Schafer, T. (2011) Interaction of bentonite colloids with Cs, Eu, Th and U in presence of humic acid: A flow field-flow fractionation study. *Geochim. Cosmochim. Acta* **75**, 3866 - 3880.

Bunker, G. (2010) *Introduction to XAFS: A practical guide to X-ray absorption fine structure spectroscopy*, Cambridge University Press, UK.

C

Charlet, L., Manceau, A. A. (1992) X-ray absorption spectroscopic study of the sorption of Cr(III) at the oxide-water interface. *J. Colloid Interface Sci.* **148**, 443 – 458.

Cheah, S. –F., Brown, G. E., Jr., Parks, G. A. (1998) XAFS spectroscopy study of Cu(II) sorption on amorphous SiO_2 and γ-Al_2O_3: Effect of substrate and time on sorption complexes. *J. Colloid Interface Sci.* **208**, 110 - 128.

Choppin, G. R. (1988) Humics and Radionuclide Migration, *Radiochim. Acta* **44/45**, 23 - 28.

Choppin, G. R., Stout, B. E. (1989) Actinide behaviour in natural waters. *Sci. Total Environ.* **83**, 203 - 216.

Choppin G. (1992) The role of natural organics in radionuclide migration in natural aquifer systems. *Radiochim. Acta* **58/59**, 113–120.

Choppin, G. R. (2006) Actinide speciation in aquatic systems. *Mar. Chem.* **99**, 83 - 92.

Claret, F., Schäfer, T., Rabung, T., Wolf, M., Bauer, A., Buckau, G. (2005) Differences in properties and Cm(III) complexation behavior of isolated humic and fulvic acid derived from Opalinus clay and Callovo-Oxfordian argillite. *Appl. Geochem.* **20**, 1158 – 1168.

Claret, F., Schäfer, T., Brevet, J., Reiller, P.E. (2008) Fractionation of Suwannee River fulvic acid and aldrich humic acid on α-Al_2O_3: spectroscopic evidence. *Environ. Sci. Technol.* **42**, 8809 – 8815.

Coppin, F., Berger, G., Bauer, A., Castet, S., Loubet, M. (2002) Sorption of lanthanides on smectite and kaolinite. *Chem. Geol.* **182**, 57 - 68.

Coston, J. A., Fuller, C. C., Davis, J. A. (1995) Pb^{2+} and Zn^{2+} adsorption by a natural Al- and Fe-bearing surface coating on an aquifer sand, *Geochim. Cosmochim. Acta* **59**, 3535 - 3548.

Courdouan, A., Christl, I., Meylan, S., Wersin, P., Kretzschmar, R. (2008) Proton and trivalent metal cation binding by dissolved organic matter in the Opalinus clay and the callovo-oxfordian formation. *Environ. Sci. Technol.* **42**, 5985 - 5991.

D

Dähn, R, Scheidegger, A. M., Manceau, A., Schlegel, M. L., Baeyens, B., Bradbury, M. H., Morales, M. (2002) Neoformation of Ni phyllosilicate upon Ni uptake on montmorillonite: A kinetics study by powder and polarized EXAFS. *Geochim. Cosmochim. Acta*, **66**, 2335 - 2347.

Dardenne, K., Schåfer, T., Denecke, M. A., Rothe, J., Kim, J. I. (2001) Identification and characterization of sorbed lutetium species on 2-line ferrihydrite by sorption data modeling, TRLFS and EXAFS. *Radiochim. Acta* **89**, 469 - 479.

Davis, J. A., Gloor, R. (1981) Adsorption of Dissolved Organics in Lake Water by Aluminum Oxide. Effect of Molecular Weight. *Enviorn. Sci. Technol.* **15**, 1223 – 1229.

Davis, J. A., Coston, J. A., Kent, D. B., Fuller, C. C. (1998) Application of surface complexation concept to complex mineral assemblages. *Environ. Sci. Technol.* **32**, 2820 - 2828.

Davies-Colley, R. J., Nelson, P.O., Williamson, K.J. (1984) Copper and cadmium uptake by estuarine sedimentary phases. *Environ. Sci. Technol.* **18**, 491-499.

Degueldre, C., Bolek, M. (2009) Modelling colloid association with plutonium: The effect of pH and redox potential. *Appl. Geochem.* **24**, 310 - 318.

Denecke, M. A. (2006) Actinide speciation using X-ray absorption fine structure spectroscopy, *Coordin. Chem. Rev.* **250**, 730 - 735.

Drot, R., Roques, J., Simoni, É (2007) Molecular approach of the Uranyl/mineral interfacial phenomena. *C. R. Chemie* **10**, 1078 – 1091.

Dumat, C., Quiquampoix, H., Staunton, S. (2000) Adsorption of cesium by synthetic clay-organic matter complexes: Effect of the nature of organic polymers. *Environ. Sci. Technol.* **34**, 2985 - 2989.

Durbin, P. W. (2010) Actinides in animal and man. Chapter 31. In: *The chemistry of the actinide and transactinde elements. Morss, L. R., Edelstein, N. M, Fuger, J. (Eds.), Springer, The Netherlands.*

Duro, L., Bruno, J., Rolin, C., Guimera, J., Geckeis, H., Schuβler, W., Vejmelka, P., Shibata, M., Yoshida, Y., Ota, K., Yui, M. (2000) Prediction of the solubility and speciation of RN in FEBEX and Grimsel waters. *Colloid and Radionuclide Retention project. NAGRA Technical Report 99 -218, Nagra, Wettingen, Switzerland*.

Dzombak, D. A., Morel, F. M. M. (1990) *Surface Complexation Modeling: Hydrous Ferric Oxide*. John Wiley & Sons.

E

Edelstein, N. M., Klenze, R., Fanghänel, T., Hubert, S. (2006) Optical properties of Cm(III) in crystals and solutions and their applications to Cm(III) speciation. *Coordin. Chem. Rev.* **250**, 948 – 973.

F

Fairhust, A. J., Warwick, P., Richardson (1995) The influence of humic acid on the adsorption of europium onto inorganic colloids as a function of pH. *Colloids Surf. A* **99**, 187 - 199.

Farr, J. D., Schulze, R. K., Honeymann, B. D. (2000) Aqueous Pu(IV) sorption on brucite. *Radiochim. Acta* **88**, 675 - 679.

Feng, X., Simpson, A. J., Simpson, M. J. (2006) Invstigating the role of mineral bound humic acid in phenanthrene sorption. *Environ. Sci. Technol.* **40,** 3260 – 3266.

Fernandes, M. M., Stumpf, T., Rabung, T., Bosbach, D., Fanghanel, Th. (2008) Incorporation of trivalent actinides into calcite: A time resolved laser fluorescence spectroscopy (TRLFS) study. *Geochim. Cosmochim. Acta* **72**, 464 - 469.

Fleet, M., Liu, X. (2000) Structure and complex twinning of dysprosium disilicate ($Dy_2Si_2O_7$), Type B. *Acta Cryst. B* **56**, 940 - 946.

Friedlander, G., Kennedy, J. W., Macias, E. S., Miller, J.M. (1981) Nuclear and Radiochemistry, John Wiley & Sons, USA.

Froideval, A., Del Nero, M., Gaillard, C., Barillon, R., Rossini, I., Hazemann, J. L. (2006) Uranyl sorption species at low coverage on Al-hydroxide: TRLFS and XAFS studies. *Geochim. Cosmochim. Acta* **70**, 5270 - 5284.

Fukushi K., Sverjensky D. A. (2007) A predictive model for arsenate adsorption and surface speciation on oxides consistent with spectroscopic and theoretical molecular evidence. *Geochim. Cosmochim. Acta* **71**, 3717 – 3745.

G

Galunin, E., Alba, M. D., Santos, M. J., Abrao, T., Vidal, M. (2010) Lanthanide sorption on smectite clays in presence of cement leachates. *Geochim. Cosmochim. Acta* **74**, 862 - 875.

Geckeis, H., Rabung, T. (2008) Actinide geochemistry: From the molecular level to the real system, *J. Contam. Hydrol*. **102**, 187 – 195.

Geipel, G (2006) Some aspects of actinide speciation by laser-induced spectroscopy, *Coordin. Chem. Rev.* **250,** 844 - 854.

Geraedts, K., Bruggeman, C., Maes, A., Van Loon, L. R., Rossberg, A., Reich, T. (2002) Evidence for the existence of Tc(IV)–humic substance species by X-ray absorption near edge spectroscopy, *Radiochim. Acta* **90**, 879 – 884.

Guo, Z., Xu, J., Shi, K., Tang, Y., Wu, W., Tao, Z. (2009) Eu(III) adsorption/desorption on Na-bentonite: Experimental and modelling studies. *Colloids Surf. A: Physicochem. Eng. Aspects* **339**, 126-133.

H

Ha, J., Trainor, P. T., Farges, F., Brown, Jr., G. E. (2009) Interaction of Aqueous Zn(II) with hematite nanoparticles and microparticles. Part 1. EXAFS Study of Zn(II) adsorption and precipitation. *Langmuir* **25**, 5574 – 5585.

Hakem, N., Apps, J. A., Moridis, G. J., Al Mahamaid, I. (2004) Sorption of fission product radionuclides, ^{137}Cs and ^{90}Sr, by Savannah River sediments impregnated with colloidal silica. *Radiochimica. Acta* **92**, 419 - 432.

Hartmann, E., Geckeis, H., Rabung, Th., Lutzenkirchen, J., Fanghanel, Th. (2008) Sorption of radionuclides onto natural clay rocks. *Radiochem. Acta* **96**, 699 - 707.

Hayes, K. F., Leckie, J. O. (1987) Modelling ionic strength effect on cation adsorption at hydrous oxide/solution interfaces. *J. Colloid Interface Sci.* **115**, 564 – 572.

Hayes, M. H. B., McCarthy, P., Malcolm, R. L., Swift, R. S. (eds.) (1989) *Humic substances II: In search of structure*. John Wiley & Sons.

Hayes, K. F., Redden, G., Ela, W., Leckie, J. O. (1991) Surface complexaion models: an evaluation of model parameter estimation using FITEQL and oxide mineral titration data. *J. Colloid Interface Sci.* **142**, 448 - 469.

Herbelin, A., Westall, J. (1994). FITEQL – *A Computer Program for Determination of Chemical Equilibrium Constants from Experimental Data*. Oregon State University, Corvallis.

Hiemstra, T., Van Riemsdijk W. H. (1990) Multiple activated complex dissolution of metal (hydr)oxides. *J. Colloid Interface Sci.* **6**, 132 – 150.

Hixon, A. E., Hu, Y. –J., Kaplan, D. I., Kukkadapu, R. K., Nitsche, H., Qafoku, O., Powell, B. A. (2010) Influence of iron redox transformations on plutonium sorption to sediments. *Radiochim. Acta* **98**, 685 – 692.

Hohl, H., Stumm, W. (1976) Interaction of Pb^{2+} with hydrous γ-Al_2O_3. *J. Colloid Interface Sci.* **55**, 281 – 288.

Honeyman, B. D. (1999) Colloidal culprits in contamination, *Nature* **397**, 23 - 24.

Horrocks, W., De, W., Sudnick, D. R. (1979) Lanthanide ion probes of structure in Biology. Laser induced luminescence decay constants provide a direct measure of the number of metal-coordinated water molecules. *J. Am. Chem. Soc.* **101**, 334 - 340.

Huittinen, N., Rabung, Th., Lutzenkirchen, J., Mitchell, S. C., Bickmore, B. R., Lehto, J., Geckeis, H. (2009) Sorption of Cm(III) and Gd(III) onto gibbsite, α-$Al(OH)_3$: A batch and TRLFS study. *J. Colloid Int. Sci.* **332**, 158 - 164.

Hur, J., Schlautman, M. A. (2003) Molecular weight fractionation of humic substances by adsorption onto minerals. *J. Colloid Interface Sci.* **264**, 313 – 321.

J

Jenne, E. A. (1998) *Adsorption of metals by geomedia: Variables, Mechanisms, and Model applications*. Academic Press, Richland, Washington.

Joseph, C., Schmeide, K., Sachs, S., Brendler, V., Geipel, G., Bernard, G. (2011) Sorption of uranium(VI) onto Opalinus clay in the absence and presence of humic acid in Opalinus clay pore water. *Chem. Geol.* **284**, 240 – 250.

K

Kaplan, D. I., Demirkanli, D. I., Gumapas, L., Powell, B. A., Fjeld, R. A., Molz, F. J., Serkiz, S. M. (2006a) Eleven-year field study of Pu migration from Pu III, IV, and VI sources. *Environ. Sci. Technol.* **40**, 443 - 448.

Kaplan, D. I., Powell, B. A., Gumapas, L., Coates, J. T., Fjeld, R. A., Diprete, D. P. (2006b) Influence of pH on plutonium desorption/solubilization from sediment. *Environ. Sci. Technol.* **40**, 5937 - 5942.

Kar, A. S., Kumar, S., Tomar, B. S., Manchanda, V. K. (2011) Sorption of curium by silica colloids: Effect of humic acid. *J. Hazard. Mater.* **186**, 1961 - 1965.

Kar, A. S., Tomar, B. S., Godbole, S. V., Manchanda, V. K. (2011) Time resolved fluorescence spectroscopy and modellling of Eu(III) sorption by silica in presence and absence of alpha hydroxyl isobutyric acid. *Coll. and Surf. A: Physicochem. Eng. Aspects* **378**, 44 - 49.

Keeney-Kennicutt, W. L., Morse, J. W. (1985) The redox chemistry of $Pu(V)O_2^+$ intercation with common mineral surfaces in dilute solutions and seawater. *Geochim. Cosmochim. Acta.* **49**, 2577 - 2588.

Kelly, S. D., Hesterberg, D., Ravel, B. (2008) Analysis of soils and minerals using X-ray absorption spectroscopy, 387-463. *In* Methods of Soil Analysis, Part 5. Mineralogical Methods. Soil Society of America, USA.

Kersting, A. B., Efurd, D. W., Finnegan, D. L., Rokop, D. J., Smith, D. K., Thompson, J. L. (1999) Migration of plutonium in ground water at the Nevada Test Site. *Nature* **397,** 56 - 59.

Kersting, A. B., Reimus, P. W., Abdel-Fattah, A., Allen, P. G., Anghel, I., Benedict, F. C., Esser, B. K., Lu, N., Kung, K. S., Nelson, J., Neu, M. P., Reily, S. D., Smith, D. K., Sylwester, E. R., Wang, L., Ware, S. D., Warren, R. G., Williams, R. W., Wang, L., Ware, S. D., Warren, R. G., Williams, R. W., Zavarin, Z., Zhao, P. (2003) Colloid-Facilitated Transport of Low-Solubility Radionuclides: A Field, Experimental, and Modeling Investigation. *LANL report, UCRL-ID-149688*.

Kim, J. (1986) Chemical behaviour of transuranic elements in natural aquatic elements. *In Handbook on the physics and chemistry of the actinides, (eds.) Freeman, A. J., Keller, C.)* Elsevier Science, chapter 8, 413 – 455.

Kim, J. I., Kanellakopulopolos, B. (1989) Solubility products of Pu(IV) oxide and hydroxide. *Radiochim. Acta* **48**, 145 - 150.

Kim, J. I., Buckau, G., Li, G. H., Duschner, H., Psarros, N. (1990) Characterization of humic and fulvic acids from Gorleben groundwater. *Fresenius J. Anal. Chem.* **338**, 245 - 252.

Kim, J. I., Czerwinski, K. R. (1996) Complexation of metal ions with humic acid: metal ion charge neutralisation model. *Radiochim. Acta* **73**, 5 – 10.

Kinniburgh, D. G., van Riemsdijk, W. H., Koopal, L. K., Borkovec, M., Benedetti, M. F., Avena, M. J. (1999) Ion binding to natural organic matter: competition, heterogeneity, stoichiometry and thermodynamic consistency. *Colloids Surf. A: Physicochem. Eng. Aspects* **151**, 147 – 166.

Koningsberger, D. C, Prins, R. (ed.) (1988) X-ray Absorption: Principles, applications, techniques of EXAFS, SEXAFS and XANES. John Wiley & Sons, New York.

Kowal-Fouchard, A., Drot, R., Simoni, E., Marmier, N., Fromage, F., Ehrhardt, J. (2004**)** Structural identification of europium(III) sorption complexes on montmorillonite. *New. J. Chem.* 28, 864-869.

Kumar, S., Rawat, N., Tomar, B. S., Manchanda, V. K., Ramanathan, S. (2007) Effect of humic acid on the sorption of technetium by hematite colloids using 95mTc and Tc tracers. *J. Radioanalytical Nucl. Chem.* **274**, 229 - 231.

Kumar, S., Rawat, N., Kar, A. S., Tomar, B. S., Manchanda, V. K. (2011) Effect of humic acid on sorption of technetium by alumina. *J. Hazard. Mater.* **192**, 1040 - 1045.

Kumar, S., Godbole, S. V., Tomar, B. S. Speciation of Am(III)/Eu(III) sorbed on γ-Alumina: Effect of metal concentration, *Radiochim. Acta*. *DOI:* 10.1524/ract.2013.1997.

Kumar, S., Kar, A.S., Tomar, B. S., Bhattacharya, D. (2012) XAFS Spectroscopy study of Eu(III) sorption products on Amorphous Silica and γ-Alumina: Effect of pH and substrate. *Polyhedron* **33**, 33-40.

Kumar, S., Kasar, S. U., Tomar, B. S. Interfacial sorption/desorption studies of Pu(IV) on Silica and alumina surfaces. *Radiochim. Acta. DOI: 10.1524/ract.2013.1997.*

L

Leiser, K. H. (1995) Radionuclides in the geosphere: Sources, mobility, reactions in natural waters and interactions with solids. *Radiochim. Acta* **70/71**, 355 – 375.

Langmuir, D. (1997) The use of laboratory adsorption data and models to predict radionuclide releases from a geological repository: a brief history. *Mater. Res. Soc. Symp. Proc.* **465**, 769 – 780.

Lenhart, J. J., Honeyman, B. D. (1999) Uranium (VI) sorption to hematite in the presence of humic acid. *Geochim. Cosmochim. Acta* **63**, 2891 - 2901.

Lenhart, J. J., Cabaniss, S. E., MacCarthy, P., Honeyman, B. D. (2000) Uranium (VI) complexation with citric, humic and fulvic acids. *Radiochim. Acta* **88**, 345 - 353.

Lu, N., Reimus, P. W., Parker, G. R., Conco, J. L., Triay, I. R. (2003) Sorption kinetics and impact of temperature, ionic strength and colloid concentration on the adsorption of plutonoium-239 by inorganic colloids. *Radiochim. Acta* **91**, 713 - 720.

Lujaniene, G., Benes, P., Stamberg, K., Sciglo, T. (2012) Kinetics of plutonium and americium sorption to natural clay. *J. Environ. Radioact.* **108**, 41 - 49.

Lutzenkirchen, J. (2012) Summary of studies on (ad)sorption as a “well-established” process within FUNMIG activities. *Appl. Geochem.* **27**, 427 - 443.

M

Maes, F A., Vancluysen, J., Geraedts, K. (1999) Studies on the reduction of Tc(VII) and the formation of Tc–Humic substance complexation in synthetic and natural systems. Effects of Humic substances on the migration of Radionuclides: Complexation and Transport of Actinides. *Second Technical Progress Report of the EC project no: FI4W-CT96-0029, Report FZKA 6324*, *(ed.) G. Buckau.*

Maes, A., Bruggeman, C., Geraedts, K., Vancluysen, J. (2003) Quantification of the interaction of Tc with dissolved boom clay humic substances, *Environ. Sci. Technol.* **37,** 747 – 753.

Maes, A., Geraedts, K., Bruggeman, C., Vancluysen, J., Rossberg, A., Hennig, C. (2004) Evidence for the interaction of technetium colloids with humic substances by X-ray absorption spectroscopy, *Environ. Sci. Technol.* **38**, 2044–2051.

Maes, N., Wang, L., Hicks, T., Bennert, D., Warwick, P., Hall, T., Walker, G., Dierckx, A. (2006) The role of natural organic matter in the migration behaviour of americium in the Boom Clay – Part I: Migration experiments. *Phys. Chem. Earth.* **31**, 541 - 547.

Marmidėe, B., Jahn, K., Ariese, F., Gooijer, C., Kumke, M. U. (2010) Direct spectroscopic evidence of 8- and 9-fold coordinated europium(III) species in H_2O and D_2O. *J. Phys. Chem. A* **114**, 13050-13054.

Marmier, N., Dumonceau, A. J., Fromage, F. (1997) Surface complexation modeling of Yb(III) sorption and desorption on hematite and alumina. *J. Contam. Hydrol.* **26**, 159 - 164.

Marmeir, N., Delisee, A., Fromage, F. (1999) Surface Complexation Modeling of Yb(III), Ni(II) and Cs(I) sorption on magnetite. *J. Colloid Int. Sci.* **211**, 54 - 60.

Marmier, N., Delisée, A., Fromage, F. (1999) Surface complexation modeling of Yb(III) and Cs(I) soption on silica. *J. Colloid Interface Sci.* **212**, 228 – 233.

Marmier, N., Fromage, F. (1999) Comparing electrostatic and nonelectrostatic surface complexation modelling of the sorption of Lanthanum on hematite. *J. Colloid Int. Sci.* **212,** 252 - 263.

Manceau, A., Schlegel, M., Nagy, K. L., Charlet, L. (1999) Evidence for the formation of trioctahedral clay upon sorption of Co^{2+} on quartz. *J. Colloid Interface Sci.* **220**, 181 – 197.

Meier, L. P., Kahr, G. (1999) Determination of the cation exchange capacity (CEC) of clay minerals using the complexes of copper(II) ion with triethylenetetramine and tetraethylenepentamine. *Clays and Clay Minerals*, **47**, 386 – 388.

Meier, M., Namjesnik-Dejanovic, K., Maurice, P., Chin, Y.-P., Aiken, G. R. (1999) Fractionation of aquatic natural organic matter upon sorption to goethite and kaolinite. *Chem. Geol.* **157**, 275-284.

Miller, A. W., Wang, Y. (2012) Radionuclide Interaction with Clays in Dilute and Heavily Compacted Systems: A Critical Review. *Environ. Sci. Technol.* **46**, 1981 - 1994.

Milne, C.J., Kinniburgh, D.G., Van Riemsdijk, W.H., Tipping, E. (2003) Generic NICA Donnan model parameters for metal–ion binding by humic substances. *Environ. Sci. Technol.* **37**, 958 – 971.

Missana, T. Alonso, U., Garcia-Gutierrez, M., Albarran, N. Lopez, T. (2009) Europium adsorption onto febex smectite. In: *4th Ann. Workshop Proc.6th EC FP –FUNMIC IP, FZKA-7461 Report, Germany*.

Morel, F. M. M., Morgan, J. J. (1971) A Numerical method for computing Equilibria in aqueous chemical systems. *Environ. Sci. Technol.* **6**, 58 - 67.

Morel, F. M. M. (1983) *Principles of Aquatic Chemistry*. Wiley, New York.

Morgenstern, A., Choppin, G. R. (2002) Kinetics of the oxidation of Pu(IV) by manganese oxide. *Radiochim. Acta* **90**, 69 - 74.

Morse, J. W., Choppin, G. R. (1991) The chemistry of transuranic elements in natural waters. *Rev. Aquat. Sci.* **4**, 1 – 22.

Morss, L. R., Edelstein, N. M., Fuger, J. (Eds.) (2010) *The chemistry of the actinides and transactinide elements, Fourth edition, Springer, The Netherlands.*

N

Novikov, A. P., Kalmylov, S. N., Utsunomiya, S., Ewing, R. C., Horreard, F., Merkulov, A., Clark, S. B., Tkachev, V. V., Myasoedov, B. F. (2006) Colloid transport of plutonium in the far-field of the Mayak production association, Russsia. *Science*, **314,** 638 - 641.

O

Olsson, M. (2006) On the stability of Pu(III) at different pH under non-inert conditions. *Radiochim. Acta* **94**, 575 - 578.

O′ Day, P. A., Chisholm-Brause, C. J., Towle, S. N., Parks, G. A., Brown, Jr., G. E. (1996) X-ray absorption spectroscopy of Co(II) sorption complexes on quartz (α-SiO_2) and rutile (TiO_2). *Geochim. Cosmochim. Acta* **60**, 2515 – 2532.

P

Pente, A. S. (2009) Characterisation of Swelling Clay Minerals for Evaluation of Their Suitability as Buffer/Backfill Material for Nuclear Waste Repository, *Ph. D Thesis. University of Mumbai, Mumbai, India.*

Piasecki, W., Sverjensky, D. A. (2008) Speciation of adsorbed yttrium and rare earth elements on oxide surfaces. *Geochim. Cosmochim. Acta* **72**, 3964 – 3979.

Piccolo, A. (2001) The supramolecular structure of humic substances. *Soil Sci.* **166**, 810-832.

Powell, B. A., Fjeld, R. A., Kaplan, D. I., Coates, J. T., Serkiz, S. M. (2004) $Pu(V)O_2^+$ adsorption and reduction by synthetic magnetite (Fe_3O_4). *Environ. Sci. Technol.* **38**, 6016 - 6024.

Powell, B. A., Fjeld, R. A., Kaplan, D. I., Coates, J. T., Serkiz, S. M. (2005) $Pu(V)O_2^+$ adsorption and reduction by synthetic hematite and goethite. *Environ. Sci. Technol.* **39** 2107 - 2114.

Powell, B. A., Duff, M. C., Kaplan, D. I., Fjeld, R. A., Newville, M., Hunter, D. B., Bertsch, P. M., Coates, J. T., Eng, P., Rivers, M. L., Serkiz, S. M., Sutton, S. R., Triay, I. R., Vaniman, D.

T. (2006) Plutonium oxidation and subsequent reduction by Mn(IV) minerals in Yucca Mountain tuff. *Environ. Sci. Technol.* **40**, 3508 - 3514.

Powell, B. A., Dai, Z., Zavarin, M., Zhao, P., Kersting, A. B. (2011) Stabilization of plutonium nano-colloids by epitaxial distortion on mineral surfaces. *Environ. Sci. Technol.* **45**, 2698 - 2703.

Prieve, D. C., Ruckenstein, E. J. (1978) The double-layer interaction between dissimilar ionisable surfaces and its effect on the rate of deposition. *J. Colloid Interface Sci.* **63**, 317 – 329.

R

Rabung, Th., Geckeis, H., Kim, J., Beck, H. P. (1998) Sorption of Eu(III) on a Natural Hematite: Application of a Surface Complexation Model. *J. Colloid Int. Sci.* **208**, 153 -161.

Rabung, Th., Stumpf, Th., Geckeis, H., Klenze, R., Kim, J. I. (2000) Sorption of Am(III) and Eu(III) onto γ-alumina: experiment and modelling. *Radiochim. Acta* **88**, 711 – 716.

Rabung, Th., Schild, D., Geckeis, H., Klenze, R., Fanghanel, Th. (2004) Cm(III) sorption onto sapphire (α-Al_2O_3) single crystals. *J. Phys. Chem. B* **108**, 17160 - 17163.

Rabung, Th., Geckeis, H., Wang, X. K., Rothe, J., Denecke, M. A., Klenze, R. (2006) Th. Fanghanel, Cm(III) sorption onto γ-Al_2O_3: New insight into sorption mechanism by time-resolved laser fluorescence spectroscopy and extended X-ray absorption fine structure. *Radiochim. Acta.* **94**, 609 - 618.

Rai, D. (1984) Solubility product of Pu(IV) hydrous oxide and equilibrium constants of Pu(IV)/ Pu(V), Pu(IV)/ Pu(IV), and Pu(V)/ Pu(VI) couples. *Radiochim. Acta* **35**, 97 - 106.

Rai, D., Moore, D. A., Felmy, A. R., Choppin, G. R., Moore, R. C. (2001) Thermodynamics of the PuO_2^+ - Na^+ - OH^- - Cl^- - ClO_4^- - H_2O system: use of NpO_2^+ pitzer parameters for PuO_2^+. *Radiochim. Acta* **89,** 491 - 498.

Randall, S. R., Sherman, D. M., Ragnarsdottir, K. V., Collins, C. R. (1999) The mechanism of cadmium surface complexation on iron oxyhydroxide minerals. *Geochim. Cosmochim. Acta* **63**, 2971 - 2976 .

Reiller, P., Casanova, F., Moulin, V. (2005) Influence of addition order and contact time on thorium(IV) retention by hematite in the presence of humic acids. *Environ. Sci. Technol.* **39**, 1641 - 1648.

Reiller, P., Moulin, V.; Casanova, F., Dautel, C. (2002) Retention behaviour of humic substances onto mineral surfaces and consequences upon thorium (IV) mobility: case of iron oxides. *Appl. Geochem.* **17**, 1551 - 1562.

Reiller, P., Bradbury, M. (2006) Report on RTD component 1. In: Reiller, P., Buckau, G., Kienzler, B., Duro, L., Montoya, V. (Eds.), *2nd Ann. Workshop Proc. of the Integrated Project "Fundamental Processes of Radionuclide Migration" (6th EC FP IP FUNMIG), Stockholm*.

Reiller, P. (2007) Report on RTD component 1. In: Buckau, G., Kienzler, B., Duro, L., Montoya, V., Delos, A. (Eds.), *3rd Ann. Workshop Proc. of the Integrated Project "Fundamental Processes of Radionuclide Migration" (6th EC FP IP FUNMIG), Edinburgh.*

Reiller, P. (2008) Report on RTD component 1. In: Buckau, G., Kienzler, B., Duro, L. (Eds.), *4th Ann. Workshop Proc. of the Integrated Project "Fundamental Processes of Radionuclide Migration" (6th EC FP IP FUNMIG), Kalsruhe.*

Reiller, P. (2012) Thermodynamic data provided through the FUNMIG project: Analyses and perspective. *Appl. Geochm.* **27**, 414 - 426.

Righetto, L., Bidoglio, G., Aziminoti, G., Bellobono, I. R. (1991) Competitive actinide interactions in colloidal humic acid-mineral oxide systems. *Environ. Sci. Technol.* **25**, 1913 - 1917.

Romanchuk, A. Y., Kalmykov, S. N., Aliev, R. A. (2011) Plutonium sorption onto hematite colloids at femto- and nanomolar concentrations. *Radiochim. Acta* **99**, 137 - 144.

Runde, W., Neu, M. P. (2010) Actindies in geosphere. *In The chemistry of the actinide and transactinide elements, (ed.) Morss, L. R., Edelstein, N. K., Fuger, J.*, volume 6, chapter 32, Springer.

S

Saito, T., Koopal, L. K., Nagasaki, S., Tanaka, S. (2005) Analysis of copper binding in the ternary system Cu(II)/humic acid/goethite at neutral and acidic pH. *Environ. Sci. Technol.* **39**, 4886 - 4893.

Samadfam, M., Jintoku, T., Sato, S., Ohashi, H., Mitsugashira, T., Hara, M., Suzuki, Y. (2000) Effects of humic acid on the sorption of Am(III) and Cm(III) on kaolinite. *Radiochim. Acta 88*, 717 - 721.

Sanchez, A. L., Murray, J. W., Sibley, T. H. (1985) The adsorption of plutonium IV and V on goethite. *Geochim. Cosmochim. Acta* **49**, 2297 - 2307.

Scheidegger, A.M., Sparks, D.L. (1996) Kinetics of the formation and the dissolution of nickel surface precipitates on pyrophyllite. *Chem. Geol.* **132**, 157–164.

Schindeler, P. W., Gamsjager, H. (1972) Acid base reactions of the TiO_2 (anatase) – water interface and the point of zero charge of TiO_2 suspensions. *Kolloid Z. Z. Polym.* **250**, 759 – 763.

Schindler, P. W. (1981) Surface complexes at oxide-water interfaces. In: M. A. Anderson and A. J. Rubin (eds.), *Adsorption of Inorganics at Solid-Liquid Interfaces*. Ann Arbor Science Publ., 1 - 49.

Schindler, P. W., Stumm, W. (1987) The surface chemistry of oxides, hydroxides, and oxide minerals. In: *Aquatic Surface Chemistry*, *W. Stumm (ed.),* John Wiley & Sons, 83 - 100.

Schlegel, M. L., Pointeau, I., Coreau, N., Reiller, P. (2004) Mechanism of europium retention by calcium silicate hydrate: An EXAFS study. *Environ. Sci. Techno.* **38**, 4423 - 4431.

Schlegel, M. L.; Pointeau, I., de Saclay, C. E. A. (2011) *Report available at http://ftp.esrf.eu/pub/UserReports/25930_A.pdf.*

Schwyn, B., Wersin, P., Ruedi, J., Schneider, J., Altmann, S., Missana, T., Noseck, U. (2012) FUNMIG integrated project results and conclusions from a safety case perspective. *Appl. Geochem.* **27**, 501 – 515.

Sekine, T., Asai, N., Mine, T., Yoshihara, K. (1997) Complexation of technetium traces with humic acid. *Radiochemistry* **39**, 309 – 311.

Shaughnessy, D. A., Nitsche, H., Booth, C. H., Shuh, D. K., Waychunas, G. A., Wilson, R. E., Gill, H., Canterll, K. J., Serne, R. J. (2003) Molecular interfacial reactions between Pu(IV) and manganese oxide minerals manganite and hausmanite. *Environ. Sci. Technol.* **37**, 3367 - 3374.

Siegel, M. D., Bryan, C. R. (2009) Environmental geochemistry of radioactive contamination. *In Treatise on Geochemistry*, Elsevier, Chapter 9, 205 - 262.

Silva, R. J., Bidoglio, G., Rand, M., Robouch, P., Wanner, H., Puigdomenech, I. (1995) In: Grenthe, G., Sandino, M. C. A., Puigdomenech, I., Rand, M. H. (Eds.), *Chemical Thermodynamics, Chemical Thermodynamics of Americium with an Appendix on Chemical Thermodynamics of Uranium*, Vol. 2, North Holland Elsevier Science Publishers B. V., Amsterdam, The Netherlands.

Sposito, G. (1984) *The Surface Chemistry of Soils*, Oxford University Press.

Stevenson, F. J. (1982) *Humus Chemistry: Genesis, Composition, Reactions*. John Wiley & Sons.

Sterne, P. A., Gonis, A., Borovoi, A. A. (1998) *Actinides in the Environment*, Kluwer, Dordrecht, The Netherlands.

Stumm, W., Huang, C. P., Jenkins, S. R. (1970) Specific chemical interactions affecting the stability of dispersed system. *Croat. Chem. Acta* 42, 223 – 244.

Stumm, W., Morgan, J. J. (1995) *Aquatic chemistry: Chemical Equilibria and rates in natural waters.* Wiley, New York.

Stumm, W. (1996) *Chemistry of the solid-Water Interface*. John Wiley & Sons.

Stumpf, Th., Rabung, Th., klenze, R., Geckeis, H., Kim, J. I. (2001) Spectroscopic study of Cm(III) sorption onto γ-alumina. *J. Colloid Interf. Sci.* **238**, 219 - 224.

Stumpf, Th., Bauer, A., Coppin, F., Kim, J. I. (2001) Time-resolved laser fluorescence spectroscopy study of the sorption of Cm(III) onto smectite and kaolinite. *Environ. Sci. Technol.* **36**, 3691 - 3694.

Stumpf, Th., Hennig, C., Bauer, A., Denecke, M. A., Fanghanel, Th. (2004) An EXAFS and TRLFS study of the sorption of trivalent actinides onto smectite and kaolinite. *Radiochem. Acta* **92**, 133 - 138.

Sutton, R., Sposito, G. (2005) Molecular structure in soil humic substances: The new view. *Environ. Sci. Technol.* **39**, 9009 - 9013.

Sverjensky D. A. (2006) Prediction of the speciation of alkaline earths adsorbed on mineral surfaces in salt solutions. *Geochim. Cosmochim. Acta* **70**, 2427 – 2453.

Swift, R. S. (1999) Macromolecular properties of soil humic substances: fact, fiction, and opinion. *Soil Sci.* **164**, 790 - 802.

T

Takahashi, Y., Kimura, T., Kato, Y., Minai, Y., Tominaga, T. (1998) Characterization of Eu(III) species sorbed on silica and montmorillonite by laser induced fluorescence spectroscopy. *Radiochim. Acta* **82**, 227 - 232.

Tertre, E., Berger, G., Simoni, E., Castet, S., Giffaut, E., Loubet, M., Catalette, H. (2006) Europium retention onto clay minerals from 25 to 150 ^{o}C : Experimental measurements, spectroscopic features and sorption modelling. *Geochim. Cosmochim. Acta* **70**, 4563 - 4578.

Ticknor, K. V., Vilks, P., Vandergraaf, T. T. (1996) The effect of fulvic acid on the sorption of actinides and fission products on granite and selected minerals. *Appl. Geochem.* **11**, 555-565.

Tipping, E., Hurley, M. A., (1992) A unifying model of cation binding by humic substances. *Geochim. Cosmochim. Acta* **56,** 3627 - 3641.

Tipping, E. (1998) Humic ion-binding model VI: an improved description of the interactions of protons and metal ions with humic substances. *Aquat. Geochem.* **4**, 3 – 48.

Tipping, E. (2002) *Cation binding by humic substances*. Cambridge University Press.

Tournassat, C., Ferrage, E., Poinsignon, C., Charlet, L. (2004) The titration of clay minerals II. Structure-based model and implications for clay reactivity. *J. Colloid Inter. Sci.* **273**, 234 – 246.

Towle, S. N.; Barger, J. R.; Brown, Jr., G. E., Parks, G. A. (1997) Surface precipitation of Co(II) (aq) on Al_2O_3. *J. Colloid Interface Sci.*, **187**, 62 - 82.

Trainor, T. P., Brown, G. E., Parks, G. A. (2000) Adsorption and precipitation of aqueous Zn(II) on alumina powders. *J. Colloid Interface Sci.* **231**, 359 – 372.

Trainor, P. T., Brown, Jr., G. E., Parks, G. A. (2000) Adsorption and precipitation of aqueous Zn(II) on alumina powders. *J. Colloid Interface Sci.* **231**, 359-372.

Triay, I. R., Meijer, A., Conca, J. L., Kung, K. S., Rundberg, R. S., Streitelmeier, B. A., Tait, C. D., Clark, D. L., Neu, M. P., Hobert, D. E. (1997) *Summary and synthesis report on radionuclide retardation for the Yucca mountain site characterization project LA-13262-MS*. Los Alamos National Laboratories.

U

Utsunomiya, S., Kersting, A. B., Ewing, R. C. (2009) Groundwater nanoparticles in the far-field at the Nevada test site: Mechanism for radionuclide transport. *Environ. Sci. Technol.* **43**, 1293 – 1298.

V

Van Riemsdijk, W. H., Koopal, L. K., Kinniburgh, D. G., Benedetti, M. F., Weng, L. (2006) Modeling the interactions between humics, ions, and mineral surfaces. *Environ. Sci. Technol.* **40**, 7473 – 7480.

Van Loon, L. R., Baeyens, B., Bradbury, M. H. (2009) The sorption behaviour of caesium on opalinus clay: A comparison between intact and crushed material. *Appl. Geochem.* **24**, 999 – 1004.

Vermeer, A. W. P., McCulloch, J. K., van Riemsdijk, W. H., Koopal, L. K. (1999) Metal ion adsorption to complexes of humic acid and metal oxides: deviation from the additivity rule. *Environ. Sci. Technol.* **33**, 3892 - 3897.

W

Wang, F., Chen, J., Forsling, W. (1997) Modeling sorption of trace metals on natural sediments by surface complexation model. *Environ. Sci. Technol.* **31**, 448 - 453.

Wang, X. K., Dong, W. M., Dai, X. X., Wang, A. X., Du, J. Z., Tao, Z. Y. (2000) Sorption and desorption of Eu and Yb on alumina: mechanisms and effect of fulvic acid. *Appl. Radiat. Isot.* **52**, 165 - 173.

Wang, K., Xing, B. (2005) Structural and sorption characteristics of adsorbed humic acid on clay minerals. *J. Environ. Qual.* **34**, 342 – 349.

Warwick, P., Lewis, T., Evans, N., Bryan, N., Knight, L. (2006) Sorption of selected radionuclides to clay in the presence of humic acid. In: *Buckau, G., Kienzler, B., Duro, L., Martell, M., Reiller, P., (eds.), 1st Ann. Workshop Proc. Integrated Project "Fundamental Processes of Radionuclide Migration" 6th EC FP IP FUNMIG, CEA report no. CEA-R-6122*, 184-189.

Weng, L. P., Koopal, L. K., Hiemstra, T., Meeussen, J. C. L., Van Riemsduk, W. H. (2005) Interactions of calcium and fulvic acid at the goethite-water interface. *Geochim. Cosmochimica Acta* **69**, 325 – 339.

Westall, J., Hohl, H. (1980) A comparison of electrostatic models for the oxide/solution interface. *Adv. Coll. Int. Sci.* **12**, 265-294.

Wronkiewicz, D. J., Buck, E. C. (1999) Uranium mineralogy and the geologic disposal of spent nuclear fuel. *In* Uranium: Mineralogy, Geochemistry, and the Environment (ed. Ribbe, P. H.) Mineralogical Society of America, Washington, D. C., 475 – 494.

Y

Yoshida, T. Tanaka, T. Yoshida, S. Hikita, S. Baba, T. Hinode, T. Ono, Y. (2000) XAFS analysis of europium species supported on aluminium oxide surface. *Appl. Surf. Sci.* **156**, 65-75.

Yun, Jong-II; Bundschuh, T.; Neck, V., Kim, J. I. (2001) Selective determination of Eu(III) oxide and hydroxide colloids in aqueous solution by laser induced breakdown spectroscopy. *Appl. Spectroscopy* **55**, 273-278.

Z

Zachara, J. M., Resch, C. T., Smith, S. C. (1994) Influence of humic substances on Co^{2+} sorption by a subsurface mineral separate and its minealogic components. *Geochim. Cosmochim. Acta* **58(2)**, 553 - 566.

Zaera, F. (2012) Probing liquid/solid interfaces at the molecular level. *Chem. Rev.* **112**, 2920 – 2986.

Zhang Z., Fenter P., Cheng L., Sturchio N. C., Bedzyk M. D., Predota M., Bandura A. V., Kubicki J. D., Lvov S. N., Cummings P. T., Chialvo A. A., Ridley M. K., Benezeth P., Anovitz L., Palmer D. A., Machesky M., Wesolowski D. J. (2004) Ion adsorption at the rutile–water interface: linking molecular and macroscopic properties. *Langmuir* **20**, 4954 – 4969.

Zhang, Z., Fenter, P., Cheng, L., Sturchio, N. C., Bedzyk, M. J., Machesky, M. L., Anovitz, L. M., Wesolowski, D. J. (2006a) Zn^{2+} and Sr^{2+} adsorption at the TiO_2 (110)–electrolyte interface: influence of ionic strength, coverage, and anions. *J. Colloid Interf. Sci.* **295**, 50 – 64.

Zhang, Z., Fenter, P., Kelly, S. D., Catalano, J. G., Bandura, A. V., Kubicki, J. D., Sofo, J. O., Wesolowski, D. J., Machesky, M. L., Sturchio, N. C., Bedzyk, M. J. (2006b) Structure of hydrated Zn^{2+} at the rutile TiO_2 (11 0)–aqueous solution interfaces: comparison of X-ray standing wave, X-ray absorption spectroscopy, and density functional theory results. *Geochim. Cosmochim. Acta* **70**, 4039 – 4056.

Zhao, P., Zavarin, M., Leif, R. N., Powell, B. A., Singleton, M. J. (2011) Mobilization of actinides by dissolved organic compounds at the Nevada Test Site. *Appl. Geochem.* **26**, 308 - 318.

Zhou, R. S., Synders, R. L. (1991) Structures and transformation mechanisms of the η, γ, and θ transition aluminas. *Acta Crystallogr. Sect. B* **47**, 617 - 620.

Zhou, Q., Maurice, P.A., Cabaniss, S.E. (2001) Size fractionation upon adsorption of fulvic acid on goethite: equilibrium and kinetic studies. *Geochim. Cosmochim. Acta* **65**, 803 – 812.

List of Publications

1. Kumar, S., Tomar, B. S., Manchanda, V. K., Ramanathan, S. (2006) Effect of humic acid on adsorption behaviour of ^{137}Cs on silica colloids, *Radiochim. Acta* **94**, 369 – 373.

2. Kumar, S., Rawat, N., Tomar, B. S., Manchanda, V. K., Ramanathan, S. (2007) Effect of humic acid on the sorption of technetium on hematite colloids using ^{95m}Tc and ^{96}Tc as tracers, *J. Radioanal. Nucl. Chem.* **274**, 229 - 231.

3. Kumar, S., Rawat, N., Kar, A. S., Tomar, B. S., Manchanda, V. K. (2011) Effect of humic acid on sorption of technetium by alumina, *J. Hazard. Mat.* **192**, 1040 – 1045.

4. Kumar, S., Godbole, S. V., Tomar, B. S., Speciation of Am(III)/Eu(III) sorbed on γ-Alumina: Effect of metal concentration, *Radiochim. Acta*. *DOI No.* 10.1524/ract.2013.1997.

5. Kumar, S., Kar, A. S., Tomar, B. S., Bhattacharya, D. (2012) XAFS Spectroscopy study of Eu(III) sorption products on Amorphous Silica and γ-Alumina: Effect of pH and substrate, *Polyhedron* **33**, 33 - 40.

6. Kumar, S., Kasar, S. U., Tomar, B. S. (2012) Interfacial sorption/desorption studies of Pu(IV) on Silica and alumina surfaces, *Radiochim. Acta*. **100**, *885 – 892.*

7. Kumar, S., Pente, A. S., Kaushik, C. P., Bajpai, R. K., Tomar, B. S., Americium sorption on smectite rich natural Clay from granitic water, *Appl. Geochem. (under review)*.